Characterization of the immune response induced by rhabdovirus-infected leukemia cell vaccines

Elena Scut

Supervisors

Dr. Natasha Kekre

Dr. Rebecca Auer

This thesis is submitted to the University of Ottawa in partial fulfillment of the requirements for the Masters of Science degree in Biochemistry

Department of Biochemistry, Microbiology & Immunology

Faculty of Medicine

University of Ottawa

Abstract

Acute lymphoblastic leukemia (ALL) and acute myeloid leukemia (AML) are blood cancers that are often treated with stem cell transplantation (SCT). Since SCT treatments have variable success, especially in adults with AML whose disease frequently relapses, novel and more effective solutions must be considered. In this thesis, I will explore one type of immunotherapy in murine models for ALL (L1210) and AML (C1498) using *in vitro* and *in vivo* techniques such as flow cytometry and transcriptomics. In my approach, I am attempting to enhance the immunogenicity of whole cell vaccines by pre-infecting the leukemia cells with oncolytic virus (OV) and thus producing leukemia infected cell vaccines (ICVs). While it has been previously shown that L1210-ICV pre-treatment works well in protecting mice from ALL challenge, I have found that pre-immunization with C1498-ICV has a limited efficacy in protecting animals from AML progression. By investigating the downstream effects of ICV, I was able to show that unlike C1498 cells, L1210 cells produce previously unknown immunogenic factors following OV infection.

Acknowledgments

While conducting my research, as well as writing this MSc thesis, I have received a great deal of assistance and encouragement from outstanding scientists to whom I will be forever grateful.

First, I would like to express my sincere gratitude to my thesis supervisors, Dr. Rebecca Auer and Dr. Natasha Kekre. Dr. Auer, thank you for your motivation, continuous support and for challenging me to think critically and grow as a scientist. Your passion for translational research and commitment to the wellness of your patients served me as a continuous source of inspiration. I feel honored for being part your research team and could not have imagined having a better mentor than you.

My sincere thanks also go to Dr. Michael Kennedy, whose expertise was invaluable in the formulating of the research questions and especially the employed methodology. Our frequent meetings and stimulating discussions on cancer immunology were incredibly resourceful for me during the last couple of years. I would especially like to thank you for the fact that the door to your office was always open whenever I faced certain challenges with my research. I am also very appreciative towards all members of my lab with whom I have had the pleasure to work with, especially to the PhD candidates Katherine Baxter and Leonard Angka that were always there for me when needing help and advice in designing my first flow cytometry experiments.

I would also like to thank the rest of my thesis committee – Dr. Tommy Alain and Dr. Carolina Solange Ilkow for their support, insightful suggestions and especially for addressing challenging questions that inspired me to orient my research into the right direction.

I also feel an immense amount of gratitude toward Dr. John Bell, whose immense knowledge and enthusiasm for science encouraged me to think outside of the box and develop my independent thinking as a scientist.

My scientific accomplishments elaborated in this thesis would have not been possible without the help of Julia Petryk, who assisted me with most of my *in vivo* work and was always ready to help me even on very short notice. I would also like to help our animal technician Christiano Tanese de Souza for helping me with the mouse IV injections without whom the DC and T cell immunophenotyping experiments would have not been accomplished. Many thanks to the Diallo lab members Andrew Chen, Naveen Haribabu and Dr. Fanny Tzelepis that assisted me with either helpful advice or borrowing reagents for certain experiments. I also very much appreciate the help of Dr. Ardolino and his PhD student Jonathan Hodgins for helping me, multiple times, salvage some complex flow cytometry experiments by running my samples even when it was very late in the day before winter holidays.

I must express my very profound gratitude to my parents for providing me with unfailing support and continuous encouragement throughout my years of study and through the process of researching and writing this thesis. A big thank you also goes to my cat Leo, who provided me with support in difficult times and helped me maintain my mental health. Last but not the least, I owe more than thanks to my loving and caring husband Adrian Pelin who was always there for me as a great advisor regarding my scientific project, moral supporter and as my absolute best friend. I would have not got anywhere without your love and encouragement.

Table of Contents

List of Abbreviations

5-AzaC – 5-azacytidine

ABL – Abelson murine leukemia viral oncogene homolog

ACK – Ammonium-Chloride-Potassium buffer

AL – Acute Leukemia

ALL – Acute Lymphoblastic Leukemia

AML – Acute Myeloid Leukemia

AML1 – Acute Myeloid Leukemia 1

APC – Antigen Presenting Cell

ATCC – American Type Culture Collection

BBB – Blood Brain Barrier

Bcl-xL – B-cell lymphoma-extra Large

BCR – Breakpoint Cluster Region

BMT – Bone Marrow Transplant

cALL – (B cell) precursor Acute Lymphoblastic Leukemia

CAR-T Chimeric Antigen Receptor T

CBFB – Core-Binding Factor Subunit Beta

CCAC – Canadian Council on Animal Care

CD-(8) – Cluster of Differentiation

cDC – classical Dendritic Cell

CL – Chronic Leukemia

CLL – Chronic Lymphocytic Leukemia

CLP – Common Lymphoid Progenitors

CML – Chronic Myelogenous Leukemia

CMP – Common Myeloid Progenitors

CNS – Central Nervous System

CR – Complete Remission

CTLA-4 - Cytotoxic T-Lymphocyte-Associated protein 4

DAMP – Damage-associated molecular patterns

DC – Dendritic Cell

DMEM – Dulbecco's Modified Eagle Medium

DMXAA – 5,6-dimethylxanthenone-4-acetic acid

DNMT3A – DNA (cytosine-5)-methyltransferase 3A

dsDNA – double-stranded deoxyribonucleic acid

eGFP - Green Fluorescent Protein

EMD – Extramedullary Disease

ETP – Early T cell Progenitors

FBS – Fetal Bovine Serum

FDA – Food and Drug Administration

FLT3 – FMS-like tyrosine kinase 3

FMO – Fluorescence Minus One

GM-CSF - Granulocyte-Macrophage Colony-Stimulating Factor

GMP – Granulocyte/Macrophage Progenitor

GRB2 – Growth factor Receptor-Bound protein 2

GVHD – Graft versus host disease

GVL – Graft versus Leukemia

HLA – Human Leukocyte Antigen

HPV – Human Papilloma Virus

HSC – Hematopoietic Stem Cell

HSPC – Hematopoietic Stem and Progenitor Cell

ICI - Immune Checkpoint Inhibitors

ICV – Infected Cell Vaccine

IFNAR - Interferon-α/β Receptor

IFN-ɣ - Interferon gamma

IL-(12) – Interleukin

IRF-(3) – Interferon Regulatory Factor (3)

ISG – Interferon Stimulated Genes

IT – Intra-Tumoral

IV – Intravenous

JAK – Janus kinase

JAK2 – Janus kinase 2 (JAK2)

KMNT2A – Lysine Methyltransferase 2A

LDLR – Low Density Lipoprotein Receptor

LPS – Lipopolysaccharide

MCP-1 – Monocyte Chemoattractant Protein 1

MEP – Megakaryocyte/Erythrocyte Progenitors

MHC – Major histocompatibility complex

MIP-1b - Macrophage Inflammatory Protein 1b

MMP-2 – Matrix Metallo-Proteinase (MMP)-2

MMP-9 – Matrix Metallo-Proteinase (MMP)-9

MOI – Multiplicity of Infection

MPP – Multipotent Progenitor

MRD – Minimal Residual Disease

MS – Myeloid Sasrcoma

MYH11 – Myosin Heavy Chain 11

NDV – New Castle Disease Virus

NF-kB – Nuclear Factor kappa-light-chain-enhancer of activated B cells

NK – Natural Killer Cell

NOS – Not Otherwise Specified

NPM 1 – Nucleophosmin 1

OV – Oncolytic Virus

PAMP –Pathogen-associated molecular patterns

PBMC – Peripheral Blood Mononuclear cells

PBS – Phosphate-Buffered Saline

PD-1 - Programmed cell Death protein 1

PDGFRB – Platelet derived growth factor receptor Beta

Ph – Philadelphia chromosome

PI - Propidium Iodide

PI-3K - Phosphoinositide 3-Kinases

PI-3K – Phosphoinositide 3-kinases

PKR – Protein Kinase RNA-activated

Poly:IC – Polyinosinic-polycytidylic acid

PRR – Pattern recognition receptors

qPCR – quantitative Polymerase Chain Reaction

RANTES - Regulated on activation, normal T cell expressed and secreted

RBC – Red Blood Cell

RT – Room Temperature

SCT – Stem Cell Transplantation

ssRNA – single-stranded Ribonucleic Acid

STAT – Signal Transducer and Activator of Transcription

STING – Stimulator of interferon genes

TAA – Tumour associated antigen

TCR – T Cell Receptor

TEL – translocation–Ets–leukemia

TIM-3 – T cell Immunoglobulin and Mucin domain-containing protein 3

TKI – Tyrosine Kinase Inhibitor

TLR-7/8 – Toll-like Receptor-7/8

t-MN – Therapy-Related Myeloid Neoplasm

TNF-α - Tumour Necrosis Factor alpha

TPM – Transcripts per Million

Tregs – Regulatory T cells

TSA – Tumour Specific Antigen

VacV – Vaccinia Virus

VSV -0 Vesicular Stromatitis Virus

WHO – World Health Organization

(c)-RPMI – (complete) Roswell Park Memorial Institute

(LT)-HSC – Long-Term Hematopoietic Stem Cell

(ST)-HSC – Short-Term Hematopoietic Stem Cell

List of Figures

List of Tables

Chapter 1 – Introduction

Normal hematopoiesis

Mature blood cells capable of carrying specialized functions like oxygen transport or immune response mediation originate from a rare population of hematopoietic stem cells (HSCs) or blood-forming cells [1]. One characteristic of HSCs is their multipotency or their ability to reconstitute all blood cell lineages during one's lifetime [2-5]. Another unique characteristic of HSCs is that they are capable of self-renewal, meaning that half of their daughter cells will commit to further lineage-specific differentiation, while the other half will be maintained as HSCs [5, 6].

At first, HSCs were considered a homogenous population, sharing the same phenotype and differentiation ability [7, 8]. However, with the help of the newly emerged technologies it was recently revealed that individual HSCs differ based on their molecular profile, cell fate and self-renewal ability [9-12]. There are long-term (LT)-HSCs that are capable of self-renewal during one's lifetime, and short-term (ST)-HSCs that originate from the LT-HSCs population and only maintain the ability to self-renew temporarily [13]. Both LT-HSCs and ST-HSCs however are multipotent and capable to recreate all blood cell lineages [14-16]. ST-HSCs differentiate into multipotent progenitors (MPPs) that are still able to differentiate into all blood cell lineages, but incapable of self-renewal [17]. MPP differentiation will give rise to two types of oligopotent or lineage –committed progenitors, namely common lymphoid progenitors (CLPs) and common myeloid progenitors (CMPs). Subsequent differentiation of CLPs will lead to the generation of terminally differentiated lymphocytes, namely natural killer (NK) cells, B cells and T cells [18, 19]. On the other hand, CMP differentiation will produce megcaryocyte/erythrocyte progenitors (MEPs), megacaryocytes and granulocyte/macrophage progenitors (GMPs) [19, 20]. MEPs will generate red blood cells (RBCs) and megacaryocytes while GMPs will differentiate into macrophages, eosinophils, basophils and neutrophils [20, 21].

Cell-fate decisions are finely regulated to maintain a functional HSCs pool and maintain blood system homeostasis. Disruption of regulatory mechanisms can lead to hematological disorders, like leukemia defined by abnormal proliferation, aberrant

differentiation and diminished apoptosis of HSCs and progenitor intermediates.

Impaired hematopoiesis and types of Leukemia

Leukemia is a hematological malignancy in which normal hematopoiesis is disrupted due to an excessive proliferation and accumulation of immature or abnormal leukocytes. Malignant transformation usually occurs at the pluripotent stem cell level, although it can involve a committed stem cell with a reduced capacity for self-renewal [22]. Types of leukemia are classified based on the blood cell in which the malignant transformation occurred. One can be diagnosed with either lymphoblastic or myelogenous leukemia, depending on whether the disease originated from an abnormal cell of lymphoid or myeloid lineage respectively. Leukemia types are further grouped based on their proliferation rate and progression. If the disease arises spontaneously with manifestation of symptoms within days or weeks, one can be diagnosed with acute leukemia (AL). On the other hand, chronic leukemia (CL) is diagnosed when malignant cell proliferation occurs over prolonged periods of time. Thus, the major diagnosed types of leukemia nowadays are acute lymphocytic leukemia (ALL), acute myelogenous leukemia (AML), chronic lymphocytic leukemia (CLL) and chronic myelogenous leukemia (CML). Further, my discussion will mostly revolve around AML and ALL, considering the fact that murine AML and ALL models were particularly used in my research.

Classification, pathophysiology and treatments of AML

According to the World Health Organization (WHO), AML subtypes were classified in several major groups defined as AML with recurrent genetic abnormalities, therapy-related myeloid neoplasms, AML that is not otherwise specified (NOS), myeloid sarcoma and myeloid proliferations related to Down syndrome. The pathology, prognosis and treatment of several of these AML subtypes are reviewed below.

AML with recurrent genetic abnormalities

Patients diagnosed with this particular type of AML carry specific mutations or chromosomal translocations. The most frequent chromosomal abnormality, diagnosed in

15% of AML cases is the t(8, 21) translocation, involving acute myeloid leukemia 1 (*AML1*) gene on chromosome 21 and the *ETO* gene on chromosome 8 [23]. A fusion protein known as *AML1-ETO* is produced as a result of this translocation and it is a transcription factor that mediates both gene repression and activation [23, 24]. The target for leukemic transformation in AML patients with t(8, 21) translocation are HSCs rather than committed progenitor cells [25-27]. The second most frequent chromosomal abnormality associated with AML is inv(16)(p13.1q22), being detected in up to 8% of all AML patients [28, 29]. Carriers of this particular inversion produce a fusion transcript in which the Core-Binding Factor Subunit Beta (*CBFB*) gene on chromosome 16q22 and the Myosin Heavy Chain 11 (*MYH11*) gene on chromosome 16p13.1 have been rearranged. The resulting C*BFB-MYH11* fusion protein was shown to impair hematopoiesis during embryogenesis at the HSPC level [30].

AML patients carrying either t(8;21) and/or inv(16) (p13.1q22) have an overall good prognosis and respond well to chemotherapy, particularly to cytarabine treatments. [28, 31, 32]. It has been shown that intensive chemotherapy, is most efficient in patients of different age categories [32]. However, some older patients that are not suitable for intensive chemotherapy are treated with low-dose cytarabine therapy [33]. Unfortunately, low-dose cytarabine therapy is less likely to result in long term remission and the prognosis of patients carrying inv(16)(p13.1q22) becomes dismal upon relapse [34, 35].

Therapy-related myeloid neoplasms

Therapy-related myeloid neoplasms (t-MN) are highly associated with the chemotherapy treatment itself and its cytotoxicity [36]. The t-MN subtypes known to date are associated with the type of leukemia treatment that patients previously received. About 70% of t-MN patients that received alkylating agents and radiation therapy carry deletions within chromosome 5 and 7 [37]. Another major t-MN subtype refers to patients to whom topoisomerase II inhibitors were administered for treatment [38, 39]. It has been shown that the most common translocation events for this subgroup affect lysine methyltransferase 2A (*KMT2A*) gene within chromosome 11 or *AML1* gene within chromosome 21 [37]. It has been established that t-MN account for 10% of all

AML cases and can develop from a couple of months to several years after the treatment of the initial disease [40, 41].

t-MN is associated with unfavorable prognosis at the onset of the disease, frequently leading to peripheral blood cytopenia [42, 43]. Treatment strategies for t-MN include intensive chemotherapy and/or SCT [44]. Some clinical studies evaluate the possibility of treating t-MN patients ineligible for intensive chemotherapy with 5-azacytidine (5-AzaC) instead [45, 46]. At this point, very little is known about the efficacy of 5-AzaC as part of t-MN treatment since most clinical studies are still at the stage of assessing the toxicity of this drug.

Myeloid sarcoma

Myeloid sarcoma (MS) is considered a fairly rare form of AML in which the extramedullary proliferation of myeloid blasts disrupt the morphology and function of the infiltrated tissue [47, 48]. Considering that MS is often defined as an extramedullary disease (EMD), it is possible that the leukemic blasts have an aberrant homing signal that does not target localization to the bone marrow. For instance, one research group stated that the interaction between the matrix metallo-proteinase (MMP)-9 and the beta (2) integrin expressed on the surface of leukocytes is necessary for migration and localization of leukemic cells [49]. The implication of MPPs in tissue blast penetration has also been supported by another study in which the expression of a MMP-2 tissue inhibitor was significantly higher on invasive AML cell lines like SHI-1 compared to AML models that are considered less invasive [50].

A comparative genomics study of several MS patient samples revealed that all patients carried genomic changes, especially within chromosome 8 [51]. Based on the fact that the mutated nucleophosmin 1 (NPM 1) gene is considered one of the most common genetic abnormalities for AML, one study determined that 15% of 181 enrolled MS patients carried this mutation [52]. Another study reported that about 33% of MS patients carried mutations in the FMS-like tyrosine kinase 3 (FLT3) gene with internal tandem duplications, which are also very commonly attributed to up to 30% of adult AML cases [53].

Considering the rarity of MS, knowledge regarding major prognostic factors in these patients is fairly scarce. It generally appears that patients having MS at the time of AML diagnosis is linked to poor prognosis and shorter survival [54]. Interestingly, allogeneic hematopoietic stem cell transplantation (SCT) was shown to be a fairly efficient treatment strategy for MS patients that achieved complete remission as a result of induction chemotherapy treatments for AML [55].

Classification, pathophysiology and treatment of ALL

Generally, 85% of ALL cases originate from B lymphocytes or B cell precursors while 15% of ALL cases can be traced to malignant transformations of T lymphocytes [56]. According to the WHO classification, ALL is classified as B-ALL not otherwise specified, B-ALL with recurrent cytogenetic abnormalities and T-ALL. The pathophysiology, prognosis and treatment regimen of several of the mentioned ALL subtypes is described below.

Precursor B-ALL with cytogenetic abnormalities

ALL with BCR-ABL

Chromosomal aberrations are considered the hallmark of ALL. In fact, the most common marker for ALL diagnosis is the Philadelphia chromosome (Ph), which is a shorter version of chromosome 22 that resulted due to the t(9, 22) reciprocal translocation, involving the Breakpoint cluster region (*BCR*) gene and Abelson murine leukemia viral oncogene homolog (*ABL*) gene located on chromosomes 22 and 9 respectively [57]. The BCR-ABL fusion gene encodes an oncogenic protein with constitutively active tyrosine kinase activity that leads to uncontrolled cell proliferation, reduced apoptosis, and impaired cell adhesion [58, 59]. It has been shown that the BCR-ABL fusion protein is expressed by the myeloid, erythroid and B lymphoid cells of most ALL patients, implying that the translocation event likely occurs in LT-HSCs [57, 60]. Although t(9, 22) translocation events do not cause neoplastic transformations by themselves, they tend to cooperate with additional mutations acquired by the cells with a pre-existing Ph+ phenotype, thus contributing to the malignancy [61]. Up to 80% of patients diagnosed with a Ph-like ALL have mutations in genes encoding for kinases and

kinase-activating proteins responsible for regulation of hematopoiesis and HSC self-renewal, like ABL-1, Janus kinase 2 (JAK2) and Platelet derived growth factor receptor Beta (PDGFRB) [61].

One clinical study pointed out that t(9, 22) is associated with extremely poor prognosis in children diagnosed with ALL [62]. ALL patients are usually treated with induction chemotherapy drugs, however the treatment also includes cranium radiation to prevent central nervous system (CNS) disease. The consolidation therapy for the Ph+ ALL cases was shown to be more efficient when the chemotherapy regiment used in Kantarjian, H.M., *et al*. [63] is combined with a Tyrosine Kinase Inhibitor (TKI) known as imatinib [64, 65]. Unfortunately, this treatment was unable to control the disease relapse in CNS due to the limited ability of imatinib to cross the Blood Brain Barrier (BBB) [66]. The next generation version of similar drugs were developed in order to easily access the BBB and prevent ALL establishment in CNS and were proven to be more efficient in several cases [67-69].

B-ALL with TEL-AML1

The chromosomal translocation involving the fusion of the translocation–Ets–leukemia (*TEL*) and *AML1* genes occurs in about 25% of pediatric patients with common B-cell precursor cell acute lymphoblastic leukaemia (cALL) [70]. The chimeric protein *TEL-AML1* identified in certain ALL patients is composed of *TEL* sequences located in most of the functional regions of the *AML1* protein [71]. It has been repeatedly shown that the *TEL-AML1* fusion occurs very early in leukaemogenesis and it could be the initiating event in the majority of identified cases [72-74].

It is generally considered that the presence of TEL-AML1 fusion gene in children diagnosed with ALL defines a subgroup of patients with a better than average treatment outcome and prognosis [75].

Precursor T lymphoblastic leukemia (T-ALL)

T-ALL is considered a hematological malignancy of immature T cells. It has been shown that early T-cell progenitors (ETP) are derived from hematopoietic stem cells that are eventually localized to the thymus with a maintained level of multilineage pluripotency [76]. The definition of ETP-ALL is recognized based on the unique

immunophenotype of the transformed cells, which are $CD1a^{-}$, $CD8^{-}$, $CD5^{-}$ and positive for certain stem cell or myeloid markers [77]. Literature shows that ETP-ALL is diagnosed in up to 12% of T-ALL cases among children as well as in up to 7% of adults suffering from T-ALL [78]. The most common genetic abnormalities observed in these patients are mutations within the FLT3 and DNA (cytosine-5)-methyltransferase 3A (*DNMT3A*) genes [79, 80].

Overall, the relapse of T-ALL is associated with a poor prognosis with only 30-50% survival. Induction chemotherapy treatment is normally used for T-ALL treatment with meticulous monitoring of Minimal residual disease (MRD) by quantitative polymerase chain reaction (qPCR) analysis of the T cell receptor (TCR) genes [81, 82].

Leukemia and its susceptibility to immunotherapy

From what has been discussed so far, the overall prognosis and chemotherapy treatment that is available for AL patients does not deliver successful outcomes, meaning that other options and strategies must be considered for this purpose.

Currently there is a significant amount of evidence that leukemia is highly susceptible to immunosurveillance and using immune strategies to control residual disease persisting after remission is the correct thing to do [83]. Several immunotherapies implemented to control leukemia progression are SCT, adoptive transfer of allogeneic or autologous T cells, vaccination with leukaemia cells, peptides, cell lysates and dendritic cells [83, 84]. The most captivating data, however, for the susceptibility of leukemic cells to immune attack is derived from the experience with allogeneic SCT and the graft versus host disease (GVHD). GVHD is a common side effect observed in leukemia patients after receiving allogeneic SCT. It has been observed that there was a strong correlation between the strength of GVHD of individuals in remission after BMT and reduced relapse rates, implying that BMT also promotes a graft versus leukemia (GVL) effect [85, 86]. In other words, the donor's cells of adaptive immunity are not only attacking the tissues of the recipient host (GVHD), but are also promoting a response against the patient's leukemic cells (GVL) [87].

Following this remarkable discovery, the SCT protocols are continuously revamped to maximize GVL, which is mediated by both T and NK cells, whose mechanisms of interaction with the transformed leukemic cells have been characterized elsewhere [83, 88] and continue to be investigated. To date, transplant protocols have been significantly adjusted in order to improve the ability to manipulate the immune environment after the procedure and control the patient's immune system recovery by avoiding GVHD and boosting GVL reactivity with vaccines or with Chimeric antigen receptor T (CAR T) cells (lymphocytes that are engineered to be cytotoxic to leukaemia cells).

Generally, allo-SCT is one of the best treatment options in reducing the risk of leukemia relapse by promoting GVL, especially for patients that are at high risk and are eligible for the procedure after they undergone induction chemotherapy. However the procedure itself is fairly invasive for elderly patients and may lead to severe complications. Another limitation in implementing SCT is the difficulty of finding a human leukocyte antigen (HLA)-matched sibling or unrelated donor.

Taken together, chemotherapy and SCT (despite the GVL effect) are not efficient enough in treating leukemia and dealing with the high relapse rates of this disease. This implies that new strategies and immunotherapeutic approaches must be implemented in targeting leukemia. Combining the current treatment options with different cancer immunotherapy approaches could potentially enhance the treatment efficacy for AL.

Cancer cells have a reduced adjuvanicity

It is generally known that different pathogens express antigens that can be recognized as non-self by our innate immune cells upon infection. Pathogen-associated molecular patterns (PAMPs), are a set of general structural components or molecules characteristic to invading pathogens and are sensed by our innate immune system. The PAMPs are sensed by pattern recognition receptors (PRRs) that are expressed on immune, non-immune and even cancer cells. Toll-like receptors (TLR)-7/8 are PRRs that sense different forms of single-stranded ribonucleic acids (ssRNA) present in endosomes and are necessary to neutralize infection with viruses like Influenza and

Vesicular Stromatitis Virus (VSV) [89, 90]. Interestingly, a recent study determined that conjugation of tumour neo-epitopes to TLR7/8 agonists is sufficient to initiate anti-tumour immunity, suggesting that these agonists work as immune adjuvants [91]. Another example of PRR is known as stimulator of interferon genes (STING) and it is able to detect double-stranded deoxyribonucleic acid (dsDNA) in cytoplasm that comes from replicating DNA viruses like Vaccinia (VacV) [92]. Interestingly, the use of STING agonists have shown a lot of promise in cancer therapy by promoting dendritic cell (DC) activation [93]. In one study, the STING agonist 5,6-dimethylxanthenone-4-acetic acid (DMXAA) was used to eradicate systemic AML in a pre-clinical mouse model (C1498) [94]. It has also been shown that STING can initiate the production of type I interferon, which is mainly implicated in the formation of adaptive immune responses by sustaining the activation of antigen presenting cells (APCs) [95]. For instance, mice that are unable to signal through type I interferon (Ifnar KO) failed to develop long lasting anti-tumour immunity, further highlighting its importance as an adjuvant [96].

In addition, the immune system keeps being alerted by damage-associated molecular patterns (DAMPs), which are components secreted by dying infected cells and are typically released in response to PAMPs and PRR signalling. In these circumstances, the components of these pathogenic agents are uptaken by phagocytes like macrophages and DCs and presented on major compatibility complex (MHC) class I and class II molecules, leading to generation of antigen-specific adaptive immunity. A similar scenario can be followed for the progression and selection of the malignant cancer cells, which have developed evasion strategies to inhibit mechanisms of DAMPs sensing and emission [97, 98]. In this sense, DAMPs that are potentially released from dying cancer cells could alert the phagocytes and act as natural adjuvants for tumour antigens. Cancer cells developed a wide range of strategies to prevent the release of DAMPs and therefore, avoid immune detection [99]. One important study found that some anti-cancer drugs like Mitoxantrone increases the level of calreticulin (DAMP) on the surface of cancer cells, resulting in a sustained anti-tumour immune response [100].

Overall, adjuvanicity depends on the release of DAMPs and sensing of PAMPs. Consequently, inducing DAMP release and triggering PRR sensing of PAMPs represent novel strategies in adjuvanating cancer antigens.

Cancer cells have a reduced antigenicity

Antigenicity refers to the mutations specific to cancer cells that result in the creation of neo-antigens to be presented on MHC molecules to T cells. The amount of neo-antigens is highly variable among different tumour types, which significantly affects the outcome of a potential immunotherapy treatment [101, 102]. For instance, unlike lung carcinoma, melanoma is considered a type of cancer that produces neo-antigens in high amounts [103, 104]. Also melanoma patients are known to respond much better to treatment with immune checkpoint inhibitors (ICIs) compared to patients suffering from lung cancer [103].

Overall, decreasing antigenicity is another strategy employed by tumour cells in order to escape immunosurveillance. One way in which cancers reduce their antigenicity is by reducing their MHC class I expression, subsequently limiting their T-lymphocyte mediated killing [105]. Another way cancer cells can decrease their antigenicity is by antigen escape. For example, residual malignant cells after CAR T cell treatment can express a modified version of the target antigen with changed extracellular epitopes that CAR T cells can no longer recognize [106, 107]. A different scenario regarding decreased tumour antigenicity involves downregulation of the target antigen expression on cell surface to levels that are inadequate for CAR T cell activation [107].

One immunotherapeutic approach attempting to increase the antigenicity of cancers cells is with the use of whole tumour cell vaccines, that are intended to generate a strong immune response against cancer-specific antigens [108, 109]. Based on the source of the used cancer cell, there are autologous and allogeneic whole tumour cell vaccines. Preparation of autologous whole tumour cell vaccines involve manipulation of patient's own cancer cells, while allogeneic whole tumour vaccines are produced from certain laboratory-grown cancer cell lines [110]. In both scenarios, the manufactured whole tumour vaccines are administered to the cancer patient and are expected to control

tumour progression by engaging the immunity of the recipient towards an anti-tumour immune response.

The upside of using the autologous cell vaccine approach is their ability to present the whole spectrum of patient-specific tumor antigens to the immune system and this is advantageous as it helps the formation of a strong anti-tumor immune response [111, 112]. However, the phenotype of cancer cells within a tumour is highly heterogeneous and an adequate amount of cells are required to produce autologous cell vaccines efficient in eliciting a broad anti-tumour immune response [113]. The disadvantage of using allogeneic cell vaccines is that tumor associated antigens (TAAs) and tumor specific antigens (TSAs) unique to one's cancer phenotype will not be targeted, however the availability of the biological material required for their production is not a limiting factor [114, 115].

Although the list of TAAs and TSAs is growing, targeting them still remains challenging. For instance, TAAs are self-antigens that preclude the development of robust T cell responses while TSAs are vulnerable to antigen downregulation and escape [107]. One employed strategy to induce tumour-specific immunity without antigen bias is to treat patients with irradiated autologous tumour vaccines, since they naturally express and present TAAs to APCs [116]. The irradiation process ensures safety of the vaccine by inhibiting the ability of the injected cancer cell vaccines to replicate and has been shown to induce release of immunogenic factors [117, 118].

Another strategy to generate efficient whole cancer cell vaccines is to increase the immunogenicity of a patient's cancer cells by encoding immune stimulatory cytokines through transduction. GVAX is an example of whole tumour cell vaccine that has been genetically altered to secrete granulocyte-macrophage colony-stimulating factor (GM-CSF), which is a cytokine that mediates recruitment of DCs and macrophages to the vaccine administration site. DCs are essential in the process of T cell priming, so GM-CSF secretion by tumour cells can improve the efficacy of the whole tumour cell vaccine. The efficacy of whole cell vaccines have been mostly explored in solid tumour models [119]. It has been shown that GVAX enhances DC activation that subsequently results in effective CD4 and CD8 T cell priming for tumour antigens [120].

It was shown that CML patients that received chemotherapy treatments and allogeneic whole tumour cell vaccines made from GM-CSF-expressing K562 leukemia cell lines had a smaller tumour burden compared to the CML patients treated with chemotherapy alone. [121-123].

Collectively, whole cell vaccines are a highly promising idea for cancer treatment and their efficacy in inducing robust anti-tumour immunity can potentially be improved when combined with other therapeutic approaches.

Immune response regulation and promising cancer immunotherapies

From everything that has been discussed so far, maintenance of cancer-specific T cell population and activation status is key to a successful extermination of the malignancy. Besides implementing treatments intended to enhance cancer adjuvanticity or antigenicity (for example, by using whole tumour cell vaccines), the use of immune checkpoint inhibitors as a strategy to overcome cancer-induced immunosuppression must be considered as well.

In an inflammatory state, activated APCs present foreign antigens on MHC class I or MHC class II to the TCR complex of the corresponding T cell subsets. However, the B7 co-stimulatory ligands expressed by activated APCs must simultaneously interact with the activating receptors CD28 to successfully prime a pathogen-specific T cell response. TCR signaling along with B7-CD28 interaction leads to the phosphorylation of the CD28 intracellular domain [124]. Phosphorylation of the CD28 intracellular subunit allows the recruitment of proteins like phosphoinositide 3-kinases (PI-3K) and growth factor receptor-bound protein 2 (GRB2) that mediate the downstream CD28 signaling [125]. Ultimately, this results in production of interleukin 12 (IL-12), interferon gamma (IFN-γ), tumor necrosis factor (TNF-α) as well as in expression of the cell cycle progression and pro-survival B-cell lymphoma-extra-large (Bcl-xL) gene and transcription factors involved in effector T cell functions [126-129]. However, long-lasting T cell activation could lead to chronic inflammation and T cells become exhausted by upregulating a wide range of non-redundant inhibitory receptors that limit their effectiveness, such as programmed cell death protein 1 (PD-1) and cytotoxic T-lymphocyte-associated protein 4 (CTLA-4) [130, 131]. Binding of these receptors to

their corresponding ligands on APCs could lead to a progressive loss of proliferative potential, effector functions and even to apoptosis of the activated T cells [132, 133].

One mechanism employed by T cells to minimize tissue damage due to prolonged immune stimulation is recruitment of the inhibitory PD-1 receptor to the immunological synapse. Engagement of PD-1 by its ligand PD-L1, whose expression increases with APC activation, leads to disruption of the TCR/CD28 signaling by inducing dephosphorylation of the intracellular domain of CD28 and other TCR complex molecules [134]. Therefore, the abrogated binding of PI3K and GRB2 to this receptor leads to a decrease in signaling pathways important for IL-2 production, survival, proliferation and maintenance of certain effector functions [135].

Another way T cell regulate the level of stimulation is by upregulating the inhibitory receptor CTLA-4 that disrupts the CD28-B7 co-stimulation cascade by binding B7 ligand molecules on APCs with a higher affinity than CD28 [136, 137]. Antigen presentation with no CD28-B7 co-stimulation is interpreted by the interacting T cells as "self", which ultimately renders them tolerant and non-responsive [138].

Immune checkpoint inhibitors in solid tumours versus AL

Even though signaling cascades induced by these inhibitory receptor/ligand interactions are naturally employed by our immune cells to prevent autoimmunity, certain cancers exploit these immune checkpoints to escape immune surveillance and continue persisting [139]. Thus, treating patients whose tumour cells employ this immune escape strategy with checkpoint inhibitors appears to be a promising immunotherapeutic approach. Among the most common checkpoint inhibitors, that were first approved by United States Food and Drug Administration (FDA) for treatment of solid tumours are Nivolumab (anti-PD-1), Pembrolizumab (anti-PD-1) and Ipilimumab (anti-CTLA-4) [140]. For example, it was shown that Nivolumab and Ipilimumab improved the survival of individuals with metastatic melanoma, squamous non-small cell lung cancer and renal cell carcinoma compared to patients that received standard chemotherapy treatment [141, 142]. Pembriolizumab was also initially used to treat metastatic melanoma as well as other metastatic solid tumours carrying specific mutations [143]. However, multiple recent pre-clinical and clinical studies revealed that

treatment with ICIs could also improve the outcome of the currently available leukemia treatments [144, 145].

Blockade of PD-1 in AL

The implication of the PD-1/PD-L1 axis as an immune evasion strategy by different types of leukemia was first assessed in pre-clinical models. For instance, one study showed that C1498 (a murine AML cell line) upregulates PD-L1 once administered IV to mice and that treatment of these animals with anti-PD-L1 monoclonal antibody reduced their tumour burden and significantly improved their survival [146]. Another research group showed that the survival of AML-bearing mice can be improved even further when treating with a combination of anti-PD-L1 blocking monoclonal antibody and T cell immunoglobulin and mucin domain-containing protein 3 (TIM-3) fusion protein [147]. It appears that C1498 cells drive CD8+ T cell exhaustion by triggering overexpression of PD-1 and TIM-3 on their surface [147]. The same research team determined that depletion of AML-associated regulatory T cells (Tregs) following PD-1/PD-L1 blockade leads to an impressive therapeutic outcome [148]. Interestingly, human AML cells collected from patients with relapsed disease were also highly expressing PD-L1 [149]. Furthermore, multi-color flow cytometry data collected on bone marrow (BM) samples of AML patients revealed high levels of PD-1 expression on T cell subsets [150], especially in cases relapsed disease after SCT [151].

Based on the accumulated pre-clinical data, the application of PD-1 inhibitors gained popularity in the clinic. For instance, one FDA-approved checkpoint inhibitor drug used to treat patients with classical Hodgkin's lymphoma is known as human IgG4 anti-PD-1 monoclonal antibody or nivolumab. It has been established that patient T cells upregulate PD-1 expression because of the demethylation of PD-1 gene promoter caused by 5-azacytidine [152], which is a standard drug used to treat older AML patients [153]. A phase II clinical trial involving 70 AML patients showed an encouraging response rate to nivolumab therapy in combination with 5-azacytidine treatment with 24% of patients achieving complete remission (CR) [154]. A follow-up clinical trial (NCT02397720) involves treatment of 14 patients with a combination of nivolumab, azacytidine and ipilimumab (a CTLA4-blocking antibody) and so far, 43% of the enrolled patients went into CR [154]. However, nivolumab therapy was shown to be unsuccessful for

individuals whose disease relapses after allo-SCT, considering that 2 out of 6 enrolled patients showed severe GVHD early after administration of the drug [155]. The efficacy of another PD-1 blockade drug known as pembrolizumab also showed modest improvement in the treatment outcome of patients with relapsed AML after allo-SCT [155]. Pembrolizumab was also involved in a phase II clinical trial (NCT02768792) in which AL patients were treated with high-doses of the chemotherapy drug cytarabine. The results of this study revealed a decent response rate to treatment and that 40-60% of the enrolled AML older patients achieved CR [156].

Blockade of CTLA-4 in AL

It has been demonstrated that treatment of human leukemia cell lines with anti-CTLA-4 enhances the frequency and cytotoxicity of AML-specific T cells [157] and that CTLA-4 blockade is highly effective at eliminating MRD in mice treated for leukemia [158]. Analysis of AML patient samples at diagnosis revealed that AML cells constitutively expressed CTLA-4 in 80% of the investigated samples [159]. High expression levels of CTLA-4 were also identified on T cell subsets of patients with T-cell lymphoma. [160]. Collectively, these findings outline the possibility that anti-CTLA-4 drugs could be highly successful in treating different types of leukemia.

Clinical trials involving treatment of relapsed AML with ipilimumab are currently in phase I/Ib trial [161]. However the safety of the drug and dose optimization is the main goal of this trial, it was observed that over 50% of enrolled patients had an extended survival of six months, also with four patients showing durable response for over a 1 year [161].

Overall, there is a massive amount of evidence that enhancing the adjuvanicity and antigenicity of cancer cells in context of whole tumour cell vaccines as well as the use of ICIs to reduce cancer-induced immunosuppression are all auspicious strategies for the future of cancer treatment. However more work needs to be done regarding the ways in which the upsides of these novel therapies can be combined and further improved.

Oncolytic viruses and their potential to enhance cancer adjuvanicity

Reports dating back a century ago linked the presence of viral infections with remissions in leukemia patients [162]. Eventually, research on oncolytic viruses (OVs)

gained popularity, involving manufacturing of viruses that preferentially target and lyse tumor cells to other normal tissues [163]. The field of OVs is rapidly evolving, with a 20-fold increase in publications in the last two decades [164].

Most OVs replicate preferentially in cancer cells due to defects in the interferon signalling pathway which is the primary cell intrinsic mechanism of fighting viral infection. This is typically initiated through PRRs binding to various viral components and triggering a phosphorylation cascade that leads to the activation of interferon regulatory factor 3 (IRF-3) and transcription of type I interferon and interferon stimulated genes (ISGs) [165]. Interferons (IFNs) are secreted soluble cytokines, with type I IFN being expressed by virtually all cell types in our body. Type I IFNs that are produced by infected cells signal nearby uninfected cells by binding to their ubiquitously-expressed receptor IFNAR, inducing an anti-viral state aimed to control viral proliferation [166]. Binding of IFNs to IFNAR triggers the Janus kinase (JAK) – signal transducer and activator of transcription (STAT) pathway, which further amplifies the signal and transcription of anti-viral ISGs [167]. It is important to note that although IRF-3 activation is the first step in anti-viral response, this role can be fulfilled by IRF-7 in immune cells in which it is constitutively expressed [168]. Aside from activating IRFs, PRRs like TLRs can also lead to nuclear factor kappa-light-chain-enhancer of activated B cells (NF-kB) activation [169].

Proliferation and hyperactive metabolism are a hallmark of cancer cells [170] with both of these states being suppressed by type I and II IFN signaling [171, 172]. This possibly explains why defects in various components of the IFN pathway are observed in several cancer types [173]. OVs are therefore engineered to be tumor-selective by being attenuated in their ability to counter IFN signaling. Therefore, OVs have the ability to enhance the adjuvanticity of certain cancers.

Oncolytic Rhabdoviruses

Two well-known rhabdoviruses currently used in the clinic are VSV and Maraba [174]. These viruses share a multitude of biological similarities, both having bullet-shaped enveloped virions with a negative-sense RNA and an 11 kb unsegmented genome [175]. The genome encodes for 5 viral proteins: nucleoprotein (N),

phosphoprotein (P), matrix protein (M), glucoprotein (G) and polymerase (L). Both viruses have been shown to infect a wide variety of mammalian hosts, including human cancer cells through the low density lipoprotein receptor (LDLR) clathrin-mediated endocytosis [176]. Inside the cell, L and P associate with N-coated genomic RNA to initiate the transcription of the first round of viral messenger RNAs [177]. Once translated, the newly produced VSV viral proteins initiate the replication of negative sense RNA genome into a positive sense intermediate [178]. It is at this stage that dsRNA forms between the negative and positive sense genomic moieties with the potential of activating RIG-I-like Receptors (RLRs) [179] and Protein Kinase RNA-activated (PKR) host anti-viral pathways [180]. This can be countered by the M protein which plays a major role in inhibiting host gene translation (such as those of IFNs) by blocking cytoplasmic transport of host mRNAs [181]. Finally, after genome replication and secondary gene transcription viral proteins and genome are assembled at the cellular membrane for budding off.

In the clinic, VSV is explored both as a vaccine platform and as an oncolytic virus. Notably, VSV has been undergoing Phase I through III clinical trials as an Ebola vaccine and has been shown to be a safe and immunogenic vector [182]. As an oncolytic in pre-clinical studies, VSV-based vectors have been employed in the treatment of various cancer types such as multiple myeloma [183] and AML [184]. The latter study also showed the ability of VSV to synergize with immune checkpoints inhibitors in AML. Another common VSV vector used in pre-clinical studies is VSV-d51, a VSV virus with a 51^{st} codon deletion in its M protein, showing a broad spectrum of activity in several tumor types [185]. Importantly, the VSV-d51 vector has been shown to be immunogenic in a cancer vaccine setting [186].

As a cancer clinical agent, VSV trials are being carried out mainly by the Mayo clinic with a viral backbone which encodes the type I IFN beta (IFN-β) cytokine. One such current trial employs VSV encoding both human IFN-β and a tumor associated antigen TYRP1 for the treatment of melanoma (NCT03865212). Similarly, to VSV, Maraba-based vector MG1 has also shown to be immunogenic in a pre-clinical cancer vaccine model [187, 188]. This in turn has prompted the use of MG1 in the clinic for a

heterologous prime-boost Phase I/Ib clinical trial against human papilloma virus (HPV) E6E7 cancer antigen (NCT03618953).

Infected Cell Vaccines (ICV) – Generating an *in vivo* autologous cell vaccine

There are several features of OVs which make them efficacious as cancer cell therapeutics. Two such important features are selectivity of OVs to cancer cells and their ability to stimulate the immune system [188]. However, despite several advantages there are still certain barriers to OVs efficacy. One such barrier is the immunogenicity of OVs acting as a "double edge sword". On one hand, OVs immunogenicity is important in leading to a proper anti-tumor immune response while on the other hand, host anti-viral response can limit OVs spread and replication, thus reducing their effect [189]. The second barrier is OV delivery to the tumor microenvironment. The most efficient method of delivery is intra-tumoral (IT) injection as high doses of viruses can be directly delivered to the tumor. This method, however, is only available in certain cancer types and is not always clinically practical. Another method of delivery is systemic intravenous (IV) delivery. This results in fewer viral particles reaching the tumor microenvironment and is not practical for OVs for which neutralizing antibodies exist in the general population (for example, HSV and Measles virus).

Another advantage of OVs is their ability to trigger an immunogenic response in the tumor microenvironment, leading to the recruitment of immune cells and development of anti-tumor immunity [188]. Furthermore, OVs like HSV, VSV and VacV have been shown to effectively synergize with immune checkpoint blockade in otherwise unresponsive tumors [190-193].

More recently, our group has shown that the immunogenic features of OVs enhance the success of whole tumor cell vaccines [186, 194]. This implies that autologous infected (cancer) cell vaccines (ICVs) combine the advantages of whole cell vaccines and OV immunotherapeutic strategies to generate a more effective cancer treatment option by inducing strong and long-lasting anti-tumour immunity. The idea behind this approach is to enhance the immunogenicity of cancer cells carrying TSAs by infecting them with virus prior to their administration as a cancer cell vaccine. In this sense, this particular form of immunotherapy has the potential to enhance both the

antigenicity and adjuvanicity of cancer cells and promote effective anti-cancer immunity.

In a clinical setting, autologous ICVs are prepared by harvesting a patient's own cancer cells, infecting them *ex vivo* with OVs followed by irradiation. It has been shown that patients treated with ICVs prepared by infecting their own melanoma cells with New Castle Disease Virus (NDV) showed a significant improvement in the 10-year death-free survival [195].

The protective effect of ICV was also shown in pre-clinical studies involving solid cancer models. In particular, it was demonstrated that 30% of mice that were pre-immunized with ICVs prepared by infecting murine colon cancer cells with VSV were protected from following challenges with viable colon cancer cells [186]. Interestingly, close to 95% of mice that were pre-treated with ICV in which the autologous colon cancer cells were engineered to secrete GM-CSF were protected from subsequent challenges [186].

Development of ICV for AL

Our lab is particularly interested in developing an ICV platform in context of leukemia to eventually provide personalized treatment for AL patients by administering autologous MG1-infected leukemia cell vaccines. In our laboratory, the leukemia ICV platform was studied in two syngeneic murine models. Namely, the vaccines were produced by infecting murine AL (L1210 or C1498 cells) with rhabdovirus followed by irradiation. The initial study identified several factors that are key to ICV success in the L1210 model. First, L1210 cells needed to be infected for a certain period of time *in vitro* prior to vaccination, as co-delivery of L1210 irradiated cells and virus had reduced efficacy. This may suggest that L1210's anti-viral response has a role in making the vaccine immunogenic. Secondly, the vaccine worked equally well when using a non-replicating rhabdo-virus (VSV G-less), suggesting viral spread is trivial to the ICV. However, TLR agonists like polyinosinic-polycytidylic acid (poly:IC) and lipopolysaccharides (LPS) failed to make the vaccine immunogenic, suggesting that the virus stimulates a different pathway. Lastly, it was important for L1210-ICV to be viable

at the time of vaccination, as necrotic or apoptotic cells failed to confer protection against L1210 challenge.

The optimal regiment for L1210 vaccination was shown to be three doses of ICV delivered systemically via the tail-vein of naïve DBA/2 mice (L1210-ICV). The ability of these vaccines to develop protective immunity in either of these syngeneic models was assessed by challenging the pre-immunized animals with viable L1210 cells and monitoring their wellness and survival.

It has been previously shown that pre-immunization with L1210-ICV protects over 90% of vaccinated mice from a following challenge with murine ALL compared to 100% mortality of the animals that did not receive prior immunization [196]. Furthermore, our preliminary data shows that the protective effects of the L1210-ICV rely on T cell responses, considering the fact that L1210-ICV was unable to protect athymic DBA/2 mice after ALL challenge [196].

Developing the ICV as a platform for treating AL patients is our long term goal and it is absolutely essential, at this point, to learn more about the mechanism(s) by which leukemia ICV induces anti-tumour immunity. For example, previous experiments suggest that L1210 vaccinations involve a T-cell mediated immune response. This was shown through the use of T-cell deficient mice [196]. However, adoptive T-cell transfer from immunized mice was insufficient to confer resistance to L1210 challenge, suggesting involvement of other immune components during vaccination [197].

Although studying the L1210-ICV-induced anti-tumour immunity is one of our main priorities, we also intend to characterize the efficacy of ICV in context of syngeneic murine AML model (C1498) that has not yet been addressed.

Thesis rationale and Objectives

Rationale

Our preliminary data suggests that ICVs in context of murine leukemia models differ in their ability to initiate anti-tumor immune response and overall effectiveness. While, the vast majority of mice pre-treated with L1210-ICV do not succumb to systemic leukemia when challenged with viable L1210 cells, pre-immunization with C1498-ICV is much less effective following challenge with viable C1498 cells. We believe that tumor models in which ICV successfully induces strong anti-tumor immunity possess immunogenic features, namely antigenicity and adjuvanicity. Lack of these or presence of immune-suppressing factors may prevent ICV from inducing long lasting anti-tumor immune response. Therefore, I will study these parameters, namely antigenicity, adjuvanicity and immune-suppressing factors in two murine leukemia models in which ICVs varies in their efficacy.

Objectives

The overall objective of my thesis is to characterize the immunogenic properties of rhabdoviral-infected autologous leukemia cell vaccine (ICV) which contribute to the variable responses observed in murine models of acute lymphoblastic (L1210) and myeloid (C1498) leukemia. I define ICV efficacy as the ability of vaccination to induce a cancer-specific immune response, which allows mice to reject the challenge of viable tumor cells. Further to this, I believe that one strategy to improve the efficacy of a vaccine is to enhance the adjuvanicity and antigenicity of leukemia cells using ICV. Lastly, I will investigate immune-suppressing factors such as immune checkpoints and their contribution to ICV efficacy

To achieve this goal I sought to investigate and compare:

- Viability versus efficacy of the ICV administered *in vivo* for prophylactic immunization treatments. Decreased viability may affect availability of antigen and therefore affect antigenicity.

- Antiviral immune response of L1210 and C1498 cells, as these could induce secretion of activating cytokines and chemokines which increase adjuvanicity.

- MHC expression of cancer cells before and after infection. Previously, virus infection has been shown to increase MHC antigen presentation increasing antigenicity.
- Presence or absence of immune-suppressing factors in both leukemia models and their impact on antigenicity.
- *In vivo* phenotypes of important immune populations such as DCs (antigen presenting) and T cells (drivers of adaptive response) after ICV administration.

Chapter 2 – Materials and Methods

2.1 Murine leukemia cell lines

L1210 (Cat#: CCL-219) murine cell line that has been derived from ascites of an 8-month-old female DBA/2 mouse strain in R. B. Jackson Memorial Laboratory [198] and C1498 (Cat#: TIB-49) murine cell line that originated spontaneously in a 10 month old female C57BL/6 (H-2^b) mouse strain [199] were obtained from American Type Culture Collection (ATCC). Both cell lines were maintained in suspension culture in Roswell Park Memorial Institute (RPMI) 1640 media supplemented with 10% fetal bovine serum (FBS) at 37°C and 5% CO_2. Leukemia cells were split every 4 days, maintaining their concentration between 1.0 to 2.0 $\times$ 10^6 cells/mL. The Vero cell line obtained from ATCC was maintained in an adherent cell culture in Dulbecco's Modified Eagle Medium (DMEM)-high glucose (HyClone) with 10% FBS. Vero cells were used for propagation, enumeration and manufacturing of virus infections particles.

2.2 Mouse *in vivo* work

DBA/2 and C57BL/6 mice were purchased from Charles River Laboratories and housed in a biosafety unit at the University of Ottawa (Ottawa, ON, Canada), accredited by the Canadian Council on Animal Care (CCAC). Institutional guidelines and review board for animal care (The Animal Care and Veterinary Service of the University of Ottawa) approved all animal studies. All mice used in these experiments were from 6 to 8 weeks of age.

2.3 Viruses

The rhabdoviruses, MG1 and VSVd51 were propagated in Vero cells and purified as previously described [200]. MG1-eGFP virus that was genetically engineered to express the enhanced Green Fluorescent Protein (eGFP) gene, was grown and purified in the same way. The enumeration of infectious particles was conducted as previously described [201]. Suspension cultures of murine leukemic cells were infected by adding virus preparations directly to the culture media (1 $\times$ 10^6 cells/mL) at a multiplicity of infection (MOI) of 10, unless specified otherwise.

2.4 Leukemia Infected Cell Vaccine (ICV) preparation

The number and viability of cultured L1210 or C1498 cells was determined using VI-Cell XR cell counter (Beckman Coulter) that distinguishes the dead cells from the live cells by assessing the cell membrane integrity using trypan blue staining. L1210 or C1498 cells were resuspended at 1×10^6 live cells/ml in RPMI 1640 media containing 10% FBS. Cells were infected with either MG1 or VSVd51 at a MOI of 10. The infected L1210 or C1498 cells were maintained at 37^0C in a humidified (5% CO_2) incubator for 6 to 18 hours as indicated for each experiment. Following infection for the indicated time periods, the cells were isolated from the media by centrifugation at 1500 RPM, 4°C for 5 minutes. The cell pellet was washed once by re-suspending it in 10 ml of Phosphate-Buffered Saline (PBS), followed by centrifugation at 1500 RPM, 4°C for 5 minutes and aspiration of the supernatant. Lastly, the infected cells were re-suspended at a final concentration of 1×10^7 cells/mL in PBS and irradiated at 30-Gy (γ-IR; HF-320; Pantak) before IV injection.

2.5 Vaccine administration and challenge

L1210-ICV or C1498-ICV (1×10^6 cells/100 µL PBS per mouse per dose) were administered intravenously via tail vein injections in either DBA/2 or C57BL/6 mice respectively. Some experimental control groups were injected with uninfected but irradiated L1210 or C1498 cells or PBS. Two distinct dosing schemes were used to assess vaccine efficacy. Naïve mice received 3 vaccine doses administered once every 7 days for 3 weeks prior to an IV challenge with 1×10^6 viable L1210 or C1498 cells re-suspended in 100 µL of PBS. The wellness of the leukemia bearing animals was closely monitored after being challenged with viable leukemia cells. Mice were euthanized upon development of predetermined signs of advanced leukemia, namely hind leg paralysis, formation of peritoneal and/or subcutaneous tumours or lack of responsiveness to external stimuli.

2.6 Murine spleen collection and processing

Spleens from either naïve or treated DBA/2 or C57BL/6 mice were harvested and mechanically dissociated in 1 ml of cRPMI media. Large aggregates were removed

by passing the cell suspensions through a 70 µm filter (Corning) along with 5 ml of PBS used to wash the vessel in which the spleens were disintegrated. The filters themselves were washed with another 5 ml of PBS and the samples was spun down at 500g for 5 minutes at 4°C. The cell pellet for each spleen sample was resuspended in 2 ml of ammonium-chloride-potassium buffer (ACK) for 3 minutes, following addition of 8 ml of PBS to stop the RBC lysing reaction. After pelleting down the cells (500g, 5 minutes at 4°C), the number of cells was counted using VI-Cell XR viability analyzer (Beckman Coulter), following the resuspension of cells at the concentration of 1×10^7 viable spleenocytes/ml. For each staining condition for flow cytometry, 100 µl of the resulting resuspensions (1×10^6 cells) were transferred per well of V-bottom 96-well plates (Corning).

2.7 Murine saphenous blood collection and processing

About 200 µl of blood was collected from C57BL/6 mice into heparinized tubes after making a puncture in the vein of one of the hind legs. The blood samples were incubated twice in 2 ml of ACK lysis buffer for 5 minutes on ice, following the addition of 2 ml of PBS to stop the RBC lysing reaction. The supernatant was removed carefully after each wash (1500 RPM for 5 minutes at 4°C) and the peripheral blood mononuclear cells (PBMCs) obtained from each mouse were resuspended in 100-150 µl of cRPMI.

2.8 Flow cytometry

2.8.1 *In vitro* infectivity and viability experiments

L1210 and/or C1498 cells were infected as outlined above with MG1-eGFP at MOI of 0.1, 1 and 10 for 17 hours or infected with MG1-eGFP at MOI of 10 for 4, 5, 7 and 17 hours. The infected leukemia cells were washed once with 10 ml of PBS (1500 RPM, 5 minutes), resuspended in either 500 µl or 600 µl of PBS and irradiated with 30-Gy. Each sample was stained with 5 µl of 1:500 diluted propidium iodide (PI) viability dye (Cat#: E1169, ThermoFisher) and the intensity of the GFP and PI signal were immediately acquired on either BD LSR Fortessa or BD Celesta from the Flow

Cytometry and Virometry core facility, University of Ottawa. Data was analyzed using FlowJo software. To determine the amount of infected and life cells, we first gated out cell debris (FSC-A vs SSC-A) and doublets (FSC-A vs FSC-H). The uninfected (MOCK) samples were used to set the gates for PI+ and/or GFP+ signals. The gating strategy is shown for a representative C1498 sample after an 18 hour-long infection with MG1-eGFP at MOI of 10 in **Supplementary Figure 1**.

2.8.2 MHC class I expression on murine leukemia cell lines

1×10^6 L1210 and/or C1498 cells were stimulated with 50U or 100U of IFN-ɣ (Cat#: 315-05, PeproTech) or left untreated for 16 hours in 2 mL of cRPMI at 37°C, 5% CO_2. The cells were washed once in 10 ml of PBS (1500 RPM, 5 minutes) and each sample was incubated in 10 µl of diluted (1:20, in PBS) FVS510 viability dye (Cat#: 564406, BD Biosciences) for 20 minutes in a dark place at RT. After washing the cells with 190 µl of PBS (1500 RPM, 5 minutes), they were incubated in 25 µl of diluted (1:100, in FACS buffer) Rat Anti-mouse CD16/CD32 (Cat#: 553142, BD Biosciences) solution for 15 minutes at 4°C in the dark. Next, the cells were washed with 175 µl of FACS buffer (1500 RPM, 5 minutes) and stained with 25 µl of diluted (1:100, in FACS buffer) MHC class I (H2Db) – FITC monoclonal antibody (ThermoFisher Scientific) for 25 minutes in the dark at 4°C. The samples were fixed in 200 µl of 1% paraformaldehyde (PFA) and ran through the BD LSR Fortessa from the Flow Cytometry and Virometry core facility, University of Ottawa. The MHC class I positive cells were identified after eliminating the doublets (FSC-A vs FSC-H), cell debris (FSC-A vs SSC-A) and dead cells (FSC-A vs BV510 positive). Data analysis and our gating strategy is shown for a representative C1498 sample that was stimulated with 50U of IFN-ɣ and stained with an isotype control antibody (**Supplementary Figure 2**). The unstimulated L1210 and C1498 samples, as well as the samples that were stained with an isotype control, were used to set the gates for MHC class I+ cells.

2.8.3 MHC class II, CD86 and CD40 expression on murine leukemia cell lines

L1210 and C1498 cells were uninfected or infected with MG1 virus at MOI of 10 for 5 and/or 17 hours in cRPMI at 37°C, 5% CO_2. The infected leukemia cells were washed once with 10 ml of PBS (1500 RPM, 5 minutes), resuspended in 100 µl of PBS

and irradiated for 30-Gy. Each sample was stained with 10 µl of diluted (1:20, in PBS) FVS510 viability dye (Cat#: 564406, BD Biosciences) for 20 minutes in a dark place at RT. After washing the cells with 190 µl of PBS (1500 RPM, 5 minutes), they were incubated in 25 µl of diluted (1:100, in FACS buffer) Rat Anti-mouse CD16/CD32 (Cat#: 553142, BD Biosciences) solution for 15 minutes at 4°C in the dark. Next, each sample was washed with 175 µl of FACS buffer (1500 RPM, 5 minutes) and incubated in 25 µl of a master mix in which MHC II-PerCP-Cy5.5 (BD Biosciences), CD86-APC-Cy7 (BioLegend) and CD40-PE-CF594 (BD Biosciences) monoclonal antibodies that were diluted 1:100 in FACS buffer. After 25 minutes of incubation at 4°C in the dark, each sample was washed with 175 µl of FACS buffer (1500 RPM, 5 minutes) and fixed in 200 µl of 1% PFA. The data was acquired using the BD LSR Fortessa from the Flow Cytometry and Virometry core facility, University of Ottawa. The MHC II+, CD86+ and CD40+ leukemia cells were identified after eliminating cell debris (FSC-A vs SSC-A), doublets (FSC-A vs FSC-H) and dead cells (FSC-A vs BV510 positive). FlowJo software was used for data analysis and our gating strategy is shown for a L1210 sample infected with MG1 for 18 hours (**Supplementary Figure 3**). Fluorescence minus one (FMO) L1210 and C1498 samples for each marker were used to set the positive gates for MHC II, CD86 and CD40.

2.8.4 PD-1 and PD-L1 expression on murine leukemia cell lines

L1210 and C1498 cells were uninfected or infected with MG1 virus at MOI of 10 for 18 hours in cRPMI at 37°C, 5% CO_2. The infected leukemia cells were washed once with 10 ml of PBS (1500 RPM, 5 minutes) and resuspended in 100 µl (per 1×10^6 cells). Each sample was stained with 50 µl of diluted (1:165, in PBS) FVS510 viability dye (Cat#: 564406, BD Biosciences) for 20 minutes in a dark place at RT. After washing the cells with 100 µl of PBS (1500 RPM, 5 minutes), they were incubated in 25 µl of diluted (1:100, in FACS buffer) Rat Anti-mouse CD16/CD32 (Cat#: 553142, BD Biosciences) solution for 5 minutes at 4°C in the dark. Next, samples were stained with PD-1 (BD Biosciences) and PD-L1 (BD Biosciences) monoclonal antibodies, both diluted (1:100) in Brilliant stain buffer (Cat#: 563794, BD Biosciences) with a total staining volume of 25 µl. After 25 minutes of incubation at 4°C in the dark, each sample was washed in 150 µl of FACS buffer (1500 RPM, 5 minutes) and fixed in 200 µl of 1%

PFA. The data was acquired using the BD LSR Fortessa from the Flow Cytometry and Virometry core facility, University of Ottawa. The PD-1+ and PD-L1+ leukemia cells were identified after eliminating cell debris (FSC-A vs SSC-A), doublets (FSC-A vs FSC-H) and dead cells (FSC-A vs BV510 positive). FlowJo software was used for data analysis and our gating strategy is shown for a L1210 sample infected with MG1 for 18 hours (**Supplementary Figure 4**). FMO samples for both L1210 and C1498 cell lines were used for each marker to set the positive gates for PD-1 and PD-L1.

2.8.5 Maturation and activation of splenic cDCs and T cell subsets *in vivo*

Naïve DBA/2 or C57BL6 mice were either unimmunized or immunized with one dose of L1210-ICV or C1498-ICV respectively. The preparation of the corresponding ICVs *in vitro* is described in the paragraph 2.4 of the Materials and Methods section. After 1, 4, 24 and 72 hours since immunization, the spleens were harvested and processed as described in the paragraph 2.6 of the Materials and Methods section. 1×10^6 spleenocytes of each mouse were seeded in two different V-bottom 96-well plates which were spun down at 500g for 5 minutes and stained with diluted (1:165, in PBS) FVS510 viability dye (Cat#: 564406, BD Biosciences) for 25 minutes at 4°C in the dark. The samples were washed once with 150 µl of PBS (500g, 5 minutes) and incubated in 50 µl of diluted (1:100, in FACS buffer) Rat Anti-mouse CD16/CD32 (Cat#: 553142, BD Biosciences) solution for 15 minutes at 4°C in the dark. Next, each sample was washed with 150 µl of FACS buffer (500g, 5 minutes). Samples from one of the V-bottom 96-well plate were resuspended in 25 µl of a master mix in which MHC II-FITC (BD Biosciences), CD11c-PE (BD Biosciences), CD103-BV421 (BD Biosciences), CD11b-APC-Cy7 (BD Biosciences), CD40-BV784 (BD Biosciences), CD86-APC (BD Biosciences) and/or CD70-APC (BD Biosciences), CD19-PE-Cy7 (Thermo Fisher Scientific), GR1-PE-Cy7 (BioLegend), CD3e-PE-Cy7 (Thermo Fisher Scientific) and F4/80-PE-Cy7 (BioLegend) monoclonal antibodies were diluted 1:100 in FACS buffer. Samples from another V-bottom 96-well plate were resuspended in 25 µl of a master mix in which CD3e-PE-Cy7 (Thermo Fisher Scientific), CD8α-PerCP-Cy 5.5 (BD Biosciences), CD28-BV786 (BD Biosciences), CD40L-APC (BioLegend), CD69-FITC (Thermo Fisher Scientific) and CD137-PE (BD Biosciences) monoclonal antibodies

were diluted 1:100 in FACS buffer. Both plates were stained for DC and T cell markers respectively for 25 minutes at 4°C in the dark. Each sample was washed with 175 µl of FACS buffer (500g, 5 minutes) and fixed in 200 µl of 1% PFA. The samples stained for DC and T cell markers were acquired using the BD LSR Fortessa from the Flow Cytometry and Virometry core facility, University of Ottawa. The cell debris (FSC-A vs SSC-A), doublets (FSC-A vs FSC-H) and dead cells (FSC-A vs BV510 positive) were eliminated from each samples in both flow panels. The cDC population was identified in the first panel as MHC II ^{high}, CD11c ^{high}, from which the cDC1 and cDC2 subsets were identified as CD103+, CD11b- and CD103-, CD11b+ respectively. The expression of CD40 and/or CD70 and CD86 were determined for individual cDC subsets or for the cDC population as a whole. The CD8+ and CD4+ T cell subsets were identified in the second panel as CD3e+, CD8α+ and CD3+, CD8α- respectively. The expression of CD28, CD40L, CD69 and CD137 was then determined individually for both T cell subsets. FlowJo software was used for data analysis and our gating strategies for cDC and T cell panels are shown for an immunized DBA/2 mouse sample after 1 hour since vaccination in **Supplementary Figures 5**. FMO controls for corresponding markers were used to set the gates for the expression of CD40, CD70 and/or CD86 as well as CD28, CD40L, CD69 and CD137.

2.8.6 Intracellular staining (ICS) for IFN-ɣ and TNF-α in CD8α+ T cells

Naïve C57BL/6 mice were either unimmunized or immunized with one dose (1×10^6 cells per mouse in 100 µl of PBS) of either irradiated C1498 cells or C1498-ICV infected with VSVd51 for 5 or 17 hours. The complete process of vaccine preparation is described in the paragraph 2.4 of the Materials and Methods section. Saphenous bleed of one of the hind legs was performed on all unimmunized and immunized animals 7 days since vaccination. After processing the blood samples, as described in the paragraph 2.7 of the Materials and Methods section, the PBMCs of each mouse were resuspended in 50 µl of cRPMI. Every sample was then incubated in 50 µl of diluted (1:250, in cRPMI) GolgiPlug (Cat#: 554715, BD Biosciences) solution for 5 hours at 37°C, 5% CO_2. The cells were then washed twice with 100-200 µl of PBS (500g for 5 minutes at 4°C) and stained with diluted (1:165, in PBS) FVS510 viability dye (Cat#: 564406, BD Biosciences,) for 25 minutes at 4°C in the dark. The samples were washed once with 150

µl of PBS (500g, 5 minutes at 4°C) and incubated in 50 µl of diluted (1:100, in FACS buffer) Rat Anti-mouse CD16/CD32 solution (Cat#: 553142, BD Biosciences) for 15 minutes the dark on ice. After washing each cell pellet with 150 µl of FACS buffer (500g for 5 minutes at 4°C), each sample was stained for extracellular markers using 25 µl of a master mix in which CD3e-AF700 (BD Biosciences) and CD8α-PE-CF594 (BD Biosciences) monoclonal antibodies were diluted 1:100 in FACS buffer. After 30 minutes of incubation at 4°C in the dark, each sample was washed in 150 µl of FACS buffer (500g for 5 minutes at 4°C) and resuspended in 100 µl of Cytofix/Cytoperm (Cat#: 554715, BD Biosciences) solution for 20 minutes at 4°C in the dark. The cells were washed twice (500g for 5 minutes at 4°C) with 100-200 µl of Perm/Wash buffer (Cat#: 554715, BD Biosciences) diluted to 1X and stained for intracellular markers using 25 µl of a master mix in which IFN-ɣ-APC (ThermoFisher Scientific) and TNF-α-PE-Cy7 (BD Biosciences) monoclonal antibodies were diluted 1:100 in 1X Perm/Wash buffer. After washing the stained PBMCs with 100-200 µl of 1X Perm/Wash buffer, the cells were fixed in 200 µl of 1% PFA. The data was acquired using the BD LSR Fortessa from the Flow Cytometry and Virometry core facility, University of Ottawa. Cell debris (FSC-A vs SSC-A), doublets (FSC-A vs FSC-H) and dead cells (FSC-A vs BV510 positive) were first eliminated in our analysis. The CD8+ and CD4+ T cell subsets were then identified from the live cell population as CD3e+, CD8α+ and CD3+, CD8α- respectively. The expression of IFN-ɣ and TNF-α was then assessed individually on each T cell subset population. Data analysis was performed using FlowJo software and our gating strategy for identifying T cells producing IFN-ɣ and TNF-α is shown for a C1498-ICV-6h immunized mouse sample in **Supplementary Figure 6**. The gates for IFN-ɣ+ and TNF-α+ T cells were established considering the FMO samples for the corresponding markers.

Table 2.1: The summarized list of the flow cytometry antibodies used in the *in vitro* and *in vivo* experiments

Species	Reactivity	Target	Fluorophore	Clone	Company	Catalogue #
Mouse	Mouse	MHC I	FITC	28-14-8	Thermo Fisher Scientific	11-5999-82
Rat	Mouse	MHC II	PerCP-Cy 5.5	M5/114	BD Biosciences	562363
Rat	Mouse	CD86	APC-Cy7	CL-1	BioLegend	105029
Rat	Mouse	CD40	PE-CF594	3/23	BD Biosciences	562847
Hamster	Mouse	PD-1	BV421	J43	BD Biosciences	565942
Rat	Mouse	PD-L1	BV786	MIH5	BD Biosciences	741014
Rat	Mouse	MHCII	FITC	2G9	BD Biosciences	562009
Hamster	Mouse	CD11c	PE	HL3	BD Biosciences	561044
Rat	Mouse	CD103	BV421	M290	BD Bioscience	562771
Rat	Mouse	CD11b	APC-Cy7	M1/70	BD Biosciences	561039
Rat	Mouse	CD40	BV786	23-Mar	BD Biosciences	740891
Rat	Mouse	CD86	APC	GL1	BD Biosciences	561964

Rat	Mouse	CD70	APC	FR70	BD Biosciences	563634
Rat	Mouse	CD19	PE-Cy7	1D3	Thermo Fisher Scientific	25-0193-81
Rat	Mouse	GR-1	PE-Cy7	RB6-8C5		108416
Armenian hamster	Mouse	CD3e	PE-Cy7	145-2C11	Thermo Fisher Scientific	25-0031-82
Rat	Mouse	F4/80	PE-Cy7	BM8	BioLegend	123113
Rat	Mouse	CD8α	PerCP-Cy 5.5	53-6.7	BD Biosciences	561109
Hamster	Mouse	CD28	BV786	37.51	BD Biosciences	740859
Armenian Hamster	Mouse	CD40L	APC	MR1	BioLegend	106510
Armenian Hamster	Mouse	CD69	FITC	H1.2F3	Thermo Fisher Scientific	11-0691-82
Rat	Mouse	CD137	PE	1AH2	BD Biosciences	558975
Hamster	Mouse	CD3e	AF700	500A2	BD Biosciences	557984
Rat	Mouse	CD8α	PE-CF594	53-6.7	BD Biosciences	562283
Rat	Mouse	IFN-ɣ	APC	XMG1.2	Thermo Fisher Scientific	17-7311-82
Rat	Mouse	TNF-α	PE-Cy7	MP6XT22	BD Biosciences	557644

2.9 RNA sequencing and analysis

L1210 and C1498 cells were infected with MG1 virus at MOI of 10 for 18 hours. The infected and uninfected leukemia cells were lysed with RLP buffer supplemented with 2-Mercaptoethanol (1% v/v). Lysates were processed through a QIAshredder column (Qiagen, Cat #: 79654) to prevent DNA binding to the column. RNA was extracted using the RNeasy Mini kit (Qiagen, Cat # 74104) according to the manufacturer's protocol. About 1 µg of RNA was sent to FASTERIS for Illumina HiSeq 4000 paired-end 150bp read sequencing. The adaptor sequences were removed from the fastq files with Trimmomatic. The trimmed reads were then mapped to the latest assembled mouse genome using HISAT2. Relative mRNA levels of annotated protein-coding genes were estimated as transcripts per million (TPM) using StringTie. The fold change between uninfected and infected samples was calculated by adding pseudoTPM values of 1 to all genes to avoid possible division by zero operations. Data was processed using the R statistical software and displayed as a heatmap using the heatmap package developed by Raivo Kolde.

2.10 Mouse IFN-β ELISA

L1210 and C1498 cells were plated at a density of 1×10^6 cells per 1 ml of RPMI and infected with MG1 at MOI of 10 for 18 hours. The supernatants from MG1-infected as well as uninfected L1210 and C1498 cells were collected by centrifuging the cells at 1500 RPM for 5 minutes. The supernatants were stored at -20°C. Mouse IFN-β Quanikine ELISA kit (R&D systems – Catalog #: MIFNB0) was performed according to the manufacturer's instruction to quantify IFN-β secretion. Briefly, 50 µl of supernatant collected from infected and uninfected leukemia cells were incubated for 2 hours at room temperature (RT) with 50 µl of Assay Diluent RD1W. After incubation, 100 µl of mouse IFN-β Conjugate was added to all samples followed by a 2 hour-long incubation at RT. Each sample was incubated for 30 minutes in 100 µl of Substrate Solution. Lastly, the reaction was stopped by adding 100 µl of Stop Solution to each well. The ELISA plate absorbance was read immediately at 450nm wavelength.

2.11 Mouse TNFα ELISA

L1210 and C1498 cells were plated at a density of 1 x 10^6 cells per 1 ml of RPMI and infected with MG1 at MOI of 10 for 18 hours. The supernatants from MG1-infected as well as uninfected L1210 and C1498 cells were collected by centrifuging the cells at 1500 RPM for 5 minutes. The supernatants were stored at -20°C. Mouse TNF-α Quanikine ELISA kit (R&D systems – Catalog #: MTA00B) was performed according to the manufacturer's instruction to quantify TNF-α secretion. Briefly, 50 µl of supernatant collected from infected and uninfected leukemia cells were incubated for 2 hours at RT with 50 µl of Assay Diluent RD1-63. After incubation, 100 µl of Mouse TNF-α Conjugate was added to all samples followed by a 2 hour-long incubation at RT. Each sample was incubated for 30 minutes in 100 µl of Substrate Solution at RT. Lastly, the reaction was stopped by adding 100 µl of Stop Solution to each well. The ELISA plate absorbance was read immediately at 450nm wavelength.

2.12 Milliplex cytokine array

L1210 and C1498 cells were resuspended at the concentration of 1 ^{x} 10^6 cells per 1 ml of RPMI media and infected with MG1 at MOI of 10 for 18 hours. Some infected and uninfected samples received 30-Gy ɣ-radiation. The supernatants from infected and uninfected cells were collected by centrifuging them at 1500 RPM for 5 minutes. The supernatants were aliquoted and stored at -80°C. The concentration of cytokines (IL-6, IL-12, MCP-1, MIP-1b, TNF-α, IFN-ɣ, GM-CSF and RANTES) in the collected supernatants was measured by performing the Milliplex Map Kit (EMD Millipore – Cat#: MCYTOMAG-70K) according to the manufacturer's protocol. Briefly, 25 µl of supernatant was incubated for 16-18 hours at 4°C with 25 µl of Mixed Beads. 25 µl of Detection Antibody solution was added to each well followed by a 1 hour-long incubation at RT. Lastly, 25 µl of Streptavidin-Phycoerythrin reagent was added to each well containing the previously added Detection Antibody, following an additional 30 minutes incubation at RT. The samples were resuspended in Sheath Fluid and the plate was run on Luminex 200, HTS, MAGPIX.

2.13 Statistical analysis

Statistical analyses were done using GraphPad Prism software. For the survival experiments, Mantel-cox (Logrank) tests were performed to determine differences among experimental groups. For the results regarding ELISA experiments measuring differences in IFN-β and TNF-α production in CT26-LacZ, L1210 and C1498 cell lines before and after MG1 infection *in vitro*, a two-way ANOVA was performed. For the experiments measuring the *in vivo* DC and T cell activation status following immunization with L1210-ICV or C1498-ICV, non-parametric, unpaired t tests were performed (assuming the populations have the same standard deviation) to determine differences in the expression of activation/maturation markers compared to the "no treatment group". The p values are represented as not significant (ns), *<0.05, ***<0.005 and ****<0.0005.

Chapter 3 – Results

Preface

This chapter outlines the results of my MSc research. The work described in this chapter was already underway when I started my MSc in Dr. Natasha Kekre's and Dr. Rebecca Auer's lab. Dr. Mike Kennedy and Holly Dempster were pivotal in helping me get started on these experiments.

I have participated in all experiments and have done the majority of the work for all the results listed in this chapter. Dr. Mike Kennedy, Leonard Angka, Katherine Baxter and Fanny Tzelepis helped me grasp flow cytometry and were occasionally present while I was running samples from my first experiments. Julia Petryk and Christiano Tanese de Souza helped me with all *in vivo* experiments, especially intravenous injections. Adrian Pelin has provided the RNA-sequencing data and analysis for the mouse cancer cell lines.

Assessing the protective effect of ICV against murine ALL

It has been shown that over 90% of mice that were pre-immunized with 3 weekly doses of L1210-ICV before being challenged with live, uninfected leukemia cells were protected from leukemic disease [196]. This implies that L1210-ICV pre-treatments established a robust immune response against this type of leukemia. Before moving forward to study the mechanism employed by L1210-ICV in generating an immune response against leukemia, I sought to ensure that I could reproduce these results.

For this purpose, naïve DBA/2 mice were either immunized with 3 weekly doses of L1210-ICV-18h or remained unimmunized. To assess the contribution of the virus infection to vaccine immunogenicity and treatment efficacy, we included a group of mice that received 3 weekly doses of uninfected but irradiated L1210 cells. One week since the third immunization, all animals were challenged with viable L1210 cells and survival was monitored. The outline and the treatment schedule is summarized in **Figure 3.1A**.

Consistent with Conrad *et al*., unimmunized mice succumbed to leukemia with the median survival of 29 days [196]. Our data shows that 60% of mice pre-immunized with L1210-ICV were protected long-term against disease progression (**Figure 3.1B**). As expected, pre-immunizations with irradiated L1210 cells alone were unable to protect the animals from ALL progression, their median survival being only 21 days (**Figure 3.1B**). These results confirm the ability of MG1 infection to create an efficacious leukemia vaccine for the L1210 model (L1210-ICV-18h).

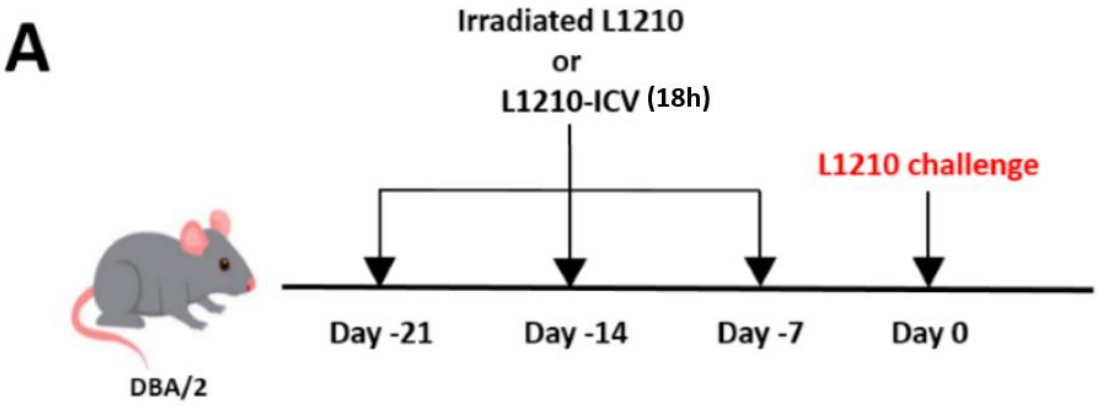
A
Irradiated L1210
or
L1210-ICV (18h)
L1210 challenge
Day -21
Day -14
Day -7
Day 0
DBA/2

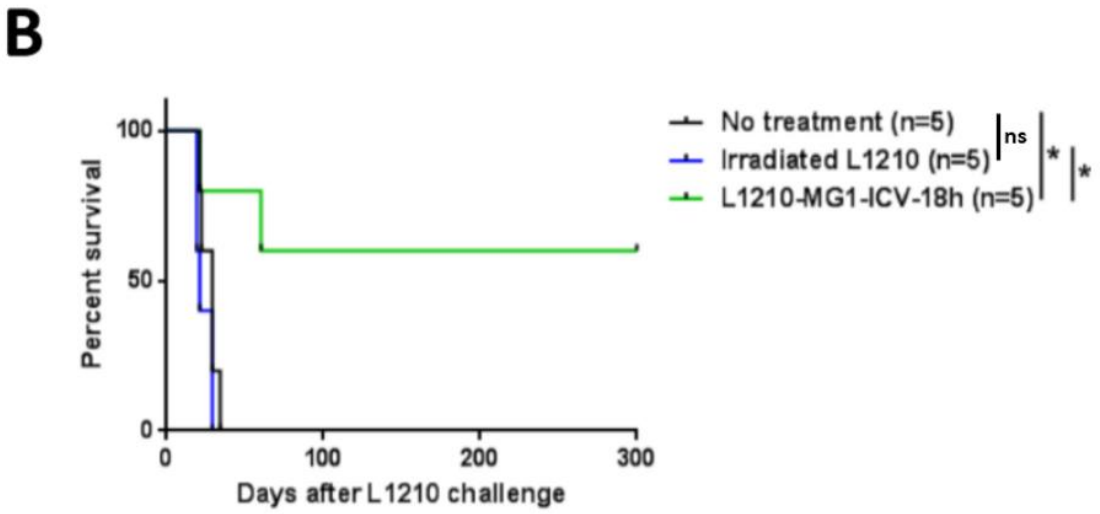
B
Percent survival
100
50
0
0
100
200
300
Days after L1210 challenge
No treatment (n=5)
Irradiated L1210 (n=5)
L1210-MG1-ICV-18h (n=5)
ns
*
*

Figure 3.1: Pre-immunization of DBA/2 mice with L1210-ICV-18h results in long-lasting protection after a subsequent L1210 leukemia challenge.

(A) Prophylactic immunization and challenge schedule of DBA/2 mice. DBA/2 mice were unimmunized or immunized IV with L1210-ICV-18h (1×10^6 cells/dose) or irradiated L1210 cells (1×10^6 cells/dose) once weekly for three weeks, followed by administration of 1×10^6 viable L1210 cells IV one week following the third immunization. The three ICV doses were prepared by infecting L1210 cells *in vitro* with MG1 virus at MOI of 10 and incubated in cRPMI media at 37°C, 5% CO_2 for 17 hours. Both infected and uninfected cells were washed and resuspended in PBS (1×10^6 cells/100 µl/dose) and received 30-Gy radiation before vaccine administration. **(B)** Survival proportion of the unimmunized and immunized DBA/2 mice. 60% of L1210-ICV- immunized mice (n=5) achieved long-term protection from ALL progression compared to unimmunized mice (n=5), p value <0.05 and animals that were treated with irradiated L1210 cells alone (n=5), p value <0.05. The survival curves were generated using GraphPad Prism software and the statistical significance in survival among experimental groups was determined by the Logrank (Mantel-Cox) test.

Assessing the protective effect of ICV against murine AML

Previous work by our group has evaluated the efficacy of the ICV platform in various solid and haematological malignancies. However, efficacy of this immunotherapeutic approach has not yet been investigated in models of acute myeloid leukemia, a malignancy that is associated with very poor prognosis and limited treatment options. Therefore, I sought to determine whether we can use ICV to also generate a robust immune response against murine AML.

Naïve C57BL/6 mice were immunized with 3 weekly doses of either irradiated C1498 cells or C1498-ICV-18h. One week following the last immunization, all animals, were challenged with 1×10^6 viable C1498 cells as outlined in **Figure 3.2A**.

Consistent with previous findings regarding this murine AML model, the median survival was 22 days for untreated mice challenged IV with C1498 cells (**Figure 3.2B**). Similarly, the median survival of mice that were pre-treated with irradiated C1498 cells alone was also 22 days (**Figure 3.2B**). Interestingly, unlike our previous results for the L1210-ICV-18h immunized DBA/2 mice, the C57BL/6 mice immunized with C1498-ICV-18h did not have a statistically significant improvement in survival compared to the unimmunized animals (median survival of 22 days versus 29 days).

Collectively, our results suggest that C1498-ICV vaccination was only able to induce a weak immune response against murine AML, as it was not strong enough to protect the mice long-term from AML progression. This data suggests ICV does not work in the C1498 AML model.

Characterizing the properties of ICV *in vitro*

We learned so far that pre-immunization of mice with L1210-ICV-18h ensures a long-lasting protection following a challenge with viable L1210 cells. Given the unexpected finding that an autologous ICV could not provide a significant survival advantage in the C1498 model of AML, I next sought to investigate the parameters that limit the ICV immunogenicity in this model.

A

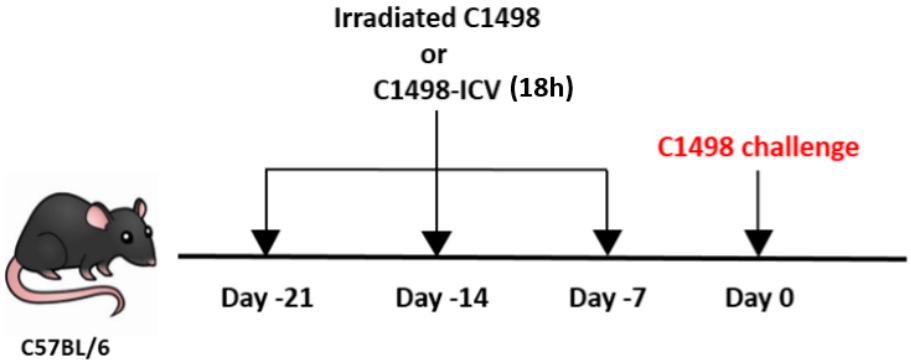
Irradiated C1498
or
C1498-ICV (18h)
C1498 challenge
Day -21
Day -14
Day -7
Day 0
C57BL/6

B

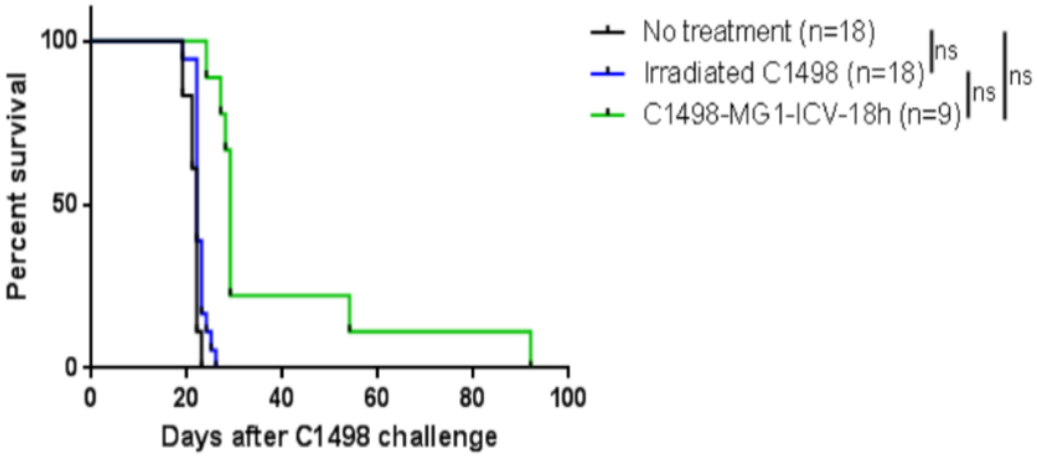
No treatment (n=18)
Irradiated C1498 (n=18)
C1498-MG1-ICV-18h (n=9)
ns
ns
ns
Percent survival
100
50
0
0
20
40
60
80
100
Days after C1498 challenge

Figure 3.2: Pre-immunization of C57BL/6 mice with C1498-ICV-18h fails to protect the animals after challenge with viable C1498 cells.

(A) Prophylactic immunization and challenge schedule of C57BL/6 mice. C57BL/6 mice were unimmunized or immunized IV with C1498-ICV-18h (1×10^6 cells/dose) or irradiated C1498 cells (1×10^6 cells/dose) once weekly for three weeks, followed by administration of 1×10^6 viable C1498 cells IV one week following immunization. The three ICV doses were prepared by infecting C1498 cells *in vitro* with MG1 virus at MOI of 10 and incubated in cRPMI media at 37°C, 5% CO_2 for 17 hours. Both infected and uninfected cells were resuspended in PBS and received 30-Gy radiation before vaccine administration. **(B)** Survival proportion of the unimmunized and immunized C57BL/6 mice. Animals pre-treated with C1498-ICV-18h (n=9) did not result in long term protection after AML challenge compared to unimmunized mice (n=18) or animals that were treated with irradiated C1498 cells alone (n=18). The survival curve representing the "No treatment group" combines 4 individual experiments with n=4 in 2 experiments and n=5 in the other 2 experiments. The survival curve representing the "Irradiated C1498" group combines 4 individual experiments with n=4 in 2 experiments and n=5 in the other 2 experiments. The survival curve representing the "C1498-MG1-ICV-18h" group combines 2 individual experiments with n=4 in one experiment and n=5 in the other experiment. The survival curves were generated using GraphPad Prism software and the statistical significance in survival among experimental groups was calculated using the Logrank (Mantel-Cox) test.

Previous work from our group has shown that viral infection and replication is a critical component of vaccine immunogenicity. Therefore, I hypothesized that the lack of efficacy observed in the C1498 model may be attributed to differences in the susceptibility of these cells to viral infection, viral killing or in the innate response of this cell line to MG1 infection. It has already been shown that both cellular and viral components of L1210-ICV-18h are necessary for the observed protective immune response against ALL [196].

C1498 cells are susceptible to *in vitro* MG1 infection

To investigate the possibility that the inferior efficacy of C1498-ICV-18h, as compared to L1210-ICV-18h, is due to the failure of the virus to infect the cells before vaccine administration, I compared the permissiveness of L1210 and C1498 cells to virus infection.

For this purpose, L1210 and C1498 cells were infected with MG1 virus following the procedures of creating murine leukemia ICVs to be administered *in vivo* (paragraph 2.4 in the Materials and Methods section). Briefly, cells were infected with MG1-eGFP at MOI of 10 for 17 hours, followed by exposure ɣ-radiation (30-Gy). The cell infectivity was assessed based on the fluorescence of the GFP signal in both leukemia cell lines before and after infection.

A microscopic examination of the cells revealed that almost all C1498 cells were GFP+ (**Figure 3.3A**), indicating that the virus is successful at infecting (viral entry and viral protein production) the cells in the context of ICV preparation. However, MG1-eGFP infection resulted in aggregation and visible necrosis of C1498 cells. In contrast, L1210 cells infected with MG1-eGFP under these conditions were entirely GFP+ (**Figure 3.3B**), however they appeared less aggregated and more viable compared to MG1-infected C1498 cells.

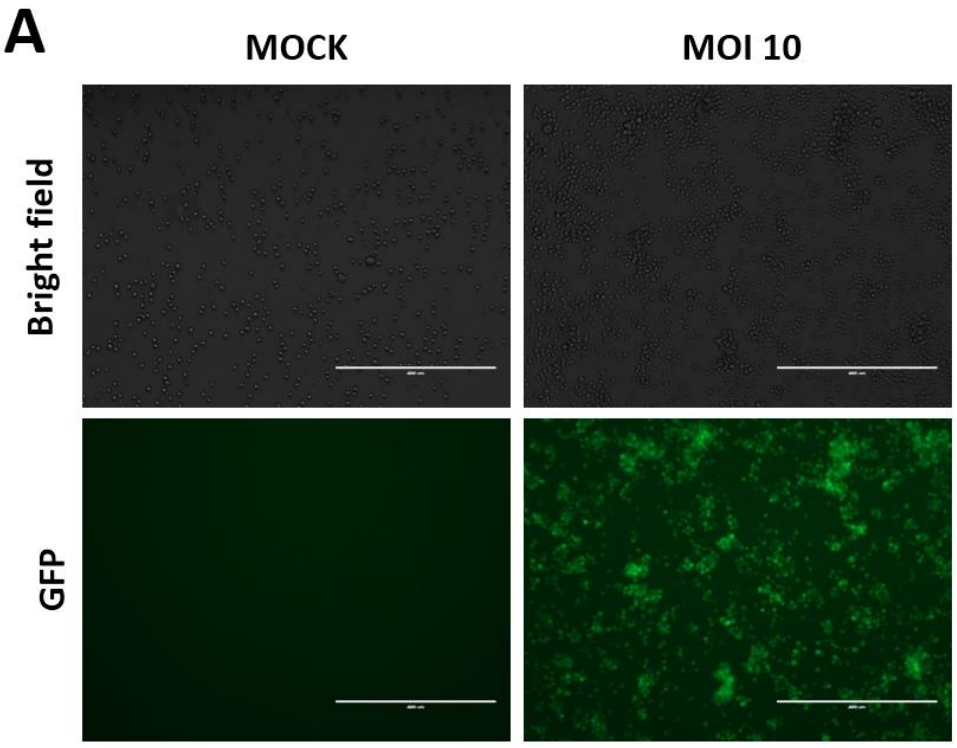
A
MOCK
MOI 10
Bright field
GFP

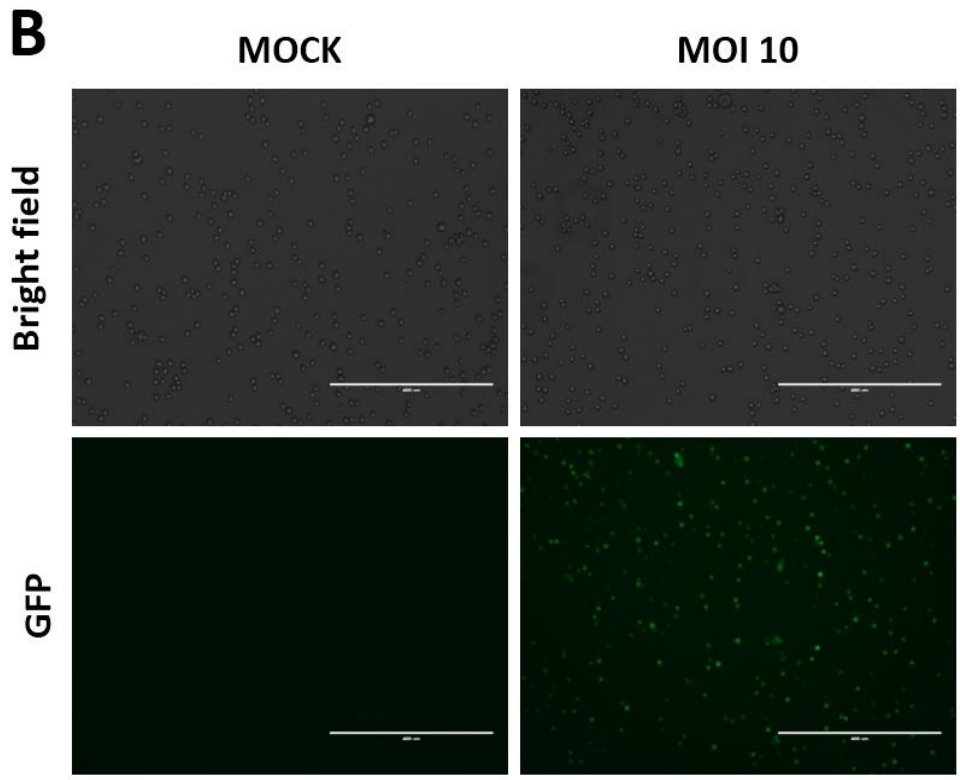
B
MOCK
MOI 10
Bright field
GFP

Figure 3.3: Both L1210 and C1498 cells are highly permissive to MG1-eGFP infection *in vitro*.

(A) 3×10^6 C1498 cells were infected with MG1-eGFP virus at MOI of 10 in 3 ml of cRPMI media and incubated at 37°C, 5% CO_2 for 17 hours. Infected C1498 cells, along with 3×10^6 uninfected cells (MOCK) were washed once in 10 ml of PBS. The cells were resuspended in 300 µl of PBS and exposed to 30-Gy radiation. GFP fluorescence signal was observed under the microscope and pictures of C1498 cells were taken before and after infection in the bright field channel (top panel) and the GFP fluorescent channel (bottom panel). All images were taken at a 400 µm scale. **(B)** 3×10^6 L1210 cells were infected with MG1-eGFP virus at MOI of 10 in 3 ml of cRPMI media and incubated at 37°C, 5% CO_2 for 17 hours. Infected L1210 cells, along with 3×10^6 uninfected cells (MOCK), were resuspended in 300 µl of PBS and exposed to 30-Gy radiation. GFP fluorescence signal was observed under the microscope and pictures of L1210 cells were taken before and after infection in the bright field channel (top panel) and the GFP fluorescent channel (bottom panel). All images were taken at a 400 µm scale.

Collectively, these results suggest that both L1210 and C1498 cells are productively infected by MG1-eGFP *in vitro*, however C1498 cells are killed more rapidly by the virus. These results also suggest that the poor immunogenicity of C1498-ICV-18h is not due to the inability of the virus to enter and replicate in the cells.

MG1 infection results in significantly reduced C1498 cell viability at high MOI *in vitro*

It has been demonstrated that immunogenic cell death occurs when dying or infected tumour cells release high amounts of DAMPs, leading to the activation of the immune system against certain pathogens or tumour antigens [202, 203]. Furthermore, Conrad, *et al*. showed that mice pre-immunized with an ICV preparation containing dead L1210 cells were unable to control the disease progression after leukemia challenge [196]. Thus, to induce a leukemia-specific immune response, MG1-infected cells have to be viable at the time of vaccination to be able to secrete DAMPs when delivered *in vivo*. Thus, the long-lasting protective effect of prophylactic ICV in murine leukemia models could be dictated by the viability of the infected cells prior immunization. Revisiting the data shown in **Figure 3.3A**, C1498 cells were forming noticeable clumps after an 18 hour long MG1 infection (MOI 10) *in vitro*, suggesting that the viability of C1498 cells might be significantly reduced at the time of vaccine administration. Thus, we decided to study the resistance of these leukemia cell lines to MG1 by comparing their post-infection viability.

First, viability of C1498-ICV-18h and L1210-ICV-18h were assessed following infection with MG1-eGFP at MOI of 10 for 17 hours and subsequent 30-Gy irradiation. Notably, only 23.7% of GFP+ C1498 cells were viable (GFP+, PI-) after 18 hours of infection (**Figure 3.4A**) in contrast to the 80.2% of L1210 cells (**Figure 3.4B**). The gating strategy for this experiment is shown for a representative C1498 sample infected with MG1-eGFP (**Supplementary Figure 1**)

These findings suggested that C1498 cells are more susceptible to MG1-mediated cytotoxicity *in vitro*. The relatively poor viability of the infected and irradiated cells could possibly explain the poor efficacy of the ICV in C57BL/6 mice immunized with C1498-ICV-18h.

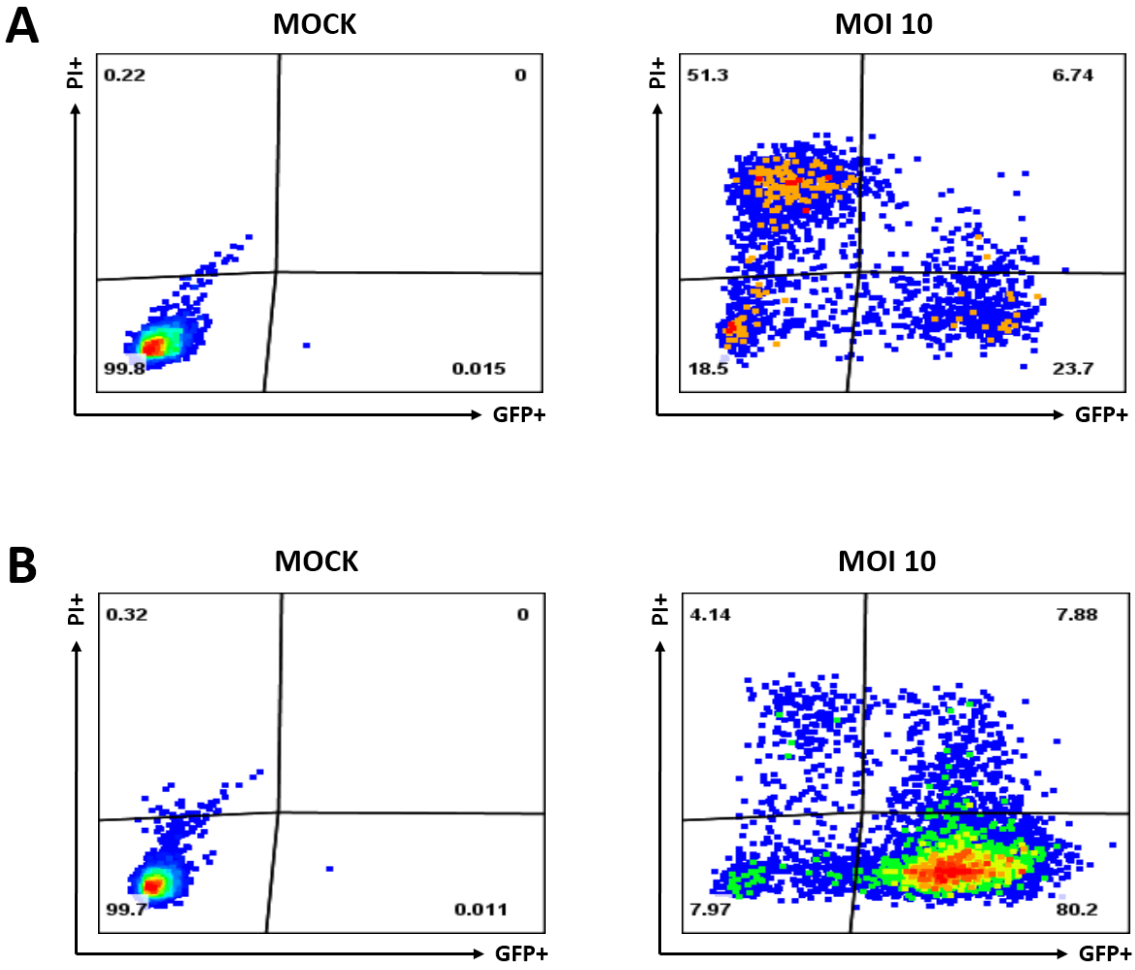
A
MOCK
MOI 10
PI+
GFP+
0.22
0
99.8
0.015
51.3
6.74
18.5
23.7
B
MOCK
MOI 10
PI+
GFP+
0.32
0
99.7
0.011
4.14
7.88
7.97
80.2

Figure 3.4: C1498 cells but not L1210 cells are significantly killed by MG1-eGFP virus *in vitro*.

(A) 5×10^6 C1498 cells were infected with MG1-eGFP virus at MOI of 10 in 5 ml of cRPMI media and incubated at 37°C, 5% CO_2 for 17 hours. Infected C1498 cells, along with 5×10^6 uninfected cells (MOCK) were washed in 10 ml of PBS. The cells were resuspended in 500 µl of PBS and exposed to 30-Gy radiation. The cells were stained with 5 µl of 1:500 diluted PI viability dye to determine the amount of dead cells before and after infection. The GFP and PI signals were immediately acquired for infected and uninfected C1498 cells by flow cytometry. The data was analyzed using FlowJo software. **(B)** 5×10^6 L1210 cells were infected with MG1-eGFP virus at MOI of 10 in 5 ml of cRPMI media and incubated at 37°C, 5% CO_2 for 17 hours. Infected L1210 cells, along with 5×10^6 uninfected cells (MOCK) were washed in 10 ml of PBS. The cells were resuspended in 500 µl of PBS and exposed to 30-Gy raddiation. The cells were stained with 5 µl of 1:500 diluted PI viability dye to determine the amount of dead cells before and after infection. The GFP and PI signals were immediately acquired for infected and uninfected L1210 cells by flow cytometry. The data was analyzed using FlowJo software.

C1498 cells are equally killed by MG1-eGFP at low and high MOIs

To determine whether viability of the vaccine at the time of immunization was impacting vaccine immunogenicity, I next sought to optimize the parameter that could improve the viability of the MG1-infected C1498 cells. First, I investigated the impact of infecting cells at lower MOIs on ICV viability.

Briefly, both murine leukemia cell lines were infected with MG1-eGFP at MOI 0.1, 1 and 10 for 17 hours followed by 2 cycles of ɣ-radiation.

The C1498 cells were observed to be highly infected at the 18 hour time point at all tested MOIs as indicated by GFP fluorescence signal (**Figure 3.5A**). Similarly, cell viability and level of aggregation was unaffected even in cases when C1498 cells were infected at lower MOIs (**Figure 3.5A**). These observations were confirmed by the obtained flow cytometry data, showing that the proportion of GFP+, PI- (viable) C1498 cells infected at MOI of 0.1 increased by only 4.37% compared to the cells infected at MOI of 10 (**Figure 3.5B**). The L1210 cells, on the other hand, maintained a high viability after MG1-eGFP infection regardless of the MOI (**Figure 3.5C and D**).

Overall, these results imply that MG1-eGFP is able to infect and replicate in C1498 cells even when exposed to smaller numbers of viral particles at the time of infection.

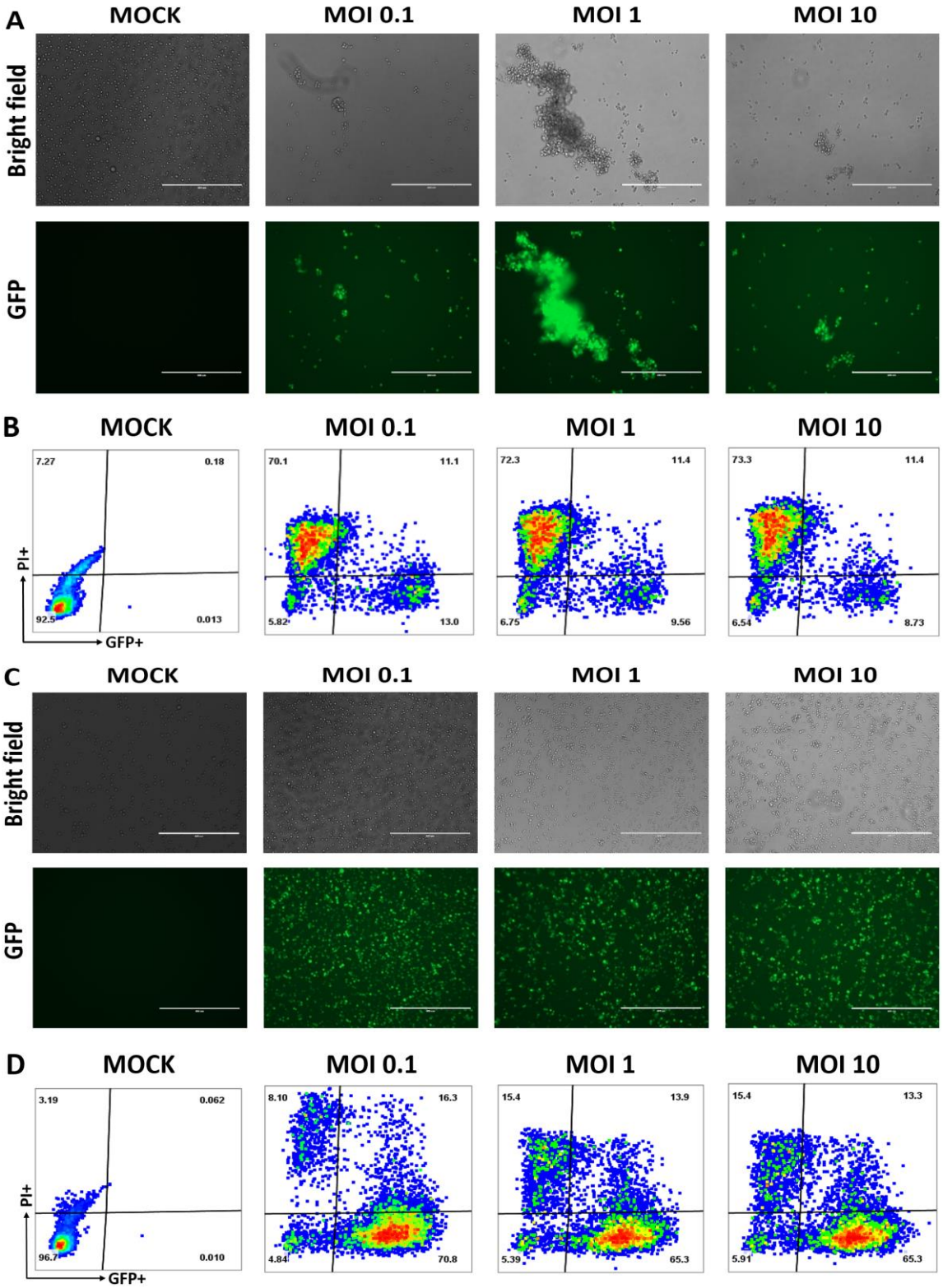
A
MOCK
MOI 0.1
MOI 1
MOI 10
Bright field
GFP
B
MOCK
MOI 0.1
MOI 1
MOI 10
7.27
0.18
92.5
0.013
70.1
11.1
5.82
13.0
72.3
11.4
6.75
9.56
73.3
11.4
6.54
8.73
PI+
GFP+
C
MOCK
MOI 0.1
MOI 1
MOI 10
Bright field
GFP
D
MOCK
MOI 0.1
MOI 1
MOI 10
3.19
0.062
96.7
0.010
8.10
16.3
4.84
70.8
15.4
13.9
5.39
65.3
15.4
13.3
5.91
65.3
PI+
GFP+

Figure 3.5: The viability of MG1-eGFP-infected murine leukemia cell lines is unchanged at lower MOIs.

(A) 6×10^6 C1498 cells were infected with MG1-eGFP virus at MOI of 0.1, 1 and 10 in 6 ml of cRPMI media and incubated at 37°C, 5% CO_2 for 17 hours. Infected C1498 cells, along with 6×10^6 uninfected cells (MOCK), were washed in 10 ml of PBS, resuspended in 600 µl of PBS and irradiated (30-Gy). GFP fluorescence signal was observed under the microscope and pictures of C1498 cells were taken before and after infection in the bright field channel (top panel) and GFP fluorescent channel (bottom panel). All images were taken at a 400 µm scale.
(B) 6×10^6 C1498 cells were infected with MG1-eGFP virus at MOI of 0.1, 1 and 10 in 6 ml of cRPMI media and incubated at 37°C, 5% CO_2 for 17 hours. Infected C1498 cells, along with 6×10^6 uninfected cells (MOCK) were washed in 10 ml of PBS, resuspended in 600 µl of PBS and irradiated (30-Gy). The cells were stained with 5 µl of 1:500 diluted PI viability dye to determine the amount of dead cells before and after infection. The GFP and PI signals were immediately acquired before and after infection by flow cytometry, by eliminating the cell debris and doublets in our gating strategy using FlowJo data analysis software.
(C) 6×10^6 L1210 cells were infected with MG1-eGFP virus at MOI of 0.1, 1 and 10 in 6 ml of cRPMI media and incubated at 37°C, 5% CO_2 for 17 hours. Infected L1210 cells, along with 6×10^6 uninfected cells (MOCK) were resuspended in 600 µl of PBS and irradiated (30-Gy). GFP fluorescence signal was observed under the microscope and pictures of L1210 cells were taken before and after infection in the bright field channel (top panel) and GFP fluorescent channel (bottom panel). All images were taken at a 400 µm scale.
(D) 6×10^6 L1210 cells were infected with MG1-eGFP virus at MOI of 0.1, 1 and 10 in 6 ml of cRPMI media and incubated at 37°C, 5% CO_2 for 17 hours. Infected L1210 cells, along with 6×10^6 uninfected cells (MOCK) were washed in 10 ml of PBS, resuspended in 600 µl of PBS and irradiated (30-Gy). The cells were stained with 5 µl of 1:500 diluted PI viability dye to determine the amount of dead cells before and after infection. The GFP and PI signals were immediately acquired before and after infection by flow cytometry, by eliminating the cell debris and doublets in our gating strategy using FlowJo data analysis software.

MG1-eGFP-infected C1498 cells are viable after 6 hours of infection

Since infecting C1498 cells *in vitro* at lower MOIs did not help improve the viability of infected cells, I next sought to examine the kinetics of viral replication.

For this purpose, C1498 and L1210 cells were infected with MG1-eGFP at MOI of 10 and the cells were collected following 4, 6, 8 and 18 hours of infection. The infected leukemia cells were irradiated correspondingly as the collection time point was reached and their infectivity was observed based on the GFP fluorescence signal using microscopy.

GFP signal was detected in the infected C1498 cells after only 6 hours of infection without significant cell aggregation (**Figure 3.6A)**. These results were confirmed by flow cytometry and importantly revealed that 53.2% of GFP+ C1498 cells were still viable at 6 hours of infection (**Figure 3.6B**). Interestingly, C1498 cells started aggregating considerably only after 8 hours of infection (**Figure 3.6A**) and our flow data confirmed that indeed the proportion of GFP+, PI- (viable) C1498 cells decreases down to 27.7% at this infection time point (**Figure 3.6B**). It appears that the GFP signal was detected in L1210 cells after 6 hours of infection as well, however the extent of cell aggregation was merely observable at any infection time point (**Figure 3.6C**). Consistent with our previous results, flow cytometry data confirmed the fact that MG1-infected L1210 cells maintain high infectivity and resistance to viral killing at any infection time point (**Figure 3.6D**).

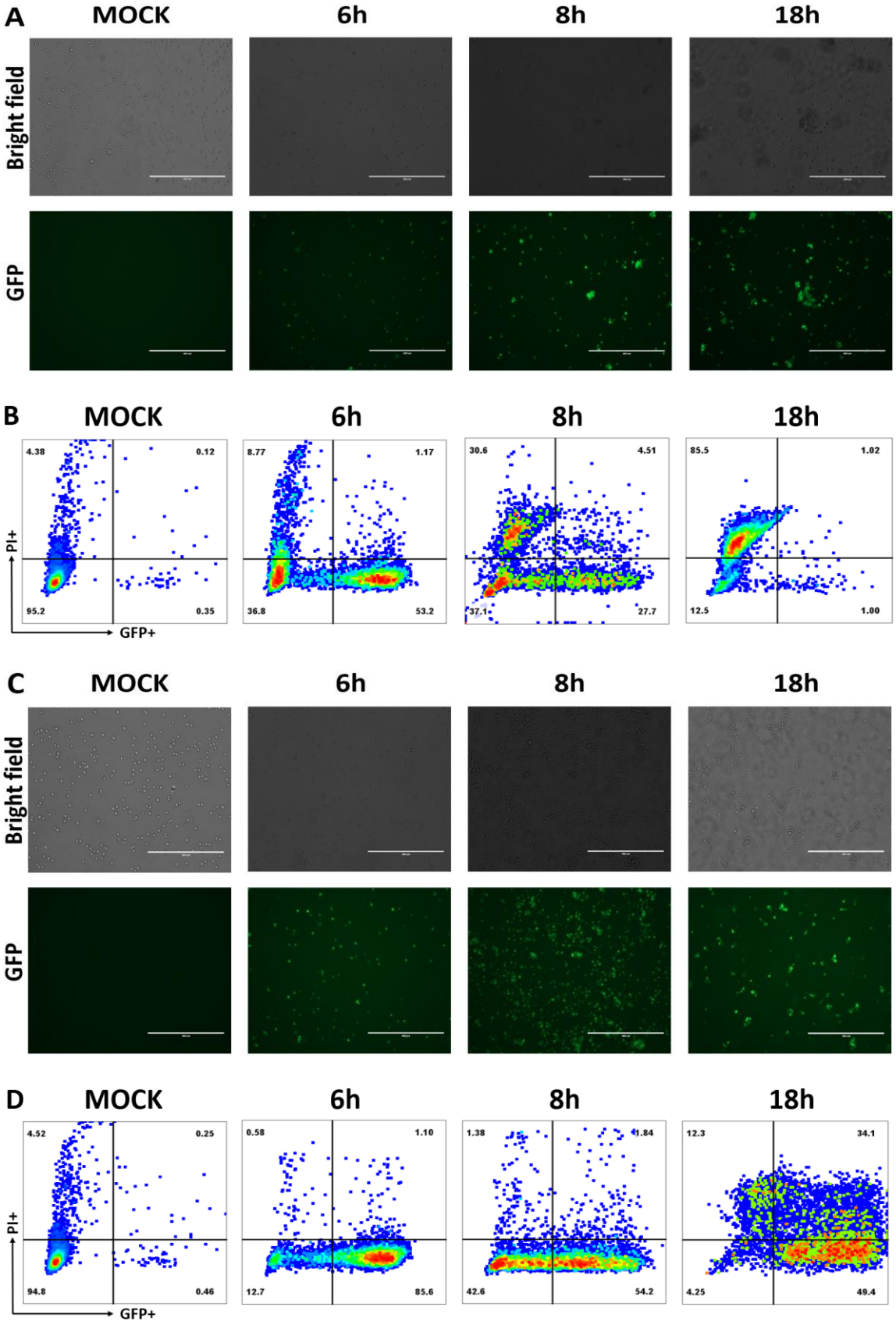
A
MOCK
6h
8h
18h
Bright field
GFP
B
MOCK
6h
8h
18h
4.38
0.12
95.2
0.35
8.77
1.17
36.8
53.2
30.6
4.51
37.1
27.7
85.5
1.02
12.5
1.00
PI+
GFP+
C
MOCK
6h
8h
18h
Bright field
GFP
D
MOCK
6h
8h
18h
4.52
0.25
94.8
0.46
0.58
1.10
12.7
85.6
1.38
1.84
42.6
54.2
12.3
34.1
4.25
49.4
PI+
GFP+

Figure 3.6: The proportion of MG1-infected and viable C1498 cells is highest after 6 hours of infection.

(A) 5×10^6 C1498 cells were infected with MG1-eGFP virus at MOI of 10 in 5 ml of cRPMI media and incubated at 37°C, 5% CO_2 for 5, 7 and 17 hours. Infected L1210 cells, along with 5×10^6 uninfected cells (MOCK) were washed once in 10 ml of PBS, resuspended in 500 µl of PBS and irradiated (30-Gy). GFP fluorescence signal was observed under the microscope and pictures of C1498 cells were taken before and after infection in the bright field channel (top panel) and GFP fluorescent channel (bottom panel). All images were taken at a 400 µm scale.
(B) 5×10^6 C1498 cells were infected with MG1-eGFP virus at MOI of 10 in 5 ml of cRPMI media and incubated at 37°C, 5% CO_2 for 17 hours. Infected C1498 cells, along with 5×10^6 uninfected cells (MOCK) were washed in 10 ml of PBS, resuspended in 500 µl of PBS and irradiated (30-Gy). The cells were stained with 5 µl of 1:500 diluted PI viability dye to determine the number of dead cells before and after infection. The GFP and PI signals were immediately acquired before and after infection by flow cytometry, by eliminating the cell debris and doublets in our gating strategy using FlowJo data analysis software.
(C) 5×10^6 L1210 cells were infected with MG1-eGFP virus at MOI of 10 in 5 ml of cRPMI media and incubated at 37°C, 5% CO_2 for 5, 7 and 17 hours. Infected L1210 cells, along with 5×10^6 uninfected cells (MOCK) were resuspended in 500 µl of PBS and irradiated (30-Gy). GFP fluorescence signal was observed under the microscope and pictures of L1210 cells were taken before and after infection in the bright field channel (top panel) and GFP fluorescent channel (bottom panel). All images were taken at a 400 µm scale.
(D) 5×10^6 L1210 cells were infected with MG1-eGFP virus at MOI of 10 in 5 ml of cRPMI media and incubated at 37°C, 5% CO_2 for 5, 7 and 17 hours. Infected L1210 cells, along with 5×10^6 uninfected cells (MOCK) were washed in 10 ml of PBS, resuspended in 500 µl of PBS and irradiated (30-Gy). The cells were stained with 5 µl of 1:500 diluted PI viability dye to determine the amount of dead cells before and after infection. The GFP and PI signals were immediately acquired before and after infection by flow cytometry, by eliminating the cell debris and doublets in our gating strategy using FlowJo data analysis software.

Validating the role of C1498-ICV-6h viability in its prophylactic efficacy *in vivo*

Having established infection conditions that lead to improved cell viability, I next sought to determine whether cell viability was indeed contributing to a more robust anti-tumour immune response and could prolong the survival of ICV-immunized C57BL/6 mice after AML challenge.

For this purpose, mice were immunized every week during three weeks with three doses of C1498-ICV prepared by infecting C1498 cells for only 6 hours (C1498-ICV-6h). To assess a potentially improved efficacy of the more viable vaccine, a group of mice were immunized with C1498-ICVs prepared by infecting the cells for 18 hours (C1498-ICV-18h). We also included a group of mice that were challenged with AML with no prior immunizations and a group of mice that were pre-immunized with irradiated, uninfected C1498 cells (Irradiated C1498). These control groups were important to compare the overall ability of the C1498-ICV in generating anti-tumour immunity in this prophylactic model. A summary of this survival experiment is shown in **Figure 3.7A**.

Interestingly, immunization with C1498-ICV-6 h resulted in a modest, although statistically significant increase in median survival (40.5 days) compared to the median survival of 22 days for both unimmunized mice and those immunized with irradiated C1498 cells alone (**Figure 3.7B**).

Even though immunizing with a highly viable vaccine was somewhat successful in protecting the pre-immunized animals from AML challenge and prolonged their median survival compared to animals from other control groups, the high viability of the infected C1498 cells alone was unable to provide long term protection in the majority of these vaccinated animals. This suggests that additional factors are preventing the creation of an immunogenic C1498 vaccine.

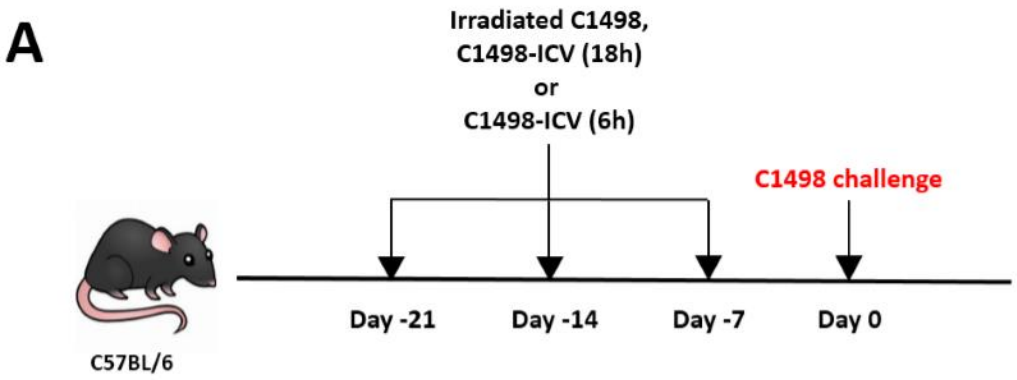
A
Irradiated C1498,
C1498-ICV (18h)
or
C1498-ICV (6h)
C1498 challenge
Day -21
Day -14
Day -7
Day 0
C57BL/6

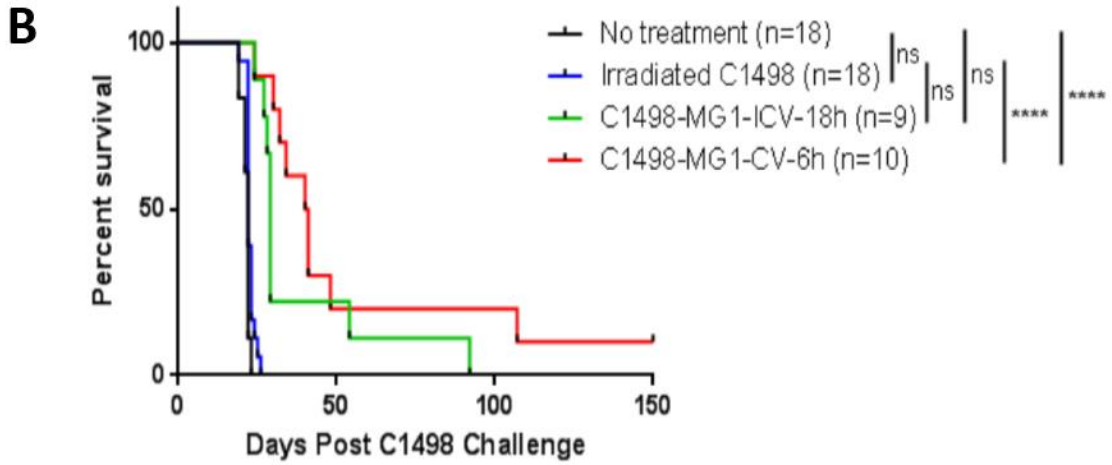
B
Percent survival
100
50
0
0
50
100
150
Days Post C1498 Challenge
No treatment (n=18)
Irradiated C1498 (n=18)
C1498-MG1-ICV-18h (n=9)
C1498-MG1-CV-6h (n=10)
ns
ns
ns
****
****

Figure 3.7: Pre-immunization with viable C1498-ICV-6h leads to a modest survival improvement of the C57BL/6 mice following challenge with viable C1498 cells.

(A) Prophylactic immunization and challenge schedule of C57BL/6 mice. C57BL/6 mice were unimmunized or immunized IV with C1498-ICV (1×10^6 cells/dose) or irradiated C1498 cells (1×10^6 cells/dose) once weekly for three weeks, followed by administration of 1×10^6 viable C1498 cells IV a week later since the third immunization. The three ICV doses were prepared by infecting C1498 cells *in vitro* with MG1 virus at MOI of 10 and incubated in cRPMI media (10% FBS) at 37°C, 5% CO_2 for either 5 or 17 hours. Both infected and uninfected cells were resuspended in PBS and were irradiated (30-Gy) before vaccine administration.
(B) Survival proportion of the unimmunized and immunized C57BL/6 mice. Animals vaccinated with C1498-ICV-18h (n=9) did not result in long term protection from AML challenge compared to unimmunized mice (n=18) or animals that were treated with irradiated C1498 cells alone (n=18). Animals vaccinated with C1498-ICV-6h (n=10) survived the longest compared to all other groups ($p<0.0001$).

C1498 cells have a deficient anti-viral response

We showed so far that C1498 cells remain viable for a shorter period of time after MG1 infection *in vitro* compared to L1210 cells and that efficacy of the vaccine is in part dependent upon viability. Next, I sought to explore the potential reasons contributing to the increased C1498 cell death following MG1 infection. To address this question, I characterized the anti-viral response of both L1210 and C1498 murine leukemia cell lines.

Cell intrinsic anti-viral response to Rhabdovirus infection is initiated by PRR (for example, RIG-I and RLRs) sensing of dsRNA in the cytoplasm, causing IRF3 activation and expression of type I interferon and interferon stimulated genes (ISGs) [167]. To assess the ability of MG1 to induce an anti-viral response, RNA has been extracted from uninfected and MG1-infected L1210 and C1498 cells to characterize global changes in transcriptional profile by RNA sequencing.

Using a recently published dataset that identified an ISG signature [204], ISG levels were compared between infected and uninfected conditions in a panel of mouse cancer cell lines. As expected ISGs were upregulated upon virus infection in the majority of cancer cell lines tested with the distinct exception of C1498 (**Figure 3.8A**). Despite a handful of ISGs being weakly expressed in infected C1498 cells, IFN-β, which is the main cytokine driving interferon signalling, is not induced at all upon MG1 infection.

To validate this finding, supernatants from MG1 infected cells were collected to quantify secreted IFN-β protein. Specifically, the supernatant of L1210 and C1498 cells infected with MG1 at a MOI of 10 were collected 18 hours after infection and an IFN-β ELISA was performed as described in the paragraph 2.10 of the Material and Methods section. In agreement with the RNA sequencing results, C1498 cells had undetectable levels of secreted IFN-β after MG1 infection (**Figure 3.8B**). In contrast, IFN-β in the supernatant of MG1-infected L1210 cells was significantly higher and exceeded the limit of detection (**Figure 3.8B**).

Collectively, these findings suggest that C1498 cells are impaired in their ability to respond appropriately to rhabdovirus infection. Therefore, the lack of an anti-viral

response and lack of type I interferon production by infected C1498 cells is potentially contributing to their rapid loss in viability after *in vitro* infection with MG1.

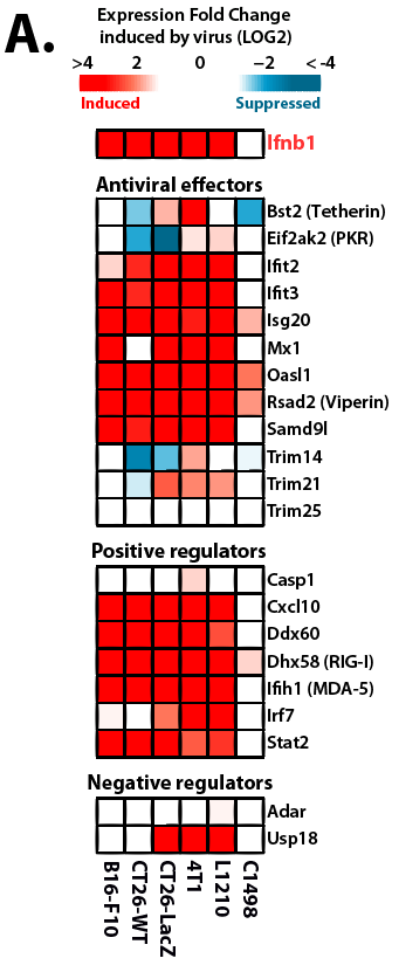
A.
Expression Fold Change
induced by virus (LOG2)
>4
2
0
−2
< -4
Induced
Suppressed
Ifnb1
Antiviral effectors
Bst2 (Tetherin)
Eif2ak2 (PKR)
Ifit2
Ifit3
Isg20
Mx1
Oasl1
Rsad2 (Viperin)
Samd9l
Trim14
Trim21
Trim25
Positive regulators
Casp1
Cxcl10
Ddx60
Dhx58 (RIG-I)
Ifih1 (MDA-5)
Irf7
Stat2
Negative regulators
Adar
Usp18
B16-F10
CT26-WT
CT26-LacZ
4T1
L1210
C1498

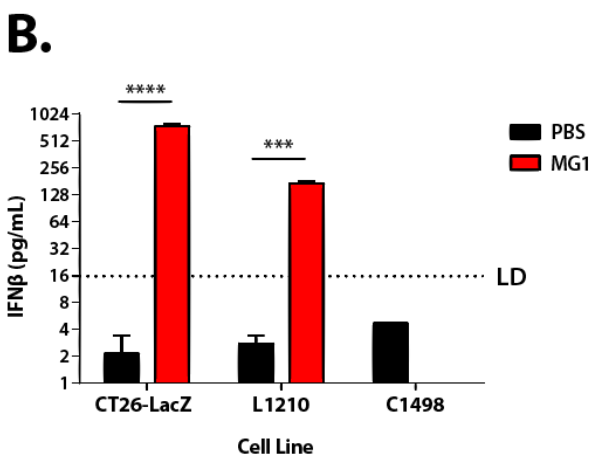
B.
****
***
1024
512
256
128
64
32
16
8
4
2
1
IFNβ (pg/mL)
LD
PBS
MG1
CT26-LacZ
L1210
C1498
Cell Line

Figure 3.8: Type I interferon signaling is impaired in C1498 cells
(A) L1210 and C1498 cells were infected with MG1 for 18 hours at an MOI of 10 after which mRNA was extracted using the RNeasy Mini kit for RNA sequencing analysis, as described in the manufacturer's protocol. The RNA for the B16-F10, CT26-WT, CT26-LacZ and 4T1 cell lines was extracted after being exposed to identical infection conditions. The data is represented as a heatmap showing fold change values between infected and uninfected samples. The selected genes are a subset of ISGs with a defined function.
(B) L1210 and C1498 cells were infected with MG1 for 18 hours at an MOI of 10 after which supernatants were collected and the amount of IFN-β protein was assessed using the mouse IFN-β Quanikine ELISA kit as recommended by the manufacturer's protocol. A two-way ANOVA was performed to determine differences in IFN-β amount produced by the L1210, C1498 and CT26-LacZ cell lines after *in vitro* MG1 infection. Each experimental group has n=2; **** p-value < 0.0001, *** p-value < 0.001.

Minimal production of pro-inflammatory cytokines and chemokines by the C1498-ICV

Virus-infected cells secrete pro-inflammatory cytokines and chemokines necessary to recruit immune cells and control the infection [205]. However, the expression of such cytokines and chemokines is induced as a result of anti-viral response and perhaps the lack of IFN-β produced in MG1-infected C1498 cells suggests that the low immunogenicity of C1498-ICV may be a result of limited production of immune-stimulatory cytokines and chemokines.

To directly test this hypothesis, I assessed the expression of all CCL chemokines, CXCL cytokines and interleukin cytokines upon viral infection in either L1210 or C1498 cells, using the available RNA sequencing data. Consistent with the impaired anti-viral response observed in C1498 cells, MG1 infection did not significantly induce immune signalling genes in C1498 cells (**Figure 3.9A**). One interesting observation was that the TNF-α expression is induced in all murine cancer cell lines with the exception of C1498 cells upon MG1 infection. Even though MG1 infection triggers TNF-α expression in L1210 cells, it is induced at a lower level compared to murine melanoma, colon and breast cancer cell lines infected with MG1 (**Figure 3.9A**).

Even though our findings from RNA sequencing are helpful and valuable, we decided to assess and confirm the expression levels of TNFα protein by performing a TNF-α ELISA on the supernatants of MG1-infected L1210 and C1498 cells. Briefly, both cell lines were infected with MG1 at MOI of 10 and the supernatants were collected 18 hours later. The supernatants were used to quantify the concentration of TNF-α secreted by these infected cells as describes in the paragraph 2.11 of the Materials and Methods section.

Consistent with RNA sequencing data, we saw a modest increase in TNF-α secretion by L1210 cells and no detectable TNF-α production by C1498 cells after infection (**Figure 3.9B**). On the other hand, the RNA sequencing data shows an increase in TNF-α transcript production in colon CT26-LacZ cells after virus infection, we were unable to detect an increase in TNF-α protein in the supernatants of CT26-LacZ cells (**Figure 3.9B**). Among other factors, this may be indicative of post-transcriptional regulation previously reported in cancer cells as one mechanism of antigen loss [206].

We have also assayed supernatants of infected L1210 and C1498 cells for a limited number of cytokines using Luminex technology. A detailed summary of this experiment is discussed in the paragraph 2.12 of the Materials and Methods section. In contrast to the ELISA data, only a modest increase (1.6 fold) of TNF-α protein was detected in the supernatant of infected L1210 cells (**Figure 3.9C**, top).

We also saw a spike in CCL5 (RANTES) and IL-6 production in infected L1210 cells (**Figure 3.9C**), consistent with the RNA sequencing data (**Figure 3.9A**). Although the expression of IL-6 is induced in infected C1498 cells at mRNA level, it was not detected at the protein level according to the cytokine array results (**Figure 3.9C**, bottom). This could be possibly explained by the fact that L1210 cells remain viable at the 18 hour collection time point since infection while C1498 cells are not (**Figure 3.6**). Thus, in addition to post-transcriptional regulation in cancer cells, cell viability is likely another factor that can affect mRNA translation.

So far, our data suggests that the immunogenic L1210-ICV produces pro-inflammatory cytokines including interferon. In contrast, infection of C1498 cells with MG1 virus does not elicit an anti-viral response or induce cytokine production. This data suggests L1210-ICV to be more immunogenic than C1498-ICV.

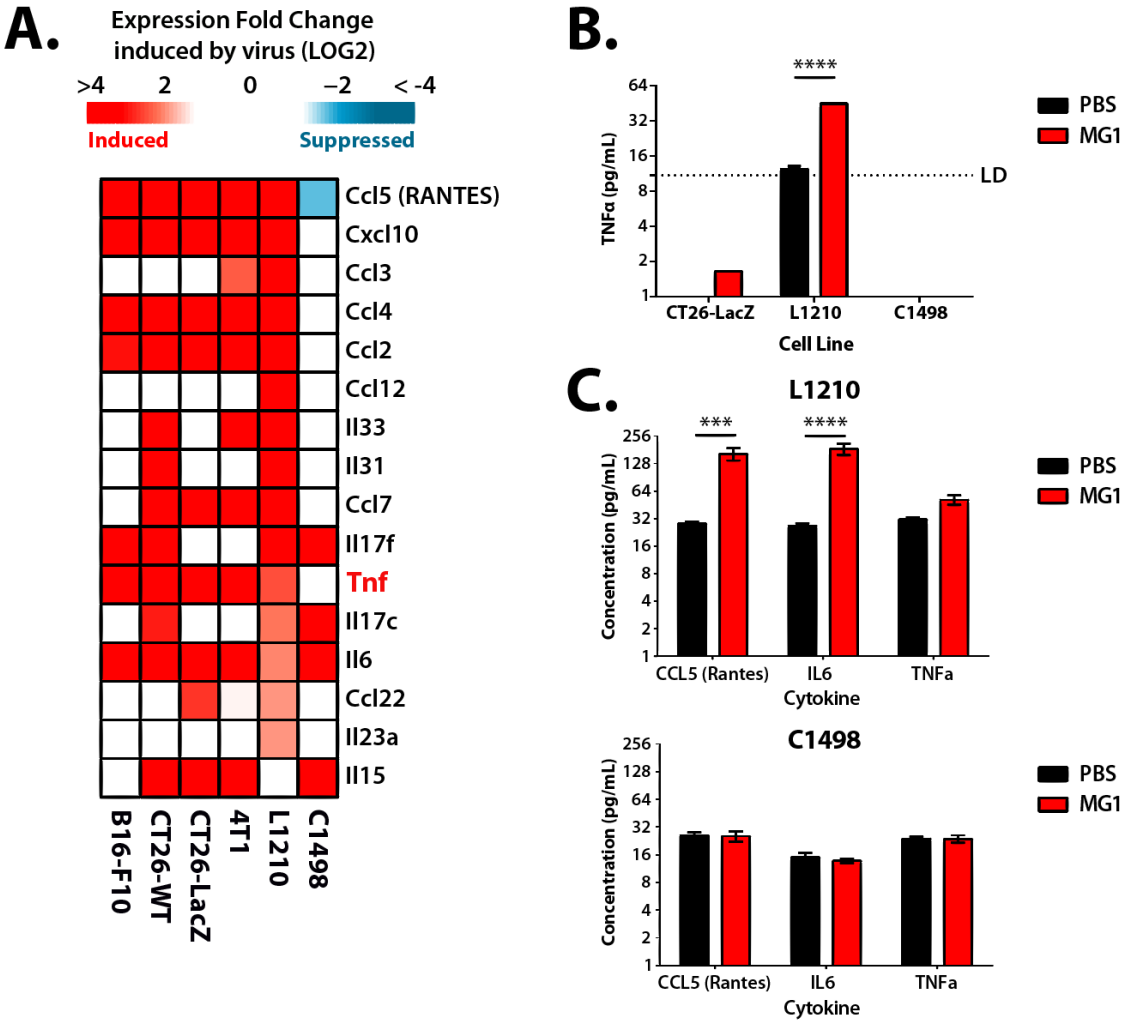
A.
Expression Fold Change induced by virus (LOG2)
>4
2
0
−2
< -4
Induced
Suppressed
Ccl5 (RANTES)
Cxcl10
Ccl3
Ccl4
Ccl2
Ccl12
Il33
Il31
Ccl7
Il17f
Tnf
Il17c
Il6
Ccl22
Il23a
Il15
B16-F10
CT26-WT
CT26-LacZ
4T1
L1210
C1498
B.
****
TNFα (pg/mL)
64
32
16
8
4
2
1
LD
CT26-LacZ
L1210
C1498
Cell Line
PBS
MG1
C.
L1210
***
****
Concentration (pg/mL)
256
128
64
32
16
8
4
2
1
CCL5 (Rantes)
IL6
TNFa
Cytokine
PBS
MG1
C1498
Concentration (pg/mL)
256
128
64
32
16
8
4
2
1
CCL5 (Rantes)
IL6
TNFa
Cytokine
PBS
MG1

Figure 3.9: Pro-inflammatory chemokines and cytokines secreted by L1210-ICV and C1498-ICV.
(A) L1210 and C1498 cells were infected with MG1 for 18 hours at an MOI of 10 after which RNA was extracted using the RNeasy Mini kit for RNA sequencing analysis, as described in the manufacturer's protocol. The RNA for the B16-F10, CT26-WT, CT26-LacZ and 4T1 cell lines was extracted after being exposed to identical infection conditions. The data is represented as a heatmap showing fold change values between infected and uninfected samples. The selected genes are all CCL chemokines, CXCL cytokines and interleukins induced in either L1210 or C1498 cells.
(B) L1210 and C1498 cells were infected with MG1 for 18 hours at an MOI of 10 after which supernatants were collected and the amount of TNF-α protein was assessed using the mouse Mouse TNF-α Quanikine ELISA kit as recommended by the manufacturer's protocol. A two-way ANOVA was performed to determine differences in TNF-α amount produced by the L1210, C1498 and CT26-LacZ cell lines after *in vitro* MG1 infection. Each experimental group has n=2; **** p-value < 0.0001, *** p-value < 0.001.
(C) Supernatants of samples from Panel **(A)** were assessed for CCL5, IL-6 and TNF-α protein amount using a Luminex cytokine array (n=3; **** p-value < 0.0001, *** p-value < 0.001)..

Both L1210 and C1498 express MHC class I but not MHC class II

In addition to induction of ISGs and cytokines upon infection, increased antigen presentation through MHC is another consequence of viral infection. Expression of MHC class I molecules on cell surface is critical for CD8+ T cell activity [207] and viral clearance. However, downregulation or lack of MHC I expression is one of the immune evasion mechanisms employed by solid tumours and leukemia cells [208]. In addition to pro-inflammatory signals created by antiviral signaling it has been documented that MHC class II molecules initiate an immune response against antigens of extracellular origin that are only expressed by professional APCs [209]. One study found that sub-clones making up a small percent of the total population of L1210 cells expressed MHC II. Interestingly, these sub-clones were shown to be immunogenic and not tumorigenic, as inoculating with these clones *in vivo* protected mice from subsequent challenge with parental L1210 [210].

In consideration of these findings, I hypothesised that MHC class I and/or II expression contributes to the antigenicity of leukemia cell vaccine and may correlate with their protective effect against leukemia challenges. To investigate this possibility, I first examined the RNA sequencing data for expression of genes which make up MHC complex I and II. Since there is no clear guidelines regarding what constitutes significant MHC expression at the RNA level, publicly available mouse RNA sequencing data of normal [211] and immune cells [212, 213] were incorporated in our analysis for comparative purposes. One study has shown that the phenotype of murine leukemia cell lines changes when delivered *in vivo* [146]. Therefore, in addition to the MG1-infected L1210 and C1498 cells, we also sequenced L1210 and C1498 cells that were stimulated *in vitro* with IFN-ɣ. This particular condition was meant to mimic the introduction of these cells in the environment they encounter when administered *in vivo*, since IFN-ɣ is one of the first cytokines produced *in vivo* only by the activated immune cells.

Consistent with the published literature, we observed that the expression level of MHC I genes was much lower in B16 cells compared to other cancer cell lines [214]. A more interesting finding was that most cancer cell types, with the exception of C1498

cells, showed an upregulation in MHC I genes after MG1 infection (**Figure 3.10A**), which is also a previously reported observation [215]. We were also able to confirm with flow cytometry that both L1210 and C1498 cells express MHC I at baseline and that an *in vitro* pre-treatment with IFN-γ did not significantly affect its level of expression (**Figure 3.10C**). A representative example regarding the gating strategy used to determine MHC I expression on murine leukemia cell lines is shown in **Supplementary Figure 2**.

In agreement with current literature, we were able to show a strong expression of 9 out of 12 MHC II genes by professional APCs like macrophages, DCs and B cells [209]. However, L1210 cells, which are considered to share the same origin as B cell precursors, express 4 out of 12 MHC II genes at much lower levels when compared to the levels expressed by APCs (**Figure 3.8B**). It also appears that MG1 infection or exposure to IFN-ɣ does not induce a population wide expression of MHC II genes in L1210 cells (**Figure 3.8B**). Using flow cytometry, we were also able to show that a very small proportion of L1210 cells express MHC II and that MG1 infection does not induce its expression (**Figure 3.10D**). The gating strategy used to assess the expression of MHC II on murine leukemia cell lines is shown in **Supplementary Figure 3**.

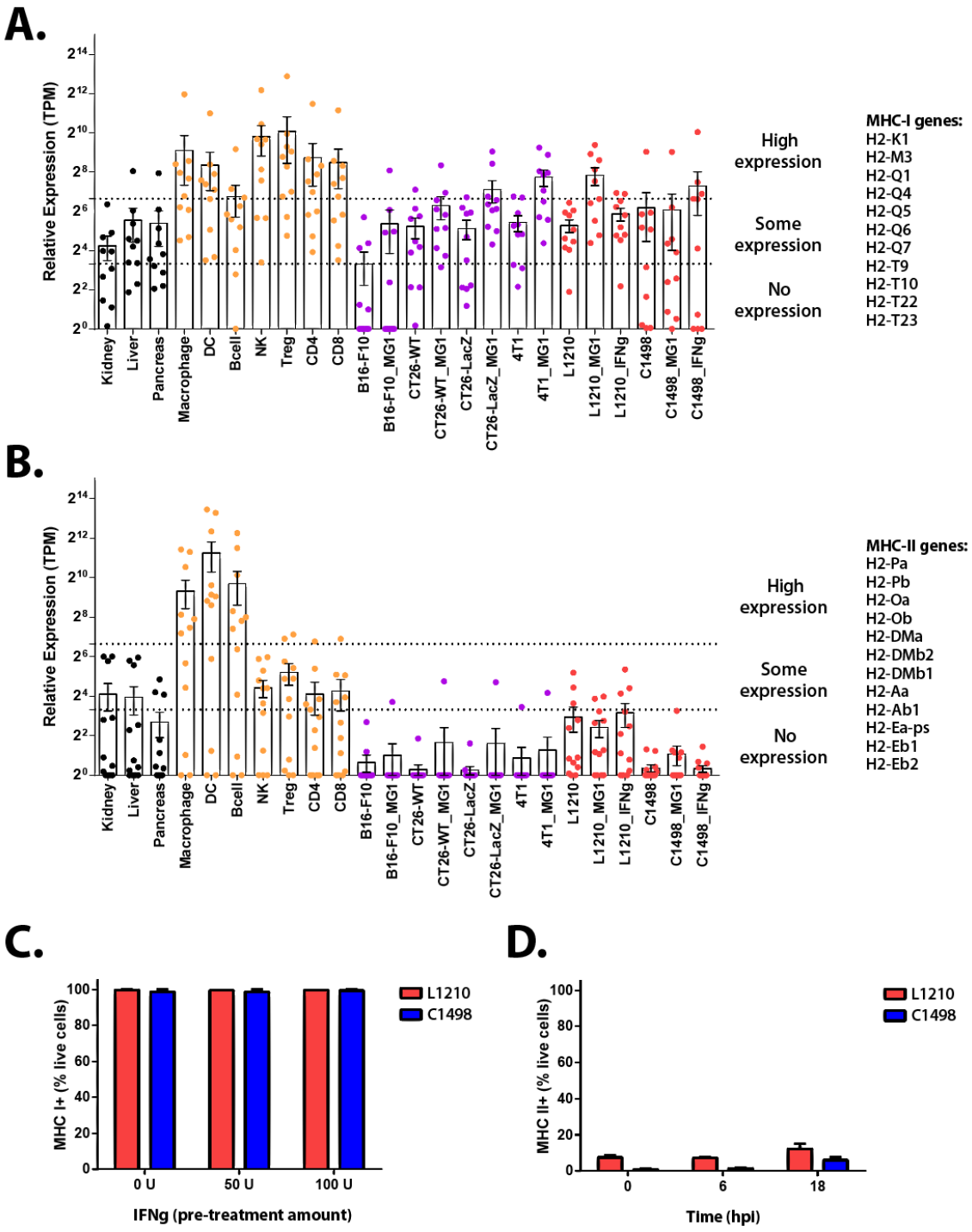
A.
Relative Expression (TPM)
High expression
Some expression
No expression
MHC-I genes:
H2-K1
H2-M3
H2-Q1
H2-Q4
H2-Q5
H2-Q6
H2-Q7
H2-T9
H2-T10
H2-T22
H2-T23
Kidney
Liver
Pancreas
Macrophage
DC
Bcell
NK
Treg
CD4
CD8
B16-F10
B16-F10_MG1
CT26-WT
CT26-WT_MG1
CT26-LacZ
CT26-LacZ_MG1
4T1
4T1_MG1
L1210
L1210_MG1
L1210_IFNg
C1498
C1498_MG1
C1498_IFNg
B.
Relative Expression (TPM)
High expression
Some expression
No expression
MHC-II genes:
H2-Pa
H2-Pb
H2-Oa
H2-Ob
H2-DMa
H2-DMb2
H2-DMb1
H2-Aa
H2-Ab1
H2-Ea-ps
H2-Eb1
H2-Eb2
C.
MHC I+ (% live cells)
L1210
C1498
0 U
50 U
100 U
IFNg (pre-treatment amount)
D.
MHC II+ (% live cells)
L1210
C1498
0
6
18
Time (hpi)

Figure 3.10: Both L1210 and C1498 express MHC class I but not MHC class II.
L1210 and C1498 cells were either uninfected, infected with MG1 for 18 hours at an MOI of 10 or stimulated with 50U IFN-ɣ for 16-18 hours, after which RNA was extracted using the RNeasy Mini kit for RNA sequencing analysis, as described in the manufacturer's protocol.
(A-B) Mouse RNA sequencing datasets were used to quantify transcripts per million (TPM) levels of genes part of **(A)** MHC class I and **(B)** MHC class II. The bar graphs show individual gene expression as well as mean gene expression. Mean TPM values between 0 and 10, 10 and 100, 100 and >1000 were classified as no expression, some expression and high level of expression respectively. The list of genes that are part of either MHC class I or MHC class II is displayed to the right of the bar graphs. Datasets used include publicly available mouse RNA sequencing data of normal tissues [211] and immune cells [212, 213].
(C) L1210 and C1498 cells were either untreated or pre-treated with 50U or 100U of IFN-γ for 16 hours after which the cells were harvested and assayed for MHC class I expression using flow cytometry.
(D) L1210 and C1498 cells were infected with MG1 at an MOI of 10 and assayed at various time-points (0, 6 and 18 hours) for MHC class II expression using flow cytometry.

Immune checkpoint inhibitors improve the survival of mice immunized with C1498-ICV

So far we have explored interferon signalling, cytokine production and antigen presentation, all of which have the potential to affect the immunogenicity of a tumor vaccine. As discussed in the introduction, another important factor affecting tumour immunogenicity and their immune escape abilities are checkpoint inhibitors.

Like other cancers, AML has been shown to upregulate ICIs in order to suppress the cancer patients' the immune system [216]. However, clinical trials testing immune checkpoints blockades have shown limited efficacy, suggesting the need for combination therapy [217]. In line with the currently available AML patient data, the syngeneic murine C1498 AML model was shown to express PD-L1 at high levels, especially after inoculating the cells *in vivo* [146].

To better describe the activating and suppressive phenotypes characteristic to L1210 and C1498 cells before and after rhabdovirus infection, we have searched our RNA sequencing datasets to assess the expression of such genes.
In children with B-cell ALL, CD40 expression was found to be beneficial and correlated with longer survival [218]. Curiously, we observed that the expression of co-stimulatory receptor CD40 was enhanced in L1210 cells after virus infection at the transcriptomic level (**Figure 3.11A**). We were also able to validate with flow cytometry that the expression of CD40 protein is indeed upregulated on the surface of L1210 cells after 18 hours of MG1 infection (**Figure 3.11B, top panel**). Another striking observation revealed from the RNA sequencing data is that L1210 cells significantly upregulate the expression of both the inhibitory PD-1 receptor and its ligand PD-L1 (**Figure 3.11A**). We were able to validate the fact that the level of both PD-1 (**Figure 3.11B, middle panel**) and PD-L1 (**Figure 3.11B, bottom panel**) expression indeed increases upon MG1 infection during the process of the L1210-ICV preparation *in vitro*. The details on the flow cytometry analysis and gating strategy are shown for MG1-infected L1210 cells in **Supplementary Figure 3** and **Supplementary Figure 4**. Interestingly, it has been recently reported that when tumour cells co-express PD-1 and PD-L1, the inhibitory receptors and its ligand will more likely interact in *cis*, thus inhibiting the ability of PD-L1 to bind T cell-intrinsic PD-1 in *trans* and repressing the canonical PD-L1/PD-1

inhibitory signaling [219]. Considering this observation, it is possible that the simultaneous upregulation of PD-1 and PD-L1 following MG1 infection could partially contribute to the L1210-ICV immunogenicity and enhanced prophylactic efficacy.

Our results also confirm the previously reported low levels of PD-L1 expression on C1498 cells [146], however we also detected low levels of CTLA-4 after infection of C1498 cells with virus (**Figure 3.11A**). In order to evaluate whether expression of these checkpoints is responsible for the failure of vaccinated mice to reject C1498, we have used monoclonal antibodies to block both checkpoints in the process of pre-immunization with C1498-ICV-6h.

For this purpose, we conducted a survival experiment in which a group of naïve C57BL/6 mice were immunized with three doses of C1498-ICV infected for 6 hours with MG1 at MOI of 10. The vaccines were administered once a week during three weeks and this group of mice were also treated with a cocktail of anti-PD-1/anti-CTLA-4 after each immunization and after challenge with viable C1498 cells. Other experimental control groups included were animals that were unimmunized or immunized with irradiated C1498 cells and C1498-ICV prepared by infecting the cells for 18 or 6 hours without administration of anti-PD-1/CTLA-4 cocktail treatment. All mice were challenged with viable C1498 cells one week since the administration of the third vaccination and survival was monitored.

Our results show a slight improvement in survival of the C1498-ICV-6h vaccinated animals that also received checkpoint inhibitors during immunization and challenge with viable C1498. Importantly, 40% of mice are long term survivors compared to groups that were not treated with anti-PD-1/anti-CTLA-4 checkpoint inhibitors cocktail (**Figure 3.11C**). However, not all mice respond to this combination therapy, suggesting additional mechanisms are responsible for C1498 relapse in C1498-ICV-immunized mice. Furthermore, these results reflect only one experiment, warranting additional experiments which can look at the effect of dosing, both in terms of timing and amounts of checkpoints administered.

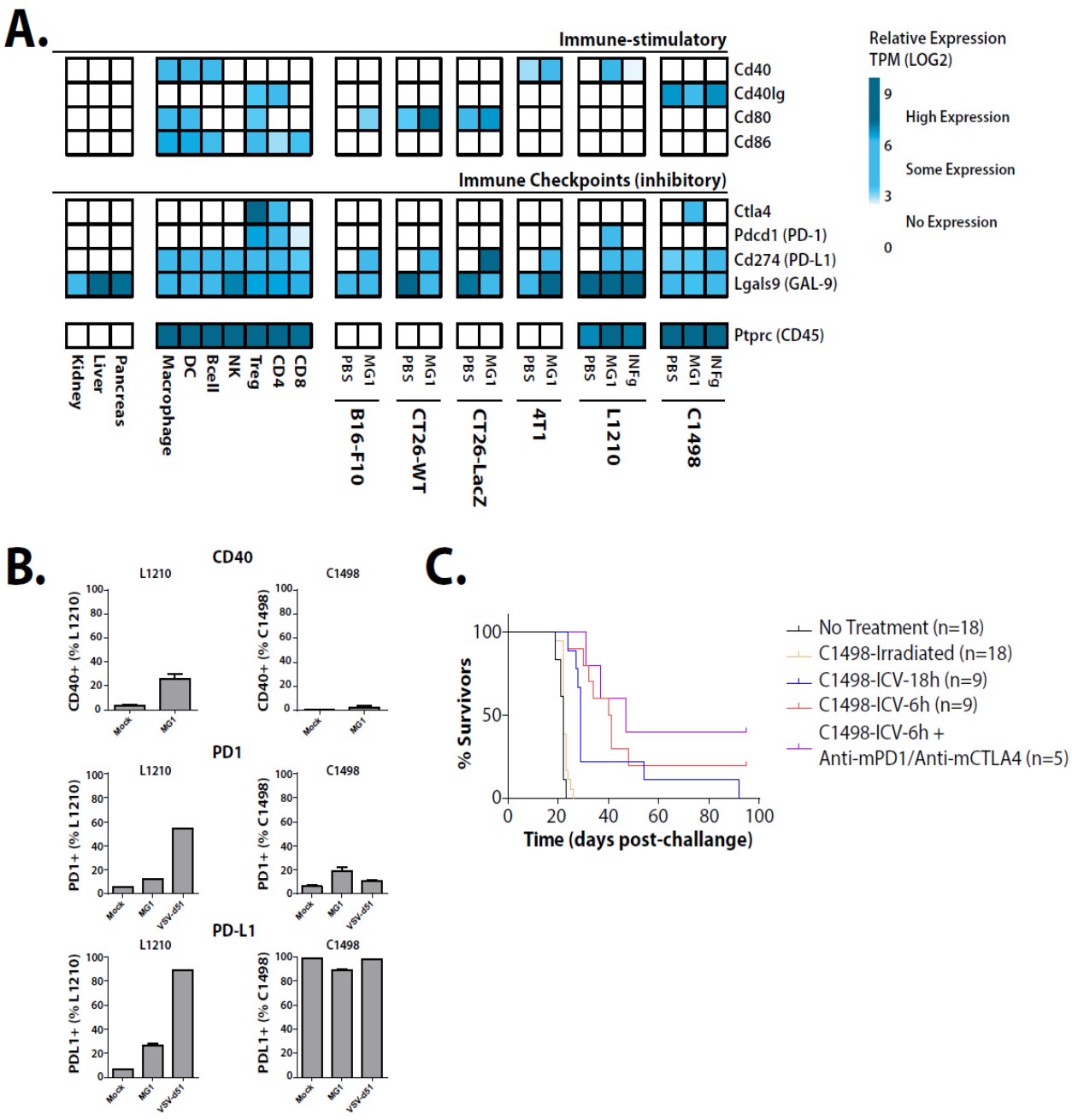
A.
Immune-stimulatory
Cd40
Cd40lg
Cd80
Cd86
Immune Checkpoints (inhibitory)
Ctla4
Pdcd1 (PD-1)
Cd274 (PD-L1)
Lgals9 (GAL-9)
Ptprc (CD45)
Relative Expression
TPM (LOG2)
9
High Expression
6
Some Expression
3
No Expression
0
Kidney
Liver
Pancreas
Macrophage
DC
BcellI
NK
Treg
CD4
CD8
PBS
MG1
INFg
B16-F10
CT26-WT
CT26-LacZ
4T1
L1210
C1498
B.
CD40
PD1
PD-L1
L1210
C1498
CD40+ (% L1210)
CD40+ (% C1498)
PD1+ (% L1210)
PD1+ (% C1498)
PDL1+ (% L1210)
PDL1+ (% C1498)
Mock
MG1
VSV-d51
C.
% Survivors
Time (days post-challange)
No Treatment (n=18)
C1498-Irradiated (n=18)
C1498-ICV-18h (n=9)
C1498-ICV-6h (n=9)
C1498-ICV-6h +
Anti-mPD1/Anti-mCTLA4 (n=5)

Figure 3.11: Expression and blockade of immune checkpoint inhibitors in context of leukemia ICV.
L1210 and C1498 cells were either uninfected, infected with MG1 for 18 hours at a MOI of 10 or stimulated with 50U IFN-ɣ for 16-18 hours, after which RNA was extracted using the RNeasy Mini kit for RNA sequencing analysis, as described in the manufacturer's protocol.
(A) Mouse RNA sequencing datasets were used to quantify transcripts per million (TPM) levels of genes involved in immune activation and suppression. TPM values between 0 and 10, 10 and 100, 100 and >1000 were classified as no expression, some expression and high level of expression respectively. Datasets used include publicly available mouse RNA-seq data of normal tissues [211] and immune cells [212, 213].
(B) L1210 and C1498 cells were infected with MG1 for 18 hours. The infected cells, along with the uninfected controls were used to determine changes in the level of CD40 (top panel), PD-1 (middle panel) and PD-L1 (bottom panel). Changes in the expression level of these markers were determined by flow cytometry and are shown as frequency of the live cell population.
(C) C57BL/6 mice were immunized IV three times one week apart with irradiated C1498 cells, or MG1 infected C1498 cells (ICV). Challenge with viable 1e6 C1498 cells was injected IV one week after the last dose. Antibodies targeting immune checkpoint inhibitors were administered IP at a dose of 100 µg per antibody per mouse during immunizations and leukemia challenge.

L1210-ICV and C1498-ICV induce maturation of splenic cDCs *in vivo*

So far, our experiments were focused on exploring differences between L1210-ICV and C1498-ICV, specifically on how *in vitro* rhabdovirus infection differentially affects the intrinsic immunogenicity of these cells. On this note, we showed that viability, possibly influenced by anti-viral response, of the administered vaccine is a factor influencing the efficacy of ICV. Namely, we showed that C1498 cells become necrotic faster than L1210 cells after MG1 infection (**Figure 3.6**). Shortening the time of infection and pre-immunizing C57BL/6 mice with viable ICVs prolonged their survival following the challenge with viable C1498 leukemia cells (**Figure 3.7**). We also determined that C1498 cells have an impaired antiviral response, explaining their increased susceptibility to OV mediated oncolysis (**Figure 3.8**). Interestingly, unlike C1498s, L1210s have an intact antiviral response and secrete several inflammatory cytokines after MG1 infection, which could be contributing to the high efficacy of L1210-ICV (**Figure 3.9**).

To understand and further improve the efficacy of ICV, it was necessary to study the immune response and changes occurring after the IV delivery of vaccine. Currently, the impact C1498-ICV has on the mouse's own immune system after vaccination is lacking, however this question has been previously addressed to some extent in the murine L1210 ALL model. Conrad *et al*. determined that survival of L1210-ICV-immunized mice following leukemia challenge is T cell-mediated [196]. Furthermore, *in vivo* T cell subset depletion experiments conducted in our lab determined that the helper CD4+ T cells were essential during the pre-immunization period to achieve this impressive result [197]. Considering that T cells are responsible for the effective outcome of the L1210-ICV pre-immunizations, I next sought to characterize the T cell priming processes after immunization with ICV, by assessing the level of classical DC (cDC) maturation as well as CD4+ and CD8+ T cells activation.

For this purpose, naïve DBA/2 and C57BL/6 mice were either unimmunized or immunized with one of dose of L1210-ICV-18h and C1498-ICV-6h respectively. The spleens were harvested and processed after 1, 4 and 24 hours since vaccination. Briefly, the level of DC maturation and T cell subset activation was assessed by staining the collected spleenocytes for cDC and T cell markers. The outline of these experiments is

shown for both models in **Figure 3.12** and a representative example of flow data analysis for cDC maturation and T cell activation is shown in **Supplementary Figure 5** and **Supplementary Figure 6** respectively.

Our results showed that the frequency of CD86+ cDCs increased in both DBA/2 and C57BL/6 mice after 24 hours since immunization with either L1210-ICV-18h (**Figure 3.13A**; p value < 0.05) or C1498-ICV-6h (**Figure 3.13C;** p value < 0.05), which is an indication of cDC maturation. On the other hand, treatment with one dose of ICV did not upregulate the expression of CD28 on CD8+ T cells in either L1210-ICV (**Figure 3.13B**) or C1498-ICV (**Figure 3.13D**). CD28 is an activating receptor, which when bound to the CD86 ligand on activated cDCs induces proliferation of effector CD8+ T cells. Lack of change in CD28 levels could be potentially explained by the fact that this marker is constitutively expressed on all T cell subsets [220], since signalling via CD28/CD86 axis is regulated at the level of CD86 ligand expression on cDCs upon activation.

It was also observed that the immunization with L1210-ICV-18h did not result in a significant cDC population expansion, considering the frequency and the count of the splenic cDCs before and after immunization (**Supplementary Figure 7A and 7B**). The same conclusion applies to the C57BL/6 mice regarding changes in the size of splenic cDC population 24 hours after administration of one dose of C1498-ICV-6h (**Supplementary Figure 7C and 7D**).

L1210-ICV, but not C1498-ICV induces CD40L on splenic CD4+ T cells *in vivo*

Next, we assessed the impact of ICV treatments on the CD40/CD40L co-stimulatory axis between cDCs and CD4+ T cell subset in both leukemia models. Considering the fact that the expression of certain T cell activation markers could be transient, spleens were collected at several time points since vaccine administration.

Our data indicates that the expression of the CD40 activating receptor did not change significantly on cDCs 24 hours after immunizing with one dose of L1210-ICV-18h (**Figure 3.14A**) or C1498-ICV-6h (**Figure 3.14C**). These results meet our expectations, since it has been previously shown that cDCs express high levels of CD40 even in steady state [221]. The regulation of CD40/CD40L co-stimulatory axis is

mediated at the level of CD4+ T cells which induce the CD40L expression on their surface exclusively upon activation [222]. We determined that one IV dose of L1210-ICV-18h could induce a significant increase in CD40L-expression on CD4+ T cells within 1 hour of immunization (**Figure 3.14B;** p value < 0.05). However, immunization with C1498-ICV-6h of C57BL/6 mice was unable to induce the expression of CD40L on the splenic CD4+ T cell subset after one hour since vaccine administration (**Figure 3.14D**).

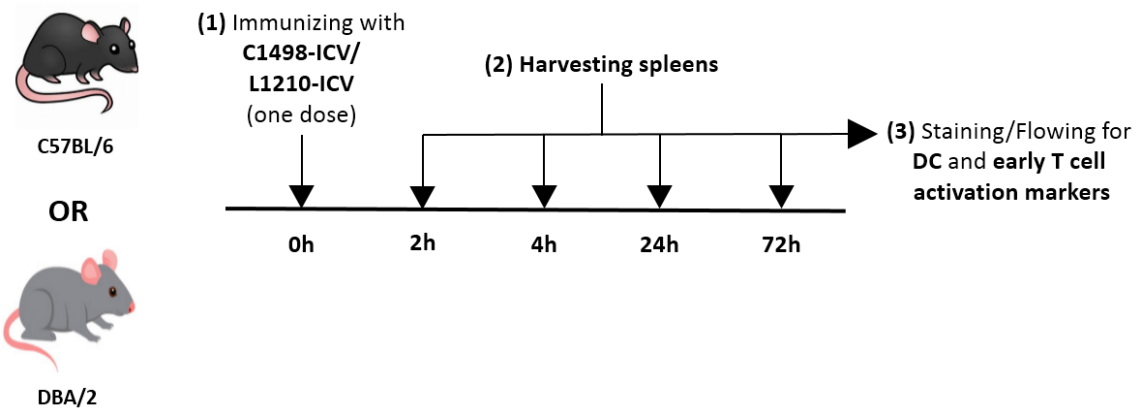
C57BL/6
OR
DBA/2
(1) Immunizing with
C1498-ICV/
L1210-ICV
(one dose)
(2) Harvesting spleens
(3) Staining/Flowing for
DC and early T cell
activation markers
0h
2h
4h
24h
72h

Figure 3.12: Outline of the immune activation experiment *in vivo* after administration of one dose of L1210-ICV and/or C1498-ICV

DBA/2 and C57BL/6 mice were unimmunized or immunized IV with one dose of L1210-ICV-18h and C1498-ICV-6h (1×10^6 cells/dose). The spleens of the immunized mice were collected after 2, 4, 24 and/or 72 hours since vaccination. The spleens were processed as described in the paragraph 2.6 of the Materials and Methods section. The spleenocytes were stained for cDC and T cell early activation markers as described in subparagraph 2.8.5 of the Materials and Methods section and the data was acquired using LSR Fortessa.

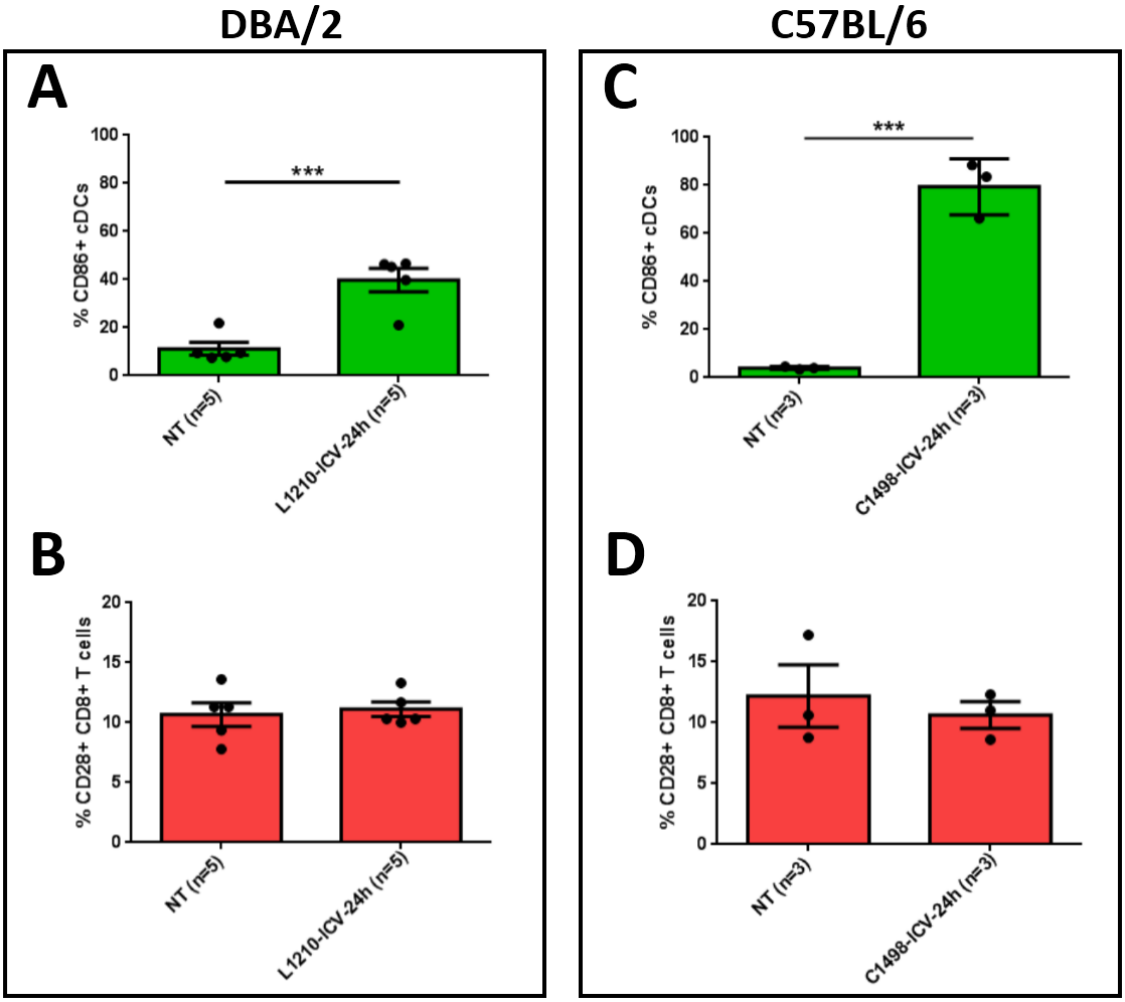
DBA/2
C57BL/6
A
B
C
D
% CD86+ cDCs
% CD28+ CD8+ T cells
***
NT (n=5)
L1210-ICV-24h (n=5)
NT (n=3)
C1498-ICV-24h (n=3)
0
20
40
60
80
100
5
10
15

Figure 3.13: DC activation status following the administration of one ICV dose in context of murine leukemia models.

Naïve DBA/2 (n=5) and C57BL/6 (n=3) mice were treated with one dose of L1210-ICV-18h and C1498-ICV-6h respectively. The spleens of the immunized mice, along with the spleens of unimmunized DBA/2 (n=5) and C57BL/6 (n=3) mice were collected 24 hours later. The harvested spleenocytes from both immunized and unimmunized animals were stained for **(B, D)** CD28 receptor on CD8+ T cell sub-population and for its CD86 ligand **(A, C)** on cDC subsets to determine changes in their levels of expression. A difference in the levels of CD86+ cDC population was detected in both ICV-immunized DBA/2 mice ($p<0.05$) and C57BL/6 mice ($p<0.05$). The statistics were obtained after performing and a non-parametric, unpaired t test using the tools from GraphPad Prism.

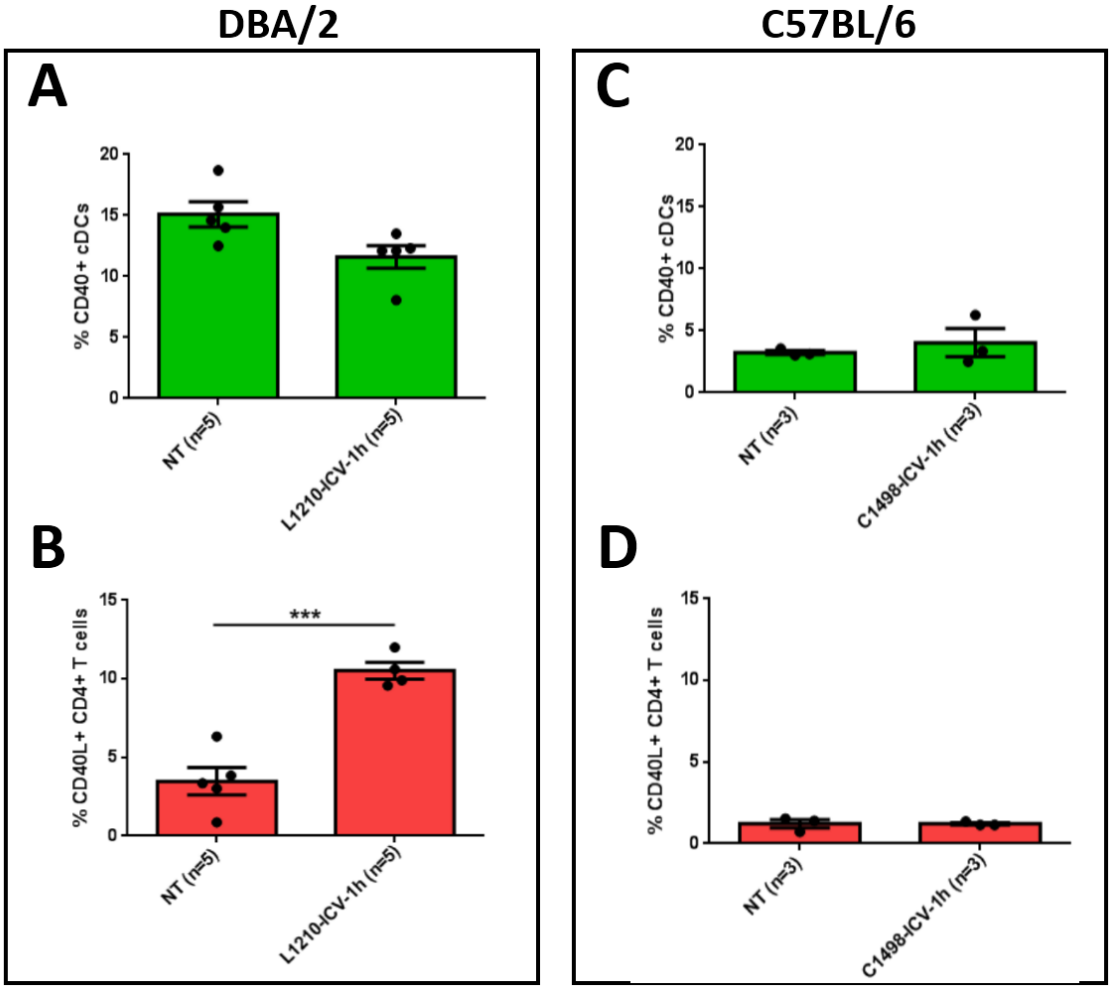
DBA/2
C57BL/6
A
% CD40+ cDCs
20
15
10
5
0
NT (n=5)
L1210-ICV-1h (n=5)
B
% CD40L+ CD4+ T cells
***
15
10
5
0
NT (n=5)
L1210-ICV-1h (n=5)
C
% CD40+ cDCs
20
15
10
5
0
NT (n=3)
C1498-ICV-1h (n=3)
D
% CD40L+ CD4+ T cells
15
10
5
0
NT (n=3)
C1498-ICV-1h (n=3)

Figure 3.14: T cell activation status following the administration of one ICV dose in context of murine leukemia models.

Naïve DBA/2 (n=5) and C57BL/6 (n=3) mice were treated with one dose of L1210-ICV-18h and C1498-ICV-6h respectively. The spleens of the immunized mice, along with the spleens of unimmunized DBA/2 (n=5) and C57BL/6 (n=3) mice were collected 24 hours later. The harvested spleenocytes from both immunized and unimmunized animals were stained for **(B, D)** CD40L ligand on CD4+ T cell sub-population and for its CD40 receptor **(A, C)** on cDC subsets to determine changes in their levels of expression.. A difference in the levels of CD40L+ CD4+ T cell population was detected in immunized DBA/2 mice ($p<0.05$) compared to the naïve group. C57BL/6 mice ($p<0.05$). The statistics were obtained after performing and a non-parametric, unpaired t test using the tools from GraphPad Prism.

Another interesting observation was revealed when analyzing the kinetics of CD40L expression on the helper T cell subset after vaccination. It has been previously shown that CD40L expression is quite transient and occurs early in the T cell priming process [222]. Indeed, expression of CD40L on CD4+ T cells started to decrease 4 hours after immunization with L1210-ICV-18h (**Supplementary Figure 8A**). On the other hand, C1498-ICV-6h failed to induce CD40L on splenic CD4+ T cells at any given time point that was assayed (**Supplementary Figure 8B**).

Collectively, our data indicates that treatment with C1498-ICV leads to cDC activation in *vivo*, however it does not seem to reverse the tolerogenic state that is characteristic to C1498 murine leukemia cells when introduced *in vivo* [223].

We also considered important to look at any potential changes in the expression of CD69 and CD137 on splenic T cell populations after immunizing with either L1210-ICV-18h or C1498-ICV-6h. Both CD69 and CD137 are well-characterized early T cell activation markers and assessment of their expression could help us further investigate the mechanism of how an efficient (L1210-ICV) versus a non-efficient (C1498-ICV) vaccine promotes the formation of a leukemia-specific immune response. Generally, CD69 is highly involved in T cell differentiation as well as lymphocyte retention in the spleen and plays a crucial role in the formation of anti-tumour immunity [224]. It has also been established that signalling via CD137 leads to the activation of cytotoxic T lymphocytes, having strong anti-cancer effects by providing costimulatory signals to T cells independently of CD28 [225].

Our data shows that immunization with one dose L1210-ICV-18h results in upregulation of CD69 on both CD8+ and CD4+ T cell subsets and in an increase in the expression of CD137 on the CD4+ T cell subset (**Supplementary Figure 9A**). Interestingly, the same trend in CD69 expression is observed for animals immunized with C1498-ICV-6h (**Supplementary Figure 9B**), however CD137 expression does not seem to change (**Supplementary Figure 9B**).

C1498-ICV-6h immunization modestly enhances the cytotoxicity of CD8+ T cells

To continue characterizing the impact C1498-ICV has on the adaptive immunity, we assessed the cytotoxic T cell response in the saphenous blood of C57BL/6 after 24

hours since administration of one C1498-ICV-6h dose. Considering the fact that we saw a slight improvement in the vaccine's protective ability when it consists of viable rather than necrotic MG1-infected cells (Figure 3.7B), we decided to compare the level of CD8+ T cell activity in mice that were immunized with C1498-ICV-6h and C1498-ICV-18h. In addition, blood samples were collected from animals that were either unimmunized or immunized with one dose of irradiated C1498 cells. The outline of the treatment regimen for this experiment is summarized in **Figure 3.15A**. The blood samples collected for every mouse in each experimental group were processed and stained for T cell subset identification markers (CD3 and CD8) as well as for intracellular IFN-ɣ and TNF-α activating markers as described in the subparagraph 2.8.6 of the Materials and Methods section. A representative example for the employed gating strategy of the acquired flow cytometry data is represented in **Supplementary Figure 10**.

According to the obtained results, we showed that mice that were pre-immunized with one dose of viable C1498-ICV-6h had an overall increased proportion of IFN-ɣ -producing CD8+ T cells compared to any other experimental group (**Figure 3.15B and C**). However, it appears that the cytotoxic T cell response is quite modest even in C1498-ICV-6h – immunized animals.

Interestingly, our results also showed that CD40L expression on splenic CD4+ T cells is rather undetectable in the mice immunized with C1498-ICV-6h (**Figure 3.14D**).

Our general understanding is that pre-activated cytotoxic CD8+ T cells become tolerant if activated CD4+ T cells do not relay help via CD40/CD40L signalling axis with cDCs [226, 227]. The strength and length of this CD40/CD40L interaction between CD4+ T cells and cDCs respectively is indispensable to the maintenance of the high level of CD8+ T cell activation (with increased IFN-ɣ production) and long-term survival [228-230].

Based on these facts, we believe the poor cytotoxicity of T cells upon immunization with C1498-ICV could be explained by the fact that CD40L expression on splenic CD4+ T cells is rather undetectable after vaccination (**Figure 3.14D**).

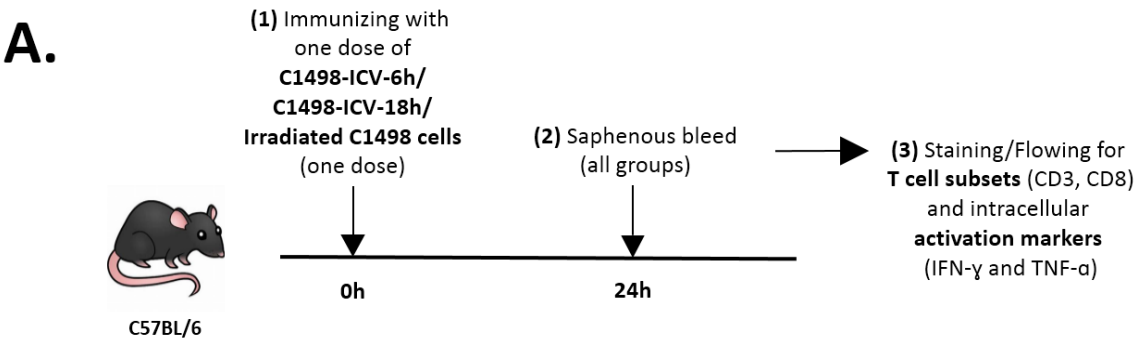
A.
(1) Immunizing with one dose of C1498-ICV-6h/ C1498-ICV-18h/ Irradiated C1498 cells (one dose)
(2) Saphenous bleed (all groups)
(3) Staining/Flowing for T cell subsets (CD3, CD8) and intracellular activation markers (IFN-ɣ and TNF-α)
C57BL/6
0h
24h

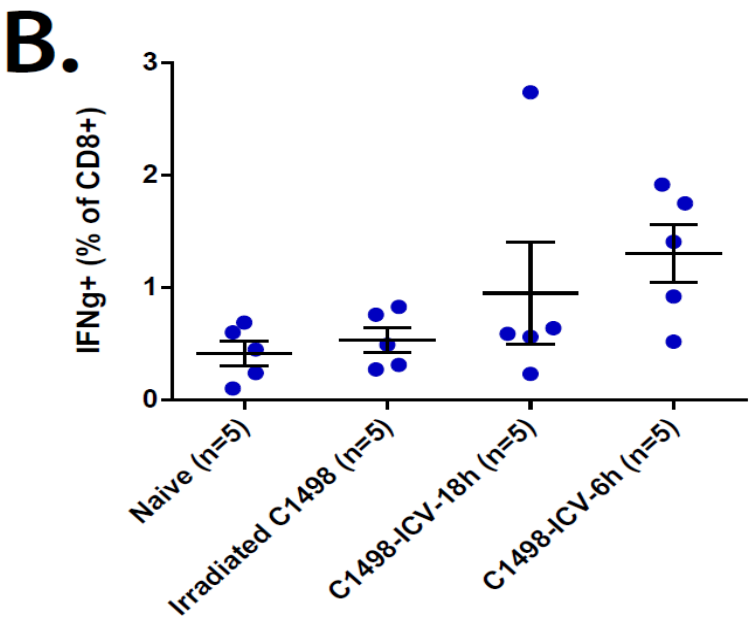
B.
IFNg+ (% of CD8+)
3
2
1
0
Naive (n=5)
Irradiated C1498 (n=5)
C1498-ICV-18h (n=5)
C1498-ICV-6h (n=5)

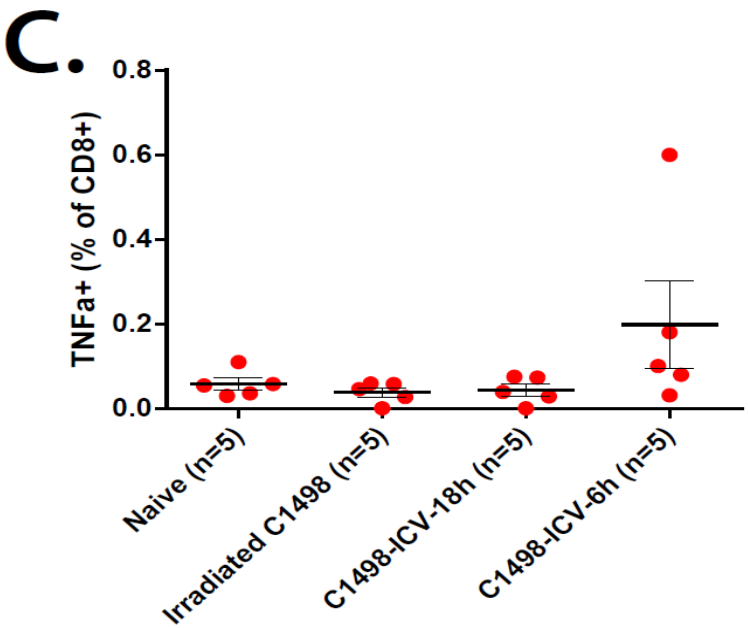
C.
TNFa+ (% of CD8+)
0.8
0.6
0.4
0.2
0.0
Naive (n=5)
Irradiated C1498 (n=5)
C1498-ICV-18h (n=5)
C1498-ICV-6h (n=5)

Figure 3.15: T cells retain a detectable level of activation after one week since the administration of one dose of C1498-ICV.

(A) The experimental outline for determining the activation level of peripheral CD8α+ T cells in C57BL/6 mice after immunization with one dose of C1498-ICV. Naïve C57BL/6 mice were either untreated or treated with irradiated C1498 cells, C1409-ICV-18h or C1498-ICV-6h. A week after the first treatment mice were saph bleed and assayed for **(B)** IFN-ɣ and **(C)** TNFα expression levels on CD8α+ T cell population. Results were acquired using LSR Fortessa and are shown as percent CD8α+ T cells that are positive for both IFN-ɣ and TNFα.

Chapter 4 – General discussion, shortcoming, future directions and concluding remarks

Current available treatments for leukemia have limited success in achieving long lasting remissions. One main reason for this is the immune escape of small populations of cancer cells that can lead to relapse. Novel treatments based on immunotherapy could be more advantageous as they aim to train the patient's immune system to recognize and kill cancer cells. Unfortunately, not all patients respond to immunotherapy. For example, treatment with immune checkpoint inhibitors (ICI) shows best results for melanoma cases, considering that 22.2% of patients receiving a combination of two ICIs achieve a complete response [231]. Lack of patient response to ICIs may be attributed to tumors not expressing immune checkpoints or simply not being infiltrated with T cells [232]. Therefore, in order to maximize the odds of success, it would be beneficial to combine immunotherapies targeting different mechanisms used by cancers for immune escape.

OVs have previously shown synergy with cancer immunotherapy [233]. Despite being effective in some cancer types, MG1 was inefficient in controlling disseminated ALL in mice [196]. Strikingly, when mice with early disseminated ALL were treated with 3 weekly doses of virus-infected and ɣ-irradiated L1210 cells (L1210-ICV), 50% of animals survived long-term after challenge with viable L1210 cells [196]. When this same ICV was given to naïve mice before challenge with ALL (prophylactic vaccination), over 90% of the mice subsequently rejected the tumor. This is suggesting that the ICV has a great potential in becoming a personalized treatment option. Personalized vaccines have a promising therapeutic perspective because they can expose cancer neo-antigens that prime the patients' immune system in recognizing and targeting the malignant tissue [234].

In this thesis, I explore the efficacy and mechanisms of ICV in two murine leukemia models, ALL (L1210) and AML (C1498). Since prophylactic vaccination was very efficient for the ALL model, the same ICV formulation and regiment in a different blood cancer model was attempted. Although we could reproduce previous findings of the ALL model and show rejection of the tumor in the majority of mice (**Figure 3.1**),

survival for the AML was poor by comparison (**Figure 3.2**). One main difference between the models was susceptibility to OV infection, with C1498 cells being much less viable compared to L1210 after an 18 hour-long MG1 infection (**Figure 3.4**). Rapid loss in viability was previously shown in C1498 using a different OV [184]. Performing a time course experiment on viability after infection demonstrated that C1498 cells were well infected and remained viable after 6 hours of infection (**Figure 3.6**). Since previous findings showed that apoptotic and necrotic cells make less effective vaccines [196], comparing a C1498-ICV infected for 18 hours (necrotic) and a C1498-ICV infected for 6 hours (viable) was relevant in the context of our prophylactic model. Indeed, our data revealed that mice pre-immunized with a more viable C1498-ICV was able to modestly improved their survival after challenge with viable C1498 cells (**Figure 3.7**), highlighting the fact that the viability of the *in vitro* infected leukemia cells partly contributes to the protective effect of ICV.

While differences in the susceptibility of cancer cell lines to virus infection were previously reported [235], the reasons for this are not always clear. To understand and explain the high susceptibility of C1498 cells to rhabdovirus infection, we decided to characterize the transcriptomic profiles of L1210 and C1498 cells lines before and after MG1 infection using RNA sequencing. Our transcriptomic analysis of L1210 and C1498 leukemia cells revealed several striking differences. First, we determined that C1498 cells fail to induce an anti-viral state through type I IFN signaling (or IRF3 activity) upon infection with virus (**Figure 3.8**). The opposite is true for L1210 cells that seem to respond to *in vitro* virus infection by upregulating type I IFN and ISGs, like other cancer cell lines. We believe that the inability of C1498 cells to induce an antiviral state could be a possible explanation for their susceptibility to OVs leading to rapid decrease in cell viability after MG1 infection. Although this experiment revealed striking results, it could benefit from the inclusion of additional controls. First, it is important to control for the effect of the vehicle. Namely, virus preps were reconstituted in DPBS which was used to infect the cells. While DPBS is not known to have any physiological effect on cells this control is nevertheless important to account for accidental contamination of the vehicle. Secondly, while we are sequencing infected cells, the in vivo ICV prep also contains an irradiation step. To account for irradiation and to get a better understanding of the

transcriptomic state of ICV cells *in vivo*, additional samples that include irradiation must be sequenced with RNA-seq.

Because transcriptome sequencing provides a global overview of gene expression, we have also looked for factors which may affect the immunogenicity of our ICV models. Interestingly, all mouse cancer models, with the exception of C1498 cells, upregulated MHC class I and PD-L1 genes (**Figure 3.10** and **Figure 3.11**). Since interferon is known to upregulate both MHC class I and PD-L1 [236], lack of such upregulation in C1498 cells can be caused by the absence of interferon upon viral infection in this model. Nevertheless, both L1210 and C1498 cells are expressing MHC I molecules to a level that is comparable to other cancer and normal cells.

Next, we showed that L1210 cells produce several pro-inflammatory cytokines upon viral infection, namely TNF-α (**Figure 3.9**). It has been previously shown that TNF-α pro-inflammatory cytokine often contributes in controlling the growth of malignant cells when highly present in tumour microenvironment [237]. Besides L1210 cells, TNF-α expression is induced in all murine cancer cell lines after MG1 infection but not in C1498 cells (**Figure 3.9A** and **B**, **top**). In fact, MG1-infected C1498 cells are not producing many other pro-inflammatory Cxcl cytokines and Ccl chemokines involved in activation and recruitment of leukocytes in an inflammatory state. For instance, we showed at both transcriptome and protein level that L1210 cells but not C1498 cells upregulate the expression of the chemotactic Ccl5 (RANTES) cytokine/chemokine upon MG1 infection (**Figure 3.9A** and **C**). It is commonly known that Ccl5 recruits granulocytes and T cells to inflammatory sites and promotes activation of NK cells in cooperation with IL-2 and IFN-ɣ produced by activated lymphocytes [238]. We consider that the weak protective effect from AML progression in C1498-ICV pre-immunized mice could be partially attributed to the insignificant production of chemotactic cytokines/chemokines like Ccl5 *in vivo*. This could possibly result in a limited recruitment or activation of various immune cell populations in the proximity of the administered ICV, making the encounter of host immune system with leukemia-specific antigens less probable.

Another immunogenic feature that L1210 cells acquire after MG1 infection is enhanced expression of CD40 (**Figure 3.11A** and **B**), which was shown to be beneficial for the treatment outcome of childhood B cell ALL [218]. Moreover, a study analyzing the immunogenicity of several isolated L1210 sub-clones determined that sub-clones that lacked or lost expression of CD40 and B7 molecules were tumorigenic and capable of establishing leukemia *in vivo*. [239]. The fact that MG1 infection induces the expression of CD40 on the surface of the entire L1210 cell population could also contribute to their incredible potential as an ICV to generate a robust immune response against murine ALL.

Our data also clearly indicates that L1210 cells highly upregulate PD-L1 and PD-1 upon MG1 infection (Figure 3.11A). It has been recently demonstrated that when the suppressive ligand (PD-L1) and the suppressive receptor (PD-1) are both highly expressed on the same cancer cell, they are likely to interact with each other in *cis* [219]. This implies that cancer cell-intrinsic PD-L1 is unable to interact in *trans* with healthy T cell-intrinsic PD-1, resulting in repression of the canonical PD-1/PD-L1 inhibitory signaling. Therefore, it is possible that the co-expression of PD-1 and PD-L1 on L1210 cells upon infection (**Figure 3.11B**) actually contributes to the immunogenicity of the vaccine and partially to its protective effect against murine ALL in the context of our prophylactic model.

Interestingly, the RNA sequencing data shows that unlike MG1-infected L1210 cells, C1498 cells express PD-L1 at detectable levels prior to infection (**Figure 3.11A**). Thus, the poor prophylactic efficacy of C1498-ICV of immunized C57BL/6 mice could be attributed to this immune suppressing phenotype, whereby C1498 render the cytotoxic T cells anergic and tolerant to C1498-specific antigens due to the PD-L1 expression. On the same note, a research team showed that PD-L1 expression increases significantly on C1498 cells after *in vivo* inoculation and provided compelling evidence that C1498 cells prevent the formation of a strong immune response against AML by promoting PD-1/PD-L1 inhibitory signalling [146]. Moreover, our data indicates that MG1 infection also boosts the expression of CTLA-4, another inhibitory receptor on C1498 cells (**Figure 3.11A**), which can induce T cell tolerance [138] by outcompeting

the stimulatory T cell co-receptor CD28 on T cell subsets for the CD80/86 ligands on activated APCs [136, 137]. A study that was characterizing the *in vivo* CD8+ T cell response induced by C1498/B7-1 cells in a subcutaneous model showed that mice have a delayed C1498/B7-1 tumour growth and an overall increased tumour-free survival after blocking CTLA-4 *in vivo* [240].

In the light of these findings, we set to characterize the *in vivo* efficacy of C1498-ICV when pre-immunizations are combined with an *in vivo* blockade of checkpoints CTLA-4 and PD-L1. Our data shows that pre-immunizing mice with viable C1498-ICV-6h while blocking PD-L1 and CTLA-4 leads to an overall better survival outcome (40%) after C1498 challenge compared to unimmunized mice and even to animals that received C1498-ICV-6h pre-treatment in absence of PD-L1 and CTLA-4 inhibition (**Figure 3.11C**). These results generally outline that *in vitro* infection of C1498 cells with MG1 in the process of ICV preparation does not sufficiently enhance the immunogenicity of the vaccine, but its protective efficacy and ability to generate a stronger anti-tumour immunity could be improved with the use of checkpoint inhibitors.

Overall, our mining of RNA sequencing data revealed several immunogenic features of L1210-ICV and mechanisms of immune evasion employed by C1498 cells. To better understand the implication of L1210-ICV and/or C1498-ICV pre-immunizations in the anti-tumour immune response priming *in vivo*, we decided to assess the level of splenic cDC maturation and T cell activation after immunization. We determined that both DBA/2 and C57BL/6 mice immunized with one dose of L1210-ICV and C1498-ICV respectively, induce the expression of CD86 co-stimulatory ligand on cDC population (**Figure 3.13A** and **C)**. This implies that pre-immunization with either L1210-ICV or C1498-ICV induces maturation of cDC population which could interact with CD28 stimulatory T cell co-receptor and theoretically contribute to generation and proliferation of virus- and/or leukemia-specific CD8+ T cells. Our flow cytometry data suggests that splenic T cell populations of both unimmunized DBA/2 and C57BL/6 mice show high levels of CD28 expression that did not seem to change after administration of one dose of either L1210-ICV or C1498-ICV correspondingly (**Figure 3.13 B** and **D**). This result is in agreement with current literature, as CD28 protein is

highly abundant on the surface of resting CD4+ and 50% of CD8+ T cells [241]. This means that signaling via CD28-CD80/86 is likely regulated at the level of the co-stimulatory ligand CD80/86 expression on cDCs upon activation rather than at the level of the T cell co-receptor. It would have been valuable to assess the expression of CTLA-4 inhibitory co-receptor on splenic CD4+ T cells after ICV, since it is typically upregulated in T cells only upon activation [242]. The CTLA-4 inhibitory receptor binds the CD80/86 co-stimulatory ligands on APCs with a higher affinity than CD28 stimulatory T cell co-receptor, thus disrupting the T cell co-stimulatory signal transduction and inducing T cell tolerance [243]. Altogether, our results showing an increase in CD86+ cDCs frequency are encouraging, but perhaps insufficient to affirm that a long-lasting cytotoxic T cell response is actually induced after immunization with either L1210-ICV or C1498-ICV. However, we can speculate that the inability of C1498-ICV to generate strong anti-tumour immunity could be due to a significant induction of CTLA-4 on helper T cells as a result of vaccination. We were also unable to define the implication the CD86+ cDC in priming of the leukemia-specific immune response after immunization with ICV. The data from a follow-up experiment showed that the expression of CD86 on cDCs was induced at a similar level in both DBA/2 and C57BL/6 pre-immunized with MG1 virus alone (not shown). This implies that the virus in ICV is responsible for the increase in splenic CD86+ cDCs in both models

The *in vivo* expression of CD40 stimulatory co-receptor on cDCs and induction of CD40L co-stimulatory ligand on helper T cell population was also characterized in context of immunization with both L1210-ICV and C1498-ICV. In murine systems, DCs normally upregulate the level of CD40 expression upon encountering certain pathogens [169, 244]. Surprisingly, our data revealed that the expression of CD40 stimulatory co-receptor did not change significantly in either DBA/2 or C57BL/6 mice after immunization with L1210-ICV or C1498-ICV respectively (**Figure 3.14A** and **C** and Supplementary Figure 8). Nevertheless, other studies determined that the expression of the stimulatory co-receptor CD40 tends to be low and constitutive on the surface of both activated and inactivated DCs [245], which seems to support our observations. It is commonly known however, that the interaction between the constitutively expressed CD40 receptor on cDCs and the CD40L ligand expressed on CD4+ T cells exclusively

upon activation is critical to the formation of an effective and long-lasting cytotoxic T cell response [230]. Our general understanding is that the formation of a CTL response against vaccines and tumours depends on antigen cross-presentation [246]. The TCR of a naïve CD8+ T cell clone recognizing an antigen loaded on the DCs' MHC I become cytotoxic with co-stimulation. However, the antigen-specific CD8+ T cells are rendered tolerant when not receiving corresponding CD4+ T cell-derived help signals during priming [226, 227]. Help is relayed to cytotoxic T cells via the interaction of CD40L on the activated CD4+ T cells and CD40 receptor on DCs [228, 229]. This interaction is known to maintain activity and survival of the effector and memory CD8+ T cells as well [230]. It was repeatedly demonstrated that C1498.SIY leukemia cells induce peripheral tolerance in mice by disrupting the accumulation of antigen-specific cytotoxic T cells when administered IV. This research team also showed that the antigen-specific T cell tolerance established in AML-bearing mice can be resolved when treating with agonistic anti-CD40 antibodies [223]. Our results show that administration of L1210-ICV but not C1498-ICV induces the expression of CD40L on CD4+ T cell population (**Figure 3.13B** and **D** and **Supplementary Figure 8**). This means that the inability of C1498-ICV to induce strong anti-tumour immunity *in vivo* is because MG1 pre-infection seems unable to overcome the ability of these leukemia cells to establish T cell tolerance. An important caveat of this experiment is the different mouse backgrounds from which the respective leukemia models come from. Different genetic backgrounds have different immune systems which affects the interplay between anti-tumor immune response and antiviral response. To account for this, tumor models from the same background need to be used, for example comparing C1498 to EL4.

Future directions and addressing shortcomings

Several of our observations regarding the success of ICV as an immunotherapy in targeting leukemia can be further explored with additional experiments. Although we showed that C1498 cells do not respond to viral infection by not producing IFN-β, it has not been yet tested whether they can respond to type I IFN. Answering this question

could be important, considering that mouse immune cells may respond to the rhabdovirus contained in every administered ICV dose by producing IFN *in viv*o. In this scenario, the potential IFN signaling in a paracrine manner could induce changes in the phenotype of C1498 cells that may be worth exploring.

Pre-treatment of C1498 cells with interferon and looking at ISG production and resistance to viral infection can help answer this question. Another question is whether C1498 cells only fail to produce interferon during dsRNA virus infection or also after encountering DNA viruses. Since different receptors recognize different patterns, we could transfect C1498 cells with immunogenic HT-DNA and assess the production of interferon and ISGs. This could potentially tell us if the defect in the antiviral response signalling is at the level of pattern recognition or in the downstream phosphorylation cascade that leads to IRF3 activation and transcription of interferon and ISGs.

The next important unresolved question is defining the implication of interferon signalling and pro-inflammatory cytokines production to the success of L1210-ICV in generating robust anti-tumour immunity. One way of addressing this is to create L1210 knockouts for IFNAR, IRF3 and other genes involved in the interferon pathway. This way we will be able to produce ICVs using the corresponding L1210 cell knockouts and attribute the role of type I IFN signaling in the immunogenicity and efficacy of the vaccine *in vivo*. A simpler way to approach this question is to compare the phenotype and/or *in vivo* efficacy of the L1210-ICV with a vaccine in which L1210 cells are pre-treated *in vitro* with either recombinant IFN-β or TNF-α. Similarly, the implication of CD40 upregulation observed on L1210 cells upon MG1 infection can be defined by comparing the protective efficacy of the L1210-ICV with an ICV prepared by using L1210 cells in which CD40 gene is knocked out with Crispr/Cas9 or knocked down with siRNA.

It is also important to further explore the *in vivo* immune response induced after immunization with L1210-ICV and/or C1498-ICV. Previous work done in our lab showed that *in vivo* depletion of the CD4+ T cell subset prior L1210-ICV immunizations significantly diminished the survival of mice [197], implying that T cell help is essential for the ICV to establish a robust anti-tumour immune response. Interestingly, our results highlight the ability of L1210-ICV (but not C1498-ICV) to induce CD40L expression on

CD4+ T cells shortly after vaccine administration (**Figure 3.13B** and **D**). A follow up experiment blocking CD40/CD40L signaling would tell us if CD40L expression on CD4 T cells is critical in inducing anti-L1210 immune response during ICV. Among other things, cytokine signaling has been implicated in upregulating CD40L on CD4 T cells [247]. Evaluating serum cytokine profiles after ICV treatment would tell us which cytokines are induced after L1210-ICV but not C1498-ICV. This short list can then be screened by co-administering recombinant forms of these cytokines with C1498-ICV, assessing possible changes in CD40L expression along with potential improvements in survival. The cytokines which improve the immunogenicity of C1498-ICV can then be cloned into this cell line using a viral vector to determine if their expression can improve the prophylactic efficacy of the C1498-ICV *in vivo*.

References

1. Boulais, P.E. and P.S. Frenette, *Making sense of hematopoietic stem cell niches.* Blood, 2015. **125**(17): p. 2621-9.
2. Till, J.E. and C.E. Mc, *A direct measurement of the radiation sensitivity of normal mouse bone marrow cells.* Radiat Res, 1961. **14**: p. 213-22.
3. Becker, A.J., C.E. Mc, and J.E. Till, *Cytological demonstration of the clonal nature of spleen colonies derived from transplanted mouse marrow cells.* Nature, 1963. **197**: p. 452-4.
4. Wu, A.M., et al., *A cytological study of the capacity for differentiation of normal hemopoietic colony-forming cells.* J Cell Physiol, 1967. **69**(2): p. 177-84.
5. Siminovitch, L., E.A. McCulloch, and J.E. Till, *The Distribution of Colony-Forming Cells among Spleen Colonies.* J Cell Comp Physiol, 1963. **62**: p. 327-36.
6. Morrison, S.J. and J. Kimble, *Asymmetric and symmetric stem-cell divisions in development and cancer.* Nature, 2006. **441**(7097): p. 1068-74.
7. Manz, M.G., et al., *Prospective isolation of human clonogenic common myeloid progenitors.* Proc Natl Acad Sci U S A, 2002. **99**(18): p. 11872-7.
8. Notta, F., et al., *Distinct routes of lineage development reshape the human blood hierarchy across ontogeny.* Science, 2016. **351**(6269): p. aab2116.
9. Buenrostro, J.D., et al., *Integrated Single-Cell Analysis Maps the Continuous Regulatory Landscape of Human Hematopoietic Differentiation.* Cell, 2018. **173**(6): p. 1535-1548 e16.
10. Bergiers, I., et al., *Single-cell transcriptomics reveals a new dynamical function of transcription factors during embryonic hematopoiesis.* Elife, 2018. **7**.
11. Copley, M.R., P.A. Beer, and C.J. Eaves, *Hematopoietic stem cell heterogeneity takes center stage.* Cell Stem Cell, 2012. **10**(6): p. 690-697.
12. Crisan, M. and E. Dzierzak, *The many faces of hematopoietic stem cell heterogeneity.* Development, 2016. **143**(24): p. 4571-4581.
13. Lanzkron, S.M., M.I. Collector, and S.J. Sharkis, *Hematopoietic stem cell tracking in vivo: a comparison of short-term and long-term repopulating cells.* Blood, 1999. **93**(6): p. 1916-21.
14. Iscove, N.N. and K. Nawa, *Hematopoietic stem cells expand during serial transplantation in vivo without apparent exhaustion.* Curr Biol, 1997. **7**(10): p. 805-8.
15. Spangrude, G.J., S. Heimfeld, and I.L. Weissman, *Purification and characterization of mouse hematopoietic stem cells.* Science, 1988. **241**(4861): p. 58-62.
16. Harrison, D.E. and R.K. Zhong, *The same exhaustible multilineage precursor produces both myeloid and lymphoid cells as early as 3-4 weeks after marrow transplantation.* Proc Natl Acad Sci U S A, 1992. **89**(21): p. 10134-8.
17. Morrison, S.J., et al., *Identification of a lineage of multipotent hematopoietic progenitors.* Development, 1997. **124**(10): p. 1929-39.
18. Kondo, M., I.L. Weissman, and K. Akashi, *Identification of clonogenic common lymphoid progenitors in mouse bone marrow.* Cell, 1997. **91**(5): p. 661-72.
19. Yamamoto, R., et al., *Clonal analysis unveils self-renewing lineage-restricted progenitors generated directly from hematopoietic stem cells.* Cell, 2013. **154**(5): p. 1112-1126.

20. Pietras, E.M., et al., *Functionally Distinct Subsets of Lineage-Biased Multipotent Progenitors Control Blood Production in Normal and Regenerative Conditions.* Cell Stem Cell, 2015. **17**(1): p. 35-46.
21. Na Nakorn, T., et al., *Myeloerythroid-restricted progenitors are sufficient to confer radioprotection and provide the majority of day 8 CFU-S.* J Clin Invest, 2002. **109**(12): p. 1579-85.
22. Lee, J.H., et al., *Brief Report: Human Acute Myeloid Leukemia Reprogramming to Pluripotency Is a Rare Event and Selects for Patient Hematopoietic Cells Devoid of Leukemic Mutations.* Stem Cells, 2017. **35**(9): p. 2095-2102.
23. Downing, J.R., et al., *Alterations of the AML1 transcription factor in human leukemia.* Semin Cell Dev Biol, 2000. **11**(5): p. 347-60.
24. Sun, X.J., et al., *A stable transcription factor complex nucleated by oligomeric AML1-ETO controls leukaemogenesis.* Nature, 2013. **500**(7460): p. 93-7.
25. Miyamoto, T., et al., *Persistence of multipotent progenitors expressing AML1/ETO transcripts in long-term remission patients with t(8;21) acute myelogenous leukemia.* Blood, 1996. **87**(11): p. 4789-96.
26. Miyamoto, T., I.L. Weissman, and K. Akashi, *AML1/ETO-expressing nonleukemic stem cells in acute myelogenous leukemia with 8;21 chromosomal translocation.* Proc Natl Acad Sci U S A, 2000. **97**(13): p. 7521-6.
27. Bonnet, D. and J.E. Dick, *Human acute myeloid leukemia is organized as a hierarchy that originates from a primitive hematopoietic cell.* Nat Med, 1997. **3**(7): p. 730-7.
28. Delaunay, J., et al., *Prognosis of inv(16)/t(16;16) acute myeloid leukemia (AML): a survey of 110 cases from the French AML Intergroup.* Blood, 2003. **102**(2): p. 462-9.
29. Marlton, P., et al., *Cytogenetic and clinical correlates in AML patients with abnormalities of chromosome 16.* Leukemia, 1995. **9**(6): p. 965-71.
30. Tirado, C.A., et al., *Acute myeloid leukemia with inv(16) with CBFB-MYH11, 3'CBFB deletion, variant t(9;22) with BCR-ABL1, and del(7)(q22q32) in a pediatric patient: case report and literature review.* Cancer Genet Cytogenet, 2010. **200**(1): p. 54-9.
31. Bloomfield, C.D., et al., *Frequency of prolonged remission duration after high-dose cytarabine intensification in acute myeloid leukemia varies by cytogenetic subtype.* Cancer Res, 1998. **58**(18): p. 4173-9.
32. Cho, E.K., et al., *Prognostic value of AML 1/ETO fusion transcripts in patients with acute myelogenous leukemia.* Korean J Intern Med, 2003. **18**(1): p. 13-20.
33. Prebet, T., et al., *Acute myeloid leukemia with translocation (8;21) or inversion (16) in elderly patients treated with conventional chemotherapy: a collaborative study of the French CBF-AML intergroup.* J Clin Oncol, 2009. **27**(28): p. 4747-53.
34. Burnett, A.K., et al., *A comparison of low-dose cytarabine and hydroxyurea with or without all-trans retinoic acid for acute myeloid leukemia and high-risk myelodysplastic syndrome in patients not considered fit for intensive treatment.* Cancer, 2007. **109**(6): p. 1114-24.
35. Marcucci, G., et al., *Prognostic factors and outcome of core binding factor acute myeloid leukemia patients with t(8;21) differ from those of patients with inv(16): a Cancer and Leukemia Group B study.* J Clin Oncol, 2005. **23**(24): p. 5705-17.
36. Singh, Z.N., et al., *Therapy-related myelodysplastic syndrome: morphologic subclassification may not be clinically relevant.* Am J Clin Pathol, 2007. **127**(2): p. 197-205.
37. McNerney, M.E., L.A. Godley, and M.M. Le Beau, *Therapy-related myeloid neoplasms: when genetics and environment collide.* Nat Rev Cancer, 2017. **17**(9): p. 513-527.

38. Rowley, J.D. and H.J. Olney, *International workshop on the relationship of prior therapy to balanced chromosome aberrations in therapy-related myelodysplastic syndromes and acute leukemia: overview report.* Genes Chromosomes Cancer, 2002. **33**(4): p. 331-45.
39. Smith, S.M., et al., *Clinical-cytogenetic associations in 306 patients with therapy-related myelodysplasia and myeloid leukemia: the University of Chicago series.* Blood, 2003. **102**(1): p. 43-52.
40. Leone, G., L. Fianchi, and M.T. Voso, *Therapy-related myeloid neoplasms.* Curr Opin Oncol, 2011. **23**(6): p. 672-80.
41. Mauritzson, N., et al., *Pooled analysis of clinical and cytogenetic features in treatment-related and de novo adult acute myeloid leukemia and myelodysplastic syndromes based on a consecutive series of 761 patients analyzed 1976-1993 and on 5098 unselected cases reported in the literature 1974-2001.* Leukemia, 2002. **16**(12): p. 2366-78.
42. Kayser, S., et al., *The impact of therapy-related acute myeloid leukemia (AML) on outcome in 2853 adult patients with newly diagnosed AML.* Blood, 2011. **117**(7): p. 2137-45.
43. Christiansen, D.H., M.K. Andersen, and J. Pedersen-Bjergaard, *Methylation of p15INK4B is common, is associated with deletion of genes on chromosome arm 7q and predicts a poor prognosis in therapy-related myelodysplasia and acute myeloid leukemia.* Leukemia, 2003. **17**(9): p. 1813-9.
44. Churpek, J.E. and R.A. Larson, *The evolving challenge of therapy-related myeloid neoplasms.* Best Pract Res Clin Haematol, 2013. **26**(4): p. 309-17.
45. Fianchi, L., et al., *Outcome of therapy-related myeloid neoplasms treated with azacitidine.* J Hematol Oncol, 2012. **5**: p. 44.
46. Minoia, C., et al., *Azacitidine in the front-line treatment of therapy-related myeloid neoplasms: a multicenter case series.* Anticancer Res, 2015. **35**(1): p. 461-6.
47. Pileri, S.A., et al., *Myeloid sarcoma: clinico-pathologic, phenotypic and cytogenetic analysis of 92 adult patients.* Leukemia, 2007. **21**(2): p. 340-50.
48. Avni, B. and M. Koren-Michowitz, *Myeloid sarcoma: current approach and therapeutic options.* Ther Adv Hematol, 2011. **2**(5): p. 309-16.
49. Stefanidakis, M., et al., *Role of leukemia cell invadosome in extramedullary infiltration.* Blood, 2009. **114**(14): p. 3008-17.
50. Wang, C., et al., *The essential roles of matrix metalloproteinase-2, membrane type 1 metalloproteinase and tissue inhibitor of metalloproteinase-2 in the invasive capacity of acute monocytic leukemia SHI-1 cells.* Leuk Res, 2010. **34**(8): p. 1083-90.
51. Deeb, G., et al., *Genomic profiling of myeloid sarcoma by array comparative genomic hybridization.* Genes Chromosomes Cancer, 2005. **44**(4): p. 373-83.
52. Falini, B., et al., *Cytoplasmic mutated nucleophosmin (NPM) defines the molecular status of a significant fraction of myeloid sarcomas.* Leukemia, 2007. **21**(7): p. 1566-70.
53. Ansari-Lari, M.A., et al., *FLT3 mutations in myeloid sarcoma.* Br J Haematol, 2004. **126**(6): p. 785-91.
54. Lan, T.Y., et al., *Prognostic factors of treatment outcomes in patients with granulocytic sarcoma.* Acta Haematol, 2009. **122**(4): p. 238-46.
55. Almond, L.M., et al., *Myeloid Sarcoma: Presentation, Diagnosis, and Treatment.* Clin Lymphoma Myeloma Leuk, 2017. **17**(5): p. 263-267.

56. Committee, C.C.S.A. *Canadian Cancer Statistics*. 2019 [cited 2020 May]; Available from: https://www.cancer.ca/en/cancer-information/cancer-type/leukemia-acute-lymphocytic-all/prognosis-and-survival/survival-statistics/?region=on.
57. Sawyers, C.L., *Chronic myeloid leukemia.* N Engl J Med, 1999. **340**(17): p. 1330-40.
58. Liu-Dumlao, T., et al., *Philadelphia-positive acute lymphoblastic leukemia: current treatment options.* Curr Oncol Rep, 2012. **14**(5): p. 387-94.
59. Lionberger, J.M., M.B. Wilson, and T.E. Smithgall, *Transformation of myeloid leukemia cells to cytokine independence by Bcr-Abl is suppressed by kinase-defective Hck.* J Biol Chem, 2000. **275**(24): p. 18581-5.
60. Fialkow, P.J., R.J. Jacobson, and T. Papayannopoulou, *Chronic myelocytic leukemia: clonal origin in a stem cell common to the granulocyte, erythrocyte, platelet and monocyte/macrophage.* Am J Med, 1977. **63**(1): p. 125-30.
61. Roberts, K.G., et al., *Genetic alterations activating kinase and cytokine receptor signaling in high-risk acute lymphoblastic leukemia.* Cancer Cell, 2012. **22**(2): p. 153-66.
62. Fletcher, J.A., et al., *Translocation (9;22) is associated with extremely poor prognosis in intensively treated children with acute lymphoblastic leukemia.* Blood, 1991. **77**(3): p. 435-9.
63. Kantarjian, H.M., et al., *Results of treatment with hyper-CVAD, a dose-intensive regimen, in adult acute lymphocytic leukemia.* J Clin Oncol, 2000. **18**(3): p. 547-61.
64. Thomas, D.A., et al., *Treatment of Philadelphia chromosome-positive acute lymphocytic leukemia with hyper-CVAD and imatinib mesylate.* Blood, 2004. **103**(12): p. 4396-407.
65. Thomas, D.A., et al., *Chemoimmunotherapy with a modified hyper-CVAD and rituximab regimen improves outcome in de novo Philadelphia chromosome-negative precursor B-lineage acute lymphoblastic leukemia.* J Clin Oncol, 2010. **28**(24): p. 3880-9.
66. Jones, D., et al., *Kinase domain point mutations in Philadelphia chromosome-positive acute lymphoblastic leukemia emerge after therapy with BCR-ABL kinase inhibitors.* Cancer, 2008. **113**(5): p. 985-94.
67. Porkka, K., et al., *Dasatinib crosses the blood-brain barrier and is an efficient therapy for central nervous system Philadelphia chromosome-positive leukemia.* Blood, 2008. **112**(4): p. 1005-12.
68. Ravandi, F., et al., *Long-term follow-up of a phase 2 study of chemotherapy plus dasatinib for the initial treatment of patients with Philadelphia chromosome-positive acute lymphoblastic leukemia.* Cancer, 2015. **121**(23): p. 4158-64.
69. Foa, R., et al., *Dasatinib as first-line treatment for adult patients with Philadelphia chromosome-positive acute lymphoblastic leukemia.* Blood, 2011. **118**(25): p. 6521-8.
70. Romana, S.P., et al., *High frequency of t(12;21) in childhood B-lineage acute lymphoblastic leukemia.* Blood, 1995. **86**(11): p. 4263-9.
71. Golub, T.R., et al., *Involvement of the TEL gene in hematologic malignancy by diverse molecular genetic mechanisms.* Curr Top Microbiol Immunol, 1996. **211**: p. 279-88.
72. Wiemels, J.L., et al., *Prenatal origin of acute lymphoblastic leukaemia in children.* Lancet, 1999. **354**(9189): p. 1499-503.
73. Hjalgrim, L.L., et al., *Presence of clone-specific markers at birth in children with acute lymphoblastic leukaemia.* Br J Cancer, 2002. **87**(9): p. 994-9.
74. Mori, H., et al., *Chromosome translocations and covert leukemic clones are generated during normal fetal development.* Proc Natl Acad Sci U S A, 2002. **99**(12): p. 8242-7.
75. Zuna, J., et al., *TEL/AML1 positivity in childhood ALL: average or better prognosis? Czech Paediatric Haematology Working Group.* Leukemia, 1999. **13**(1): p. 22-4.

76. Bell, J.J. and A. Bhandoola, *The earliest thymic progenitors for T cells possess myeloid lineage potential.* Nature, 2008. **452**(7188): p. 764-7.
77. Coustan-Smith, E., et al., *Early T-cell precursor leukaemia: a subtype of very high-risk acute lymphoblastic leukaemia.* Lancet Oncol, 2009. **10**(2): p. 147-56.
78. Jain, N., et al., *Early T-cell precursor acute lymphoblastic leukemia/lymphoma (ETP-ALL/LBL) in adolescents and adults: a high-risk subtype.* Blood, 2016. **127**(15): p. 1863-9.
79. Neumann, M., et al., *Clinical and molecular characterization of early T-cell precursor leukemia: a high-risk subgroup in adult T-ALL with a high frequency of FLT3 mutations.* Blood Cancer J, 2012. **2**(1): p. e55.
80. Neumann, M., et al., *Whole-exome sequencing in adult ETP-ALL reveals a high rate of DNMT3A mutations.* Blood, 2013. **121**(23): p. 4749-52.
81. Pui, C.H., et al., *Improved prognosis for older adolescents with acute lymphoblastic leukemia.* J Clin Oncol, 2011. **29**(4): p. 386-91.
82. van Dongen, J.J., et al., *Minimal residual disease diagnostics in acute lymphoblastic leukemia: need for sensitive, fast, and standardized technologies.* Blood, 2015. **125**(26): p. 3996-4009.
83. Barrett, A.J., *Understanding and harnessing the graft-versus-leukaemia effect.* Br J Haematol, 2008. **142**(6): p. 877-88.
84. Barrett, A.J. and K. Le Blanc, *Immunotherapy prospects for acute myeloid leukaemia.* Clin Exp Immunol, 2010. **161**(2): p. 223-32.
85. Barnes, D.W., et al., *Treatment of murine leukaemia with X rays and homologous bone marrow; preliminary communication.* Br Med J, 1956. **2**(4993): p. 626-7.
86. Weiden, P.L., et al., *Antileukemic effect of graft-versus-host disease in human recipients of allogeneic-marrow grafts.* N Engl J Med, 1979. **300**(19): p. 1068-73.
87. Kolb, H.J., et al., *Donor leukocyte transfusions for treatment of recurrent chronic myelogenous leukemia in marrow transplant patients.* Blood, 1990. **76**(12): p. 2462-5.
88. Kolb, H.J., et al., *Graft-versus-leukemia reactions in allogeneic chimeras.* Blood, 2004. **103**(3): p. 767-76.
89. Van Hoeven, N., et al., *A Formulated TLR7/8 Agonist is a Flexible, Highly Potent and Effective Adjuvant for Pandemic Influenza Vaccines.* Sci Rep, 2017. **7**: p. 46426.
90. Shi, Z., et al., *A novel Toll-like receptor that recognizes vesicular stomatitis virus.* J Biol Chem, 2011. **286**(6): p. 4517-24.
91. Lynn, G.M., et al., *Impact of Polymer-TLR-7/8 Agonist (Adjuvant) Morphology on the Potency and Mechanism of CD8 T Cell Induction.* Biomacromolecules, 2019. **20**(2): p. 854-870.
92. Georgana, I., et al., *Virulent Poxviruses Inhibit DNA Sensing by Preventing STING Activation.* J Virol, 2018. **92**(10).
93. Su, T., et al., *STING activation in cancer immunotherapy.* Theranostics, 2019. **9**(25): p. 7759-7771.
94. Curran, E., et al., *STING Pathway Activation Stimulates Potent Immunity against Acute Myeloid Leukemia.* Cell Rep, 2016. **15**(11): p. 2357-66.
95. Zhu, Y., et al., *STING: a master regulator in the cancer-immunity cycle.* Mol Cancer, 2019. **18**(1): p. 152.
96. Sistigu, A., et al., *Cancer cell-autonomous contribution of type I interferon signaling to the efficacy of chemotherapy.* Nat Med, 2014. **20**(11): p. 1301-9.
97. Mittal, D., et al., *New insights into cancer immunoediting and its three component phases--elimination, equilibrium and escape.* Curr Opin Immunol, 2014. **27**: p. 16-25.

98. Fucikova, J., et al., *Prognostic and Predictive Value of DAMPs and DAMP-Associated Processes in Cancer.* Front Immunol, 2015. **6**: p. 402.
99. Galluzzi, L., et al., *Immunogenic cell death in cancer and infectious disease.* Nat Rev Immunol, 2017. **17**(2): p. 97-111.
100. Obeid, M., et al., *Calreticulin exposure dictates the immunogenicity of cancer cell death.* Nat Med, 2007. **13**(1): p. 54-61.
101. Yarchoan, M., et al., *Targeting neoantigens to augment antitumour immunity.* Nat Rev Cancer, 2017. **17**(4): p. 209-222.
102. Rajasagi, M., et al., *Systematic identification of personal tumor-specific neoantigens in chronic lymphocytic leukemia.* Blood, 2014. **124**(3): p. 453-62.
103. Lu, Y.C. and P.F. Robbins, *Cancer immunotherapy targeting neoantigens.* Semin Immunol, 2016. **28**(1): p. 22-7.
104. Jiang, T., et al., *Tumor neoantigens: from basic research to clinical applications.* J Hematol Oncol, 2019. **12**(1): p. 93.
105. Morrison, B.J., J.C. Steel, and J.C. Morris, *Reduction of MHC-I expression limits T-lymphocyte-mediated killing of Cancer-initiating cells.* BMC Cancer, 2018. **18**(1): p. 469.
106. Majzner, R.G., S. Heitzeneder, and C.L. Mackall, *Harnessing the Immunotherapy Revolution for the Treatment of Childhood Cancers.* Cancer Cell, 2017. **31**(4): p. 476-485.
107. Majzner, R.G. and C.L. Mackall, *Tumor Antigen Escape from CAR T-cell Therapy.* Cancer Discov, 2018. **8**(10): p. 1219-1226.
108. Chiang, C.L., G. Coukos, and L.E. Kandalaft, *Whole Tumor Antigen Vaccines: Where Are We?* Vaccines (Basel), 2015. **3**(2): p. 344-72.
109. Van Acker, H.H., et al., *Dendritic Cell-Based Immunotherapy of Acute Myeloid Leukemia.* J Clin Med, 2019. **8**(5).
110. Srivatsan, S., et al., *Allogeneic tumor cell vaccines: the promise and limitations in clinical trials.* Hum Vaccin Immunother, 2014. **10**(1): p. 52-63.
111. Moingeon, P., *Cancer vaccines.* Vaccine, 2001. **19**(11-12): p. 1305-26.
112. Guo, C., et al., *Therapeutic cancer vaccines: past, present, and future.* Adv Cancer Res, 2013. **119**: p. 421-75.
113. Gerlinger, M., et al., *Intratumor heterogeneity and branched evolution revealed by multiregion sequencing.* N Engl J Med, 2012. **366**(10): p. 883-892.
114. Copier, J. and A. Dalgleish, *Overview of tumor cell-based vaccines.* Int Rev Immunol, 2006. **25**(5-6): p. 297-319.
115. Ueda, R., et al., *Cell surface antigens of human renal cancer defined by autologous typing.* J Exp Med, 1979. **150**(3): p. 564-79.
116. Li, J., et al., *Whole tumor cell vaccine with irradiated S180 cells as adjuvant.* Vaccine, 2009. **27**(4): p. 558-64.
117. Deacon, D.H., et al., *The use of gamma-irradiation and ultraviolet-irradiation in the preparation of human melanoma cells for use in autologous whole-cell vaccines.* BMC Cancer, 2008. **8**: p. 360.
118. Carvalho, H.A. and R.C. Villar, *Radiotherapy and immune response: the systemic effects of a local treatment.* Clinics (Sao Paulo), 2018. **73**(suppl 1): p. e557s.
119. Eager, R. and J. Nemunaitis, *GM-CSF gene-transduced tumor vaccines.* Mol Ther, 2005. **12**(1): p. 18-27.
120. Dranoff, G., et al., *Vaccination with irradiated tumor cells engineered to secrete murine granulocyte-macrophage colony-stimulating factor stimulates potent, specific, and long-lasting anti-tumor immunity.* Proc Natl Acad Sci U S A, 1993. **90**(8): p. 3539-43.

121. Smith, B.D., et al., *K562/GM-CSF immunotherapy reduces tumor burden in chronic myeloid leukemia patients with residual disease on imatinib mesylate.* Clin Cancer Res, 2010. **16**(1): p. 338-47.
122. Lowenberg, B., et al., *Use of recombinant GM-CSF during and after remission induction chemotherapy in patients aged 61 years and older with acute myeloid leukemia: final report of AML-11, a phase III randomized study of the Leukemia Cooperative Group of European Organisation for the Research and Treatment of Cancer and the Dutch Belgian Hemato-Oncology Cooperative Group.* Blood, 1997. **90**(8): p. 2952-61.
123. Rossi, H.A., et al., *Granulocyte-macrophage colony-stimulating factor (GM-CSF) priming with successive concomitant low-dose Ara-C for elderly patients with secondary/refractory acute myeloid leukemia or advanced myelodysplastic syndrome.* Leukemia, 2002. **16**(3): p. 310-5.
124. Hutchcroft, J.E. and B.E. Bierer, *Activation-dependent phosphorylation of the T-lymphocyte surface receptor CD28 and associated proteins.* Proc Natl Acad Sci U S A, 1994. **91**(8): p. 3260-4.
125. Nurieva, R., et al., *T-cell tolerance or function is determined by combinatorial costimulatory signals.* EMBO J, 2006. **25**(11): p. 2623-33.
126. Raab, M., et al., *p56Lck and p59Fyn regulate CD28 binding to phosphatidylinositol 3-kinase, growth factor receptor-bound protein GRB-2, and T cell-specific protein-tyrosine kinase ITK: implications for T-cell costimulation.* Proc Natl Acad Sci U S A, 1995. **92**(19): p. 8891-5.
127. Patsoukis, N., et al., *Selective effects of PD-1 on Akt and Ras pathways regulate molecular components of the cell cycle and inhibit T cell proliferation.* Sci Signal, 2012. **5**(230): p. ra46.
128. Chemnitz, J.M., et al., *SHP-1 and SHP-2 associate with immunoreceptor tyrosine-based switch motif of programmed death 1 upon primary human T cell stimulation, but only receptor ligation prevents T cell activation.* J Immunol, 2004. **173**(2): p. 945-54.
129. Carter, L., et al., *PD-1:PD-L inhibitory pathway affects both CD4(+) and CD8(+) T cells and is overcome by IL-2.* Eur J Immunol, 2002. **32**(3): p. 634-43.
130. Parry, R.V., et al., *CTLA-4 and PD-1 receptors inhibit T-cell activation by distinct mechanisms.* Mol Cell Biol, 2005. **25**(21): p. 9543-53.
131. Blackburn, S.D., et al., *Coregulation of CD8+ T cell exhaustion by multiple inhibitory receptors during chronic viral infection.* Nat Immunol, 2009. **10**(1): p. 29-37.
132. Wherry, E.J., *T cell exhaustion.* Nat Immunol, 2011. **12**(6): p. 492-9.
133. Ishida, Y., et al., *Induced expression of PD-1, a novel member of the immunoglobulin gene superfamily, upon programmed cell death.* EMBO J, 1992. **11**(11): p. 3887-95.
134. Sheppard, K.A., et al., *PD-1 inhibits T-cell receptor induced phosphorylation of the ZAP70/CD3zeta signalosome and downstream signaling to PKCtheta.* FEBS Lett, 2004. **574**(1-3): p. 37-41.
135. Bennett, F., et al., *Program death-1 engagement upon TCR activation has distinct effects on costimulation and cytokine-driven proliferation: attenuation of ICOS, IL-4, and IL-21, but not CD28, IL-7, and IL-15 responses.* J Immunol, 2003. **170**(2): p. 711-8.
136. Krummel, M.F. and J.P. Allison, *CD28 and CTLA-4 have opposing effects on the response of T cells to stimulation.* J Exp Med, 1995. **182**(2): p. 459-65.
137. Walunas, T.L., C.Y. Bakker, and J.A. Bluestone, *CTLA-4 ligation blocks CD28-dependent T cell activation.* J Exp Med, 1996. **183**(6): p. 2541-50.
138. Harding, F.A., et al., *CD28-mediated signalling co-stimulates murine T cells and prevents induction of anergy in T-cell clones.* Nature, 1992. **356**(6370): p. 607-9.

139. Speiser, D.E., et al., *T cell differentiation in chronic infection and cancer: functional adaptation or exhaustion?* Nat Rev Immunol, 2014. **14**(11): p. 768-74.
140. Barbee, M.S., et al., *Current status and future directions of the immune checkpoint inhibitors ipilimumab, pembrolizumab, and nivolumab in oncology.* Ann Pharmacother, 2015. **49**(8): p. 907-37.
141. Sundar, R., et al., *Nivolumab in NSCLC: latest evidence and clinical potential.* Ther Adv Med Oncol, 2015. **7**(2): p. 85-96.
142. Hodi, F.S., et al., *Improved survival with ipilimumab in patients with metastatic melanoma.* N Engl J Med, 2010. **363**(8): p. 711-23.
143. Syn, N.L., et al., *De-novo and acquired resistance to immune checkpoint targeting.* Lancet Oncol, 2017. **18**(12): p. e731-e741.
144. Naidoo, J., D.B. Page, and J.D. Wolchok, *Immune checkpoint blockade.* Hematol Oncol Clin North Am, 2014. **28**(3): p. 585-600.
145. Ok, C.Y. and K.H. Young, *Checkpoint inhibitors in hematological malignancies.* J Hematol Oncol, 2017. **10**(1): p. 103.
146. Zhang, L., T.F. Gajewski, and J. Kline, *PD-1/PD-L1 interactions inhibit antitumor immune responses in a murine acute myeloid leukemia model.* Blood, 2009. **114**(8): p. 1545-52.
147. Zhou, Q., et al., *Coexpression of Tim-3 and PD-1 identifies a CD8+ T-cell exhaustion phenotype in mice with disseminated acute myelogenous leukemia.* Blood, 2011. **117**(17): p. 4501-10.
148. Zhou, Q., et al., *Program death-1 signaling and regulatory T cells collaborate to resist the function of adoptively transferred cytotoxic T lymphocytes in advanced acute myeloid leukemia.* Blood, 2010. **116**(14): p. 2484-93.
149. Chen, X., et al., *Clinical significance of B7-H1 (PD-L1) expression in human acute leukemia.* Cancer Biol Ther, 2008. **7**(5): p. 622-7.
150. Williams, P., et al., *The distribution of T-cell subsets and the expression of immune checkpoint receptors and ligands in patients with newly diagnosed and relapsed acute myeloid leukemia.* Cancer, 2019. **125**(9): p. 1470-1481.
151. Schnorfeil, F.M., et al., *T cells are functionally not impaired in AML: increased PD-1 expression is only seen at time of relapse and correlates with a shift towards the memory T cell compartment.* J Hematol Oncol, 2015. **8**: p. 93.
152. Zhang, M., et al., *DNA demethylation in PD-1 gene promoter induced by 5-azacytidine activates PD-1 expression on Molt-4 cells.* Cell Immunol, 2011. **271**(2): p. 450-4.
153. Kantarjian, H.M., et al., *Multicenter, randomized, open-label, phase III trial of decitabine versus patient choice, with physician advice, of either supportive care or low-dose cytarabine for the treatment of older patients with newly diagnosed acute myeloid leukemia.* J Clin Oncol, 2012. **30**(21): p. 2670-7.
154. Daver, N., et al., *Efficacy, Safety, and Biomarkers of Response to Azacitidine and Nivolumab in Relapsed/Refractory Acute Myeloid Leukemia: A Nonrandomized, Open-Label, Phase II Study.* Cancer Discov, 2019. **9**(3): p. 370-383.
155. Liao, D., et al., *A Review of Efficacy and Safety of Checkpoint Inhibitor for the Treatment of Acute Myeloid Leukemia.* Front Pharmacol, 2019. **10**: p. 609.
156. Dohner, H., et al., *Diagnosis and management of AML in adults: 2017 ELN recommendations from an international expert panel.* Blood, 2017. **129**(4): p. 424-447.
157. Zhong, R.K., et al., *CTLA-4 blockade by a human MAb enhances the capacity of AML-derived DC to induce T-cell responses against AML cells in an autologous culture system.* Cytotherapy, 2006. **8**(1): p. 3-12.

158. Saudemont, A. and B. Quesnel, *In a model of tumor dormancy, long-term persistent leukemic cells have increased B7-H1 and B7.1 expression and resist CTL-mediated lysis.* Blood, 2004. **104**(7): p. 2124-33.
159. Pistillo, M.P., et al., *CTLA-4 is not restricted to the lymphoid cell lineage and can function as a target molecule for apoptosis induction of leukemic cells.* Blood, 2003. **101**(1): p. 202-9.
160. Xerri, L., et al., *In vivo expression of the CTLA4 inhibitory receptor in malignant and reactive cells from human lymphomas.* J Pathol, 1997. **183**(2): p. 182-7.
161. Davids, M.S., et al., *Ipilimumab for Patients with Relapse after Allogeneic Transplantation.* N Engl J Med, 2016. **375**(2): p. 143-53.
162. Bierman, H.R., et al., *Remissions in leukemia of childhood following acute infectious disease: staphylococcus and streptococcus, varicella, and feline panleukopenia.* Cancer, 1953. **6**(3): p. 591-605.
163. Russell, S.J., K.W. Peng, and J.C. Bell, *Oncolytic virotherapy.* Nat Biotechnol, 2012. **30**(7): p. 658-70.
164. Zou, Y., et al., *Bibliometric analysis of oncolytic virus research, 2000 to 2018.* Medicine (Baltimore), 2019. **98**(35): p. e16817.
165. Thompson, M.R., et al., *Pattern recognition receptors and the innate immune response to viral infection.* Viruses, 2011. **3**(6): p. 920-40.
166. Talemi, S.R. and T. Hofer, *Antiviral interferon response at single-cell resolution.* Immunol Rev, 2018. **285**(1): p. 72-80.
167. Platanias, L.C., *Mechanisms of type-I- and type-II-interferon-mediated signalling.* Nat Rev Immunol, 2005. **5**(5): p. 375-86.
168. Prakash, A., et al., *Tissue-specific positive feedback requirements for production of type I interferon following virus infection.* J Biol Chem, 2005. **280**(19): p. 18651-7.
169. Kawai, T. and S. Akira, *Signaling to NF-kappaB by Toll-like receptors.* Trends Mol Med, 2007. **13**(11): p. 460-9.
170. Hanahan, D. and R.A. Weinberg, *Hallmarks of cancer: the next generation.* Cell, 2011. **144**(5): p. 646-74.
171. Borsellino, N., et al., *Antiproliferative and chemomodulatory effects of interferon-gamma on doxorubicin-sensitive and -resistant tumor cell lines.* Anticancer Drugs, 1993. **4**(2): p. 265-72.
172. Bekisz, J., et al., *Antiproliferative Properties of Type I and Type II Interferon.* Pharmaceuticals (Basel), 2010. **3**(4): p. 994-1015.
173. Katsoulidis, E., S. Kaur, and L.C. Platanias, *Deregulation of Interferon Signaling in Malignant Cells.* Pharmaceuticals (Basel), 2010. **3**(2): p. 406-418.
174. Zemp, F., J. Rajwani, and D.J. Mahoney, *Rhabdoviruses as vaccine platforms for infectious disease and cancer.* Biotechnol Genet Eng Rev, 2018. **34**(1): p. 122-138.
175. Nishizono, A. and K. Yamada, *[Rhabdoviruses].* Uirusu, 2012. **62**(2): p. 183-96.
176. Tong, J.G., et al., *Spatial and temporal epithelial ovarian cancer cell heterogeneity impacts Maraba virus oncolytic potential.* BMC Cancer, 2017. **17**(1): p. 594.
177. Baltimore, D., A.S. Huang, and M. Stampfer, *Ribonucleic acid synthesis of vesicular stomatitis virus, II. An RNA polymerase in the virion.* Proc Natl Acad Sci U S A, 1970. **66**(2): p. 572-6.
178. Baltimore, D., *Expression of animal virus genomes.* Bacteriol Rev, 1971. **35**(3): p. 235-41.
179. Kell, A.M. and M. Gale, Jr., *RIG-I in RNA virus recognition.* Virology, 2015. **479-480**: p. 110-21.

180. Stojdl, D.F., et al., *The murine double-stranded RNA-dependent protein kinase PKR is required for resistance to vesicular stomatitis virus.* J Virol, 2000. **74**(20): p. 9580-5.
181. von Kobbe, C., et al., *Vesicular stomatitis virus matrix protein inhibits host cell gene expression by targeting the nucleoporin Nup98.* Mol Cell, 2000. **6**(5): p. 1243-52.
182. Suder, E., et al., *The vesicular stomatitis virus-based Ebola virus vaccine: From concept to clinical trials.* Hum Vaccin Immunother, 2018. **14**(9): p. 2107-2113.
183. Naik, S., et al., *Potent systemic therapy of multiple myeloma utilizing oncolytic vesicular stomatitis virus coding for interferon-beta.* Cancer Gene Ther, 2012. **19**(7): p. 443-50.
184. Shen, W., et al., *Immunovirotherapy with vesicular stomatitis virus and PD-L1 blockade enhances therapeutic outcome in murine acute myeloid leukemia.* Blood, 2016. **127**(11): p. 1449-58.
185. Wu, L., et al., *rVSV(M Delta 51)-M3 is an effective and safe oncolytic virus for cancer therapy.* Hum Gene Ther, 2008. **19**(6): p. 635-47.
186. Lemay, C.G., et al., *Harnessing oncolytic virus-mediated antitumor immunity in an infected cell vaccine.* Mol Ther, 2012. **20**(9): p. 1791-9.
187. Pol, J.G., et al., *Maraba virus as a potent oncolytic vaccine vector.* Mol Ther, 2014. **22**(2): p. 420-429.
188. Bourgeois-Daigneault, M.C., et al., *Neoadjuvant oncolytic virotherapy before surgery sensitizes triple-negative breast cancer to immune checkpoint therapy.* Sci Transl Med, 2018. **10**(422).
189. Marchini, A., E.M. Scott, and J. Rommelaere, *Overcoming Barriers in Oncolytic Virotherapy with HDAC Inhibitors and Immune Checkpoint Blockade.* Viruses, 2016. **8**(1).
190. Saha, D., R.L. Martuza, and S.D. Rabkin, *Macrophage Polarization Contributes to Glioblastoma Eradication by Combination Immunovirotherapy and Immune Checkpoint Blockade.* Cancer Cell, 2017. **32**(2): p. 253-267 e5.
191. Andtbacka, R.H., et al., *Talimogene Laherparepvec Improves Durable Response Rate in Patients With Advanced Melanoma.* J Clin Oncol, 2015. **33**(25): p. 2780-8.
192. Shim, K.G., et al., *Inhibitory Receptors Induced by VSV Viroimmunotherapy Are Not Necessarily Targets for Improving Treatment Efficacy.* Mol Ther, 2017. **25**(4): p. 962-975.
193. Liu, Z., et al., *Rational combination of oncolytic vaccinia virus and PD-L1 blockade works synergistically to enhance therapeutic efficacy.* Nat Commun, 2017. **8**: p. 14754.
194. Alkayyal, A.A., et al., *NK-Cell Recruitment Is Necessary for Eradication of Peritoneal Carcinomatosis with an IL12-Expressing Maraba Virus Cellular Vaccine.* Cancer Immunol Res, 2017. **5**(3): p. 211-221.
195. Cassel, W.A. and D.R. Murray, *A ten-year follow-up on stage II malignant melanoma patients treated postsurgically with Newcastle disease virus oncolysate.* Med Oncol Tumor Pharmacother, 1992. **9**(4): p. 169-71.
196. Conrad, D.P., et al., *Leukemia cell-rhabdovirus vaccine: personalized immunotherapy for acute lymphoblastic leukemia.* Clin Cancer Res, 2013. **19**(14): p. 3832-43.
197. Dempster, H., *Characterization of the Anti-Tumour Immune Response Following Treatment with an Infected Leukemia Cell Vaccine*, in *BMI*. 2018, University of Ottawa.
198. Moore, G.E., A.A. Sandberg, and K. Ulrich, *Suspension cell culture and in vivo and in vitro chromosome constitution of mouse leukemia L1210.* J Natl Cancer Inst, 1966. **36**(3): p. 405-13, 415-21.
199. Goldie, H., et al., *Growth characteristics of free C1498 granulocytic leukemia tumor cells in the peritoneal fluid and the blood of C57 mice.* Cancer Res, 1953. **13**(2): p. 125-9.

200. Stojdl, D.F., et al., *Exploiting tumor-specific defects in the interferon pathway with a previously unknown oncolytic virus.* Nat Med, 2000. **6**(7): p. 821-5.
201. Breitbach, C.J., et al., *Targeted inflammation during oncolytic virus therapy severely compromises tumor blood flow.* Mol Ther, 2007. **15**(9): p. 1686-93.
202. Zitvogel, L., et al., *Immune response against dying tumor cells.* Adv Immunol, 2004. **84**: p. 131-79.
203. Matzinger, P., *The danger model: a renewed sense of self.* Science, 2002. **296**(5566): p. 301-5.
204. Liu, H., et al., *Tumor-derived IFN triggers chronic pathway agonism and sensitivity to ADAR loss.* Nat Med, 2019. **25**(1): p. 95-102.
205. Glass, W.G., H.F. Rosenberg, and P.M. Murphy, *Chemokine regulation of inflammation during acute viral infection.* Curr Opin Allergy Clin Immunol, 2003. **3**(6): p. 467-73.
206. Han, B.S., et al., *Regulation of the translation activity of antigen-specific mRNA is responsible for antigen loss and tumor immune escape in a HER2-expressing tumor model.* Sci Rep, 2019. **9**(1): p. 2855.
207. Leone, P., et al., *MHC class I antigen processing and presenting machinery: organization, function, and defects in tumor cells.* J Natl Cancer Inst, 2013. **105**(16): p. 1172-87.
208. Curran, E.K., J. Godfrey, and J. Kline, *Mechanisms of Immune Tolerance in Leukemia and Lymphoma.* Trends Immunol, 2017. **38**(7): p. 513-525.
209. Holling, T.M., E. Schooten, and P.J. van Den Elsen, *Function and regulation of MHC class II molecules in T-lymphocytes: of mice and men.* Hum Immunol, 2004. **65**(4): p. 282-90.
210. Murphy, S.P., et al., *DNA alkylating agents alleviate silencing of class II transactivator gene expression in L1210 lymphoma cells.* J Immunol, 2002. **169**(6): p. 3085-93.
211. Sollner, J.F., et al., *An RNA-Seq atlas of gene expression in mouse and rat normal tissues.* Sci Data, 2017. **4**: p. 170185.
212. Oh, J., et al., *Age-related tumor growth in mice is related to integrin alpha 4 in CD8+ T cells.* JCI Insight, 2018. **3**(21).
213. Fowler, T., et al., *Divergence of transcriptional landscape occurs early in B cell activation.* Epigenetics Chromatin, 2015. **8**: p. 20.
214. Seliger, B., et al., *Characterization of the major histocompatibility complex class I deficiencies in B16 melanoma cells.* Cancer Res, 2001. **61**(3): p. 1095-9.
215. Welsh, R.M., et al., *Type 1 interferons and antiviral CD8 T-cell responses.* PLoS Pathog, 2012. **8**(1): p. e1002352.
216. Berthon, C., et al., *In acute myeloid leukemia, B7-H1 (PD-L1) protection of blasts from cytotoxic T cells is induced by TLR ligands and interferon-gamma and can be reversed using MEK inhibitors.* Cancer Immunol Immunother, 2010. **59**(12): p. 1839-49.
217. Stahl, M. and A.D. Goldberg, *Immune Checkpoint Inhibitors in Acute Myeloid Leukemia: Novel Combinations and Therapeutic Targets.* Curr Oncol Rep, 2019. **21**(4): p. 37.
218. Troeger, A., et al., *High expression of CD40 on B-cell precursor acute lymphoblastic leukemia blasts is an independent risk factor associated with improved survival and enhanced capacity to up-regulate the death receptor CD95.* Blood, 2008. **112**(4): p. 1028-34.
219. Zhao, Y., et al., *Antigen-Presenting Cell-Intrinsic PD-1 Neutralizes PD-L1 in cis to Attenuate PD-1 Signaling in T Cells.* Cell Rep, 2018. **24**(2): p. 379-390 e6.
220. Beyersdorf, N., T. Kerkau, and T. Hunig, *CD28 co-stimulation in T-cell homeostasis: a recent perspective.* Immunotargets Ther, 2015. **4**: p. 111-22.

221. Mayer, C.T., et al., *Selective and efficient generation of functional Batf3-dependent CD103+ dendritic cells from mouse bone marrow.* Blood, 2014. **124**(20): p. 3081-91.
222. Elgueta, R., et al., *Molecular mechanism and function of CD40/CD40L engagement in the immune system.* Immunol Rev, 2009. **229**(1): p. 152-72.
223. Zhang, L., et al., *CD40 ligation reverses T cell tolerance in acute myeloid leukemia.* J Clin Invest, 2013. **123**(5): p. 1999-2010.
224. Mita, Y., et al., *Crucial role of CD69 in anti-tumor immunity through regulating the exhaustion of tumor-infiltrating T cells.* Int Immunol, 2018. **30**(12): p. 559-567.
225. Vinay, D.S. and B.S. Kwon, *4-1BB (CD137), an inducible costimulatory receptor, as a specific target for cancer therapy.* BMB Rep, 2014. **47**(3): p. 122-9.
226. Schuurhuis, D.H., et al., *Immature dendritic cells acquire CD8(+) cytotoxic T lymphocyte priming capacity upon activation by T helper cell-independent or -dependent stimuli.* J Exp Med, 2000. **192**(1): p. 145-50.
227. Bijker, M.S., et al., *CD8+ CTL priming by exact peptide epitopes in incomplete Freund's adjuvant induces a vanishing CTL response, whereas long peptides induce sustained CTL reactivity.* J Immunol, 2007. **179**(8): p. 5033-40.
228. Ridge, J.P., F. Di Rosa, and P. Matzinger, *A conditioned dendritic cell can be a temporal bridge between a CD4+ T-helper and a T-killer cell.* Nature, 1998. **393**(6684): p. 474-8.
229. Diehl, L., et al., *CD40 activation in vivo overcomes peptide-induced peripheral cytotoxic T-lymphocyte tolerance and augments anti-tumor vaccine efficacy.* Nat Med, 1999. **5**(7): p. 774-9.
230. Schoenberger, S.P., et al., *T-cell help for cytotoxic T lymphocytes is mediated by CD40-CD40L interactions.* Nature, 1998. **393**(6684): p. 480-3.
231. Postow, M.A., et al., *Nivolumab and ipilimumab versus ipilimumab in untreated melanoma.* N Engl J Med, 2015. **372**(21): p. 2006-17.
232. Ottaviano, M., S. De Placido, and P.A. Ascierto, *Recent success and limitations of immune checkpoint inhibitors for cancer: a lesson from melanoma.* Virchows Arch, 2019. **474**(4): p. 421-432.
233. Tsun, A., et al., *Oncolytic Immunotherapy for Treatment of Cancer.* Adv Exp Med Biol, 2016. **909**: p. 241-83.
234. Aldous, A.R. and J.Z. Dong, *Personalized neoantigen vaccines: A new approach to cancer immunotherapy.* Bioorg Med Chem, 2018. **26**(10): p. 2842-2849.
235. Chan, J.F., et al., *Differential cell line susceptibility to the emerging Zika virus: implications for disease pathogenesis, non-vector-borne human transmission and animal reservoirs.* Emerg Microbes Infect, 2016. **5**: p. e93.
236. Bazhin, A.V., et al., *Interferon-alpha Up-Regulates the Expression of PD-L1 Molecules on Immune Cells Through STAT3 and p38 Signaling.* Front Immunol, 2018. **9**: p. 2129.
237. Wajant, H., *The role of TNF in cancer.* Results Probl Cell Differ, 2009. **49**: p. 1-15.
238. Maghazachi, A.A., A. Al-Aoukaty, and T.J. Schall, *CC chemokines induce the generation of killer cells from CD56+ cells.* Eur J Immunol, 1996. **26**(2): p. 315-9.
239. Cycon, K.A., et al., *The immunogenicity of L1210 lymphoma clones correlates with their ability to function as antigen-presenting cells.* Immunology, 2009. **128**(1 Suppl): p. e641-51.
240. LaBelle, J.L., et al., *Negative effect of CTLA-4 on induction of T-cell immunity in vivo to B7-1+, but not B7-2+, murine myelogenous leukemia.* Blood, 2002. **99**(6): p. 2146-53.
241. Riley, J.L. and C.H. June, *The CD28 family: a T-cell rheostat for therapeutic control of T-cell activation.* Blood, 2005. **105**(1): p. 13-21.

242. Alegre, M.L., et al., *Regulation of surface and intracellular expression of CTLA4 on mouse T cells.* J Immunol, 1996. **157**(11): p. 4762-70.
243. van Elsas, A., A.A. Hurwitz, and J.P. Allison, *Combination immunotherapy of B16 melanoma using anti-cytotoxic T lymphocyte-associated antigen 4 (CTLA-4) and granulocyte/macrophage colony-stimulating factor (GM-CSF)-producing vaccines induces rejection of subcutaneous and metastatic tumors accompanied by autoimmune depigmentation.* J Exp Med, 1999. **190**(3): p. 355-66.
244. Ip, W.K. and Y.L. Lau, *Distinct maturation of, but not migration between, human monocyte-derived dendritic cells upon ingestion of apoptotic cells of early or late phases.* J Immunol, 2004. **173**(1): p. 189-96.
245. Banchereau, J., et al., *The CD40 antigen and its ligand.* Annu Rev Immunol, 1994. **12**: p. 881-922.
246. Joffre, O.P., et al., *Cross-presentation by dendritic cells.* Nat Rev Immunol, 2012. **12**(8): p. 557-69.
247. Skov, S., et al., *IL-2 and IL-15 regulate CD154 expression on activated CD4 T cells.* J Immunol, 2000. **164**(7): p. 3500-5.

Appendices

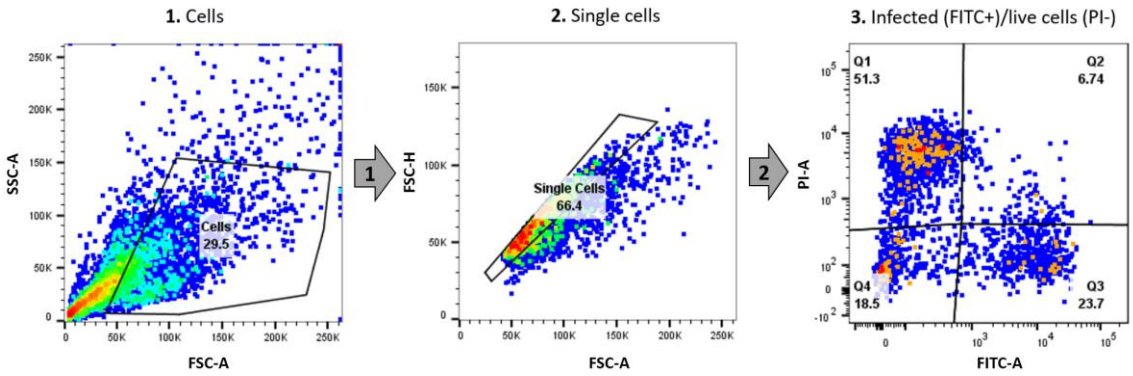
1. Cells
SSC-A
FSC-A
Cells
29.5
1
2. Single cells
FSC-H
FSC-A
Single Cells
66.4
2
3. Infected (FITC+)/live cells (PI-)
PI-A
FITC-A
Q1
51.3
Q2
6.74
Q4
18.5
Q3
23.7

Supplementary Figure 1: The gating strategy employed in the data analysis from *in vitro* infectivity/viability experiments.

The complete gating strategy is showed for a representative C1498 – infected sample. 5 x 10^6 C1498 cells were infected with MG1-eGFP virus at MOI of 10 in 5 ml of cRPMI media for 17 hours at 37°C, 5% CO_2 The cells were then washed 10 ml of PBS (1500 RPM, 5 minutes), resuspended in 500 µl of PBS and exposed to 30-Gy radiation for 1 hour. The cells were stained with 5 µl of a 1:500 diluted PI viability dye and the intensity of the GFP and PI signal were immediately acquired using BD Celesta. Data was analyzed using FlowJo software. To determine the amount of infected and life cells, we first gated out cell debris that is identified as FSC-A^{low} and SSC-A^{low}, then the doublets were eliminated using the FSC-A and FSC-H.

A

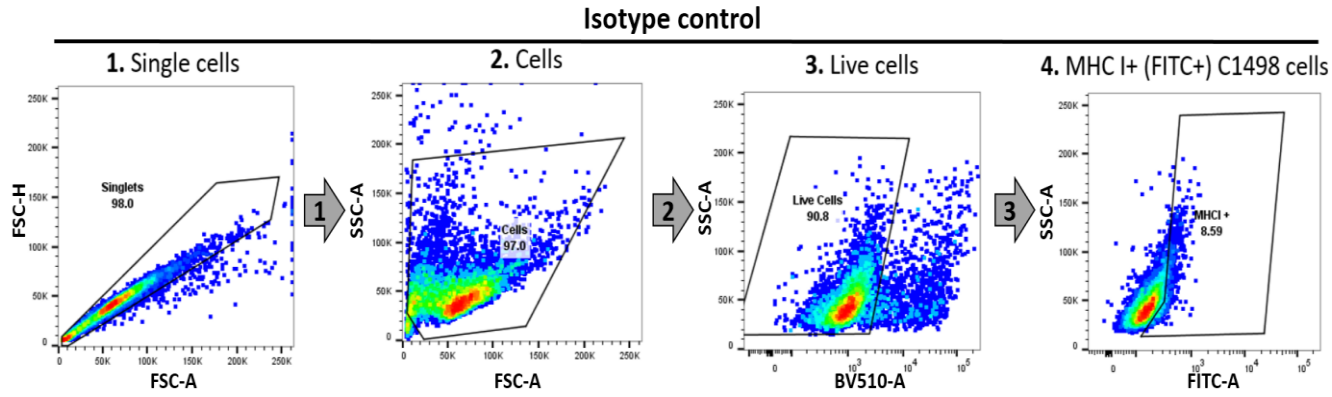
Isotype control
1. Single cells
2. Cells
3. Live cells
4. MHC I+ (FITC+) C1498 cells
Singlets
98.0
FSC-H
FSC-A
1
SSC-A
Cells
97.0
FSC-A
2
SSC-A
Live Cells
90.8
BV510-A
3
SSC-A
MHCI +
8.59
FITC-A

B

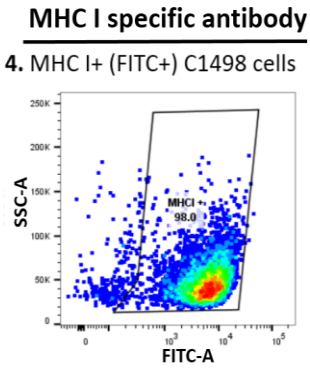
MHC I specific antibody
4. MHC I+ (FITC+) C1498 cells
SSC-A
MHCI +
98.0
FITC-A

Supplementary Figure 2: The gating strategy employed in the data analysis from the MHC I expression assessment experiments on leukemia cell lines.

1×10^6 cells C1498 cells were stimulated with 50U of IFN-ɣ at 37°C, 5% CO_2 in 1 ml of cRPMI media. After 16 hours, cells were washed in PBS (1500 RPM, 5 minutes) and incubated in 10 µl of diluted (1:20, in PBS) FVS510 viability dye for 20 minutes in the dark at RT. Then the cells were washed in PBS (1500 RPM, 5 minutes) and incubated in 25 µl of diluted (1:100, in FACS buffer) Rat Anti-mouse CD16/CD32 solution for 15 minutes at 4°C in the dark. Then cells were stained with 25 µl of either diluted (1:100, in FACS buffer) an isotype control or MHC I – FITC monoclonal antibodies for 25 minutes in the dark at 4°C. Lastly, the samples were fixed in 200 µl of 1% PFA and ran through the BD LSR Fortessa. FlowJo software was used for data analysis. First, doublets were excluded on the FSC-A vs FSC-H plots, following the elimination of cell debris that was identified as $FSC\text{-}A^{low}$ and $SSC\text{-}A^{low}$. The population of live cells, identified as BV510-, was used to determine the MHC I – expressing cells as being FITC+ along the SSC-A axis.
(A) An example of a complete gating strategy is shown for an IFN-ɣ - stimulated C1498 cells stained with an isotype control antibody, along with
(B) a single dot plot of an IFN-ɣ - stimulated C1498 sample stained with an antibody with binding specificity to the murine MHC I complex.

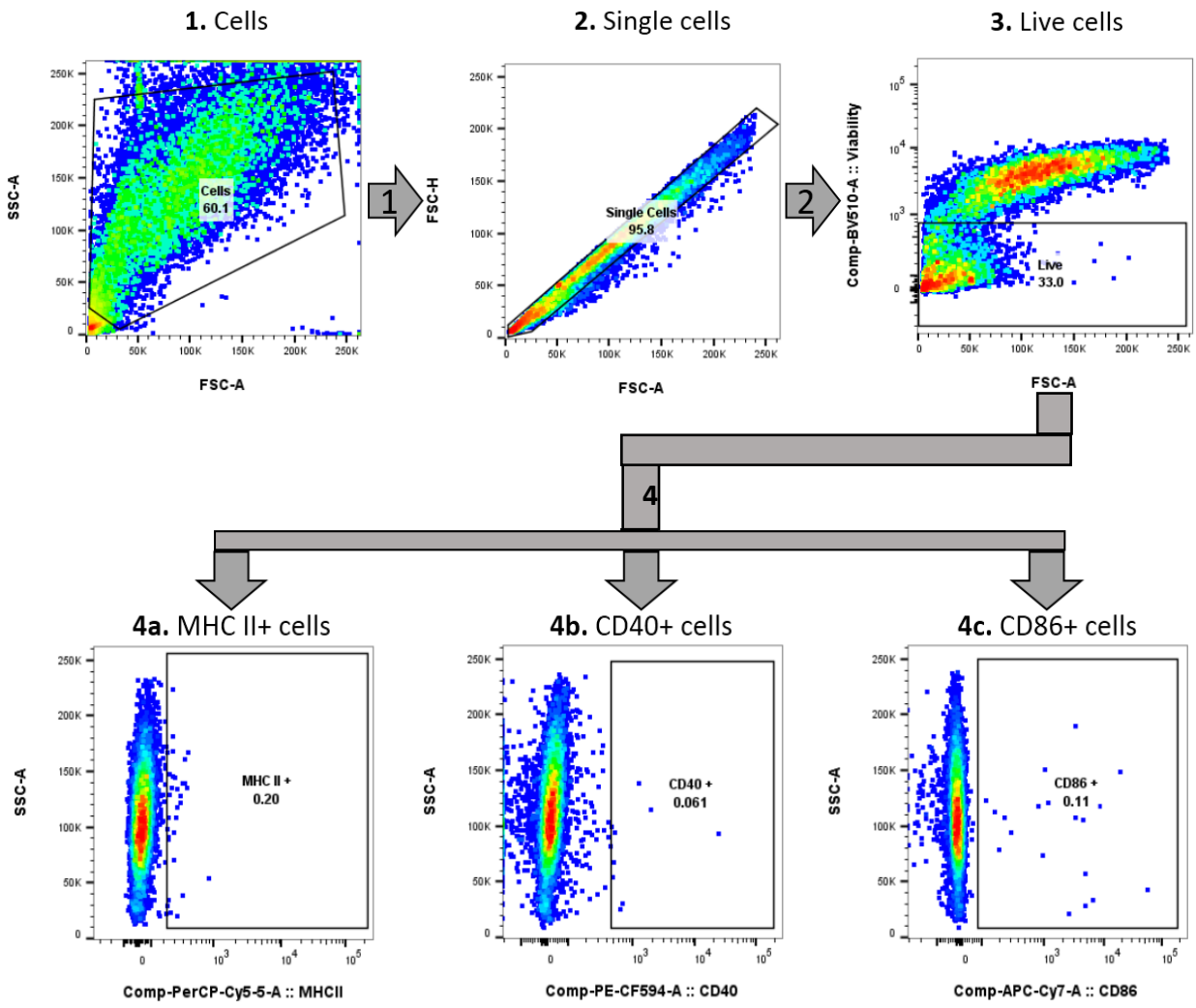
1. Cells
2. Single cells
3. Live cells
SSC-A
FSC-A
Cells
60.1
1
FSC-H
FSC-A
Single Cells
95.8
2
Comp-BV510-A :: Viability
FSC-A
Live
33.0
4
4a. MHC II+ cells
4b. CD40+ cells
4c. CD86+ cells
SSC-A
MHC II +
0.20
Comp-PerCP-Cy5-5-A :: MHCII
SSC-A
CD40 +
0.061
Comp-PE-CF594-A :: CD40
SSC-A
CD86 +
0.11
Comp-APC-Cy7-A :: CD86

Supplementary Figure 3: The gating strategy employed in the data analysis from the experiments assessing the expression of MHC II, CD40 and CD86 on murine leukemia cell lines.

1×10^6 L1210 cells were infected with MG1 virus at MOI of 10 for 17 hours in 1 ml of cRPMI at 37°C, 5% CO_2. The infected cells were washed with PBS (1500 RPM, 5 minutes), resuspended in 100 µl of PBS and exposed to 30-Gy for about an hour. Each sample was stained with 10 µl of diluted (1:20, in PBS) for 20 minutes in a dark place at RT. The cells were washed with PBS (1500 RPM, 5 minutes) and incubated in 25 µl of diluted (1:100, in FACS buffer) Rat Anti-mouse CD16/CD32 (Cat#: 553142, BD Biosciences) solution for 15 minutes at 4°C in the dark. Next, the cells were incubated in 25 µl of a master mix in which MHC II – PerC-Cy 5.5, CD86 – APC-Cy7 and CD40 – PE-CF594 monoclonal antibodies were diluted 1:100 in FACS buffer. After 25 minutes of incubation at 4°C in the dark, each sample was washed with FACS buffer (1500 RPM, 5 minutes) and fixed in 200 µl of 1% PFA. The data was acquired using the BD LSR Fortessa and the data was analysed using FlowJo software. First, cell debris identified as FSC-A ^{low} and SSC-A ^{low} was eliminated from the analysis, following the exclusion of the doublets on the FSC-A vs FSC-H plots. The population of live cells, identified as BV510-, was used to determine the MHC II+, CD40+ and CD86+ L1210 cells along the SSC-A axis.

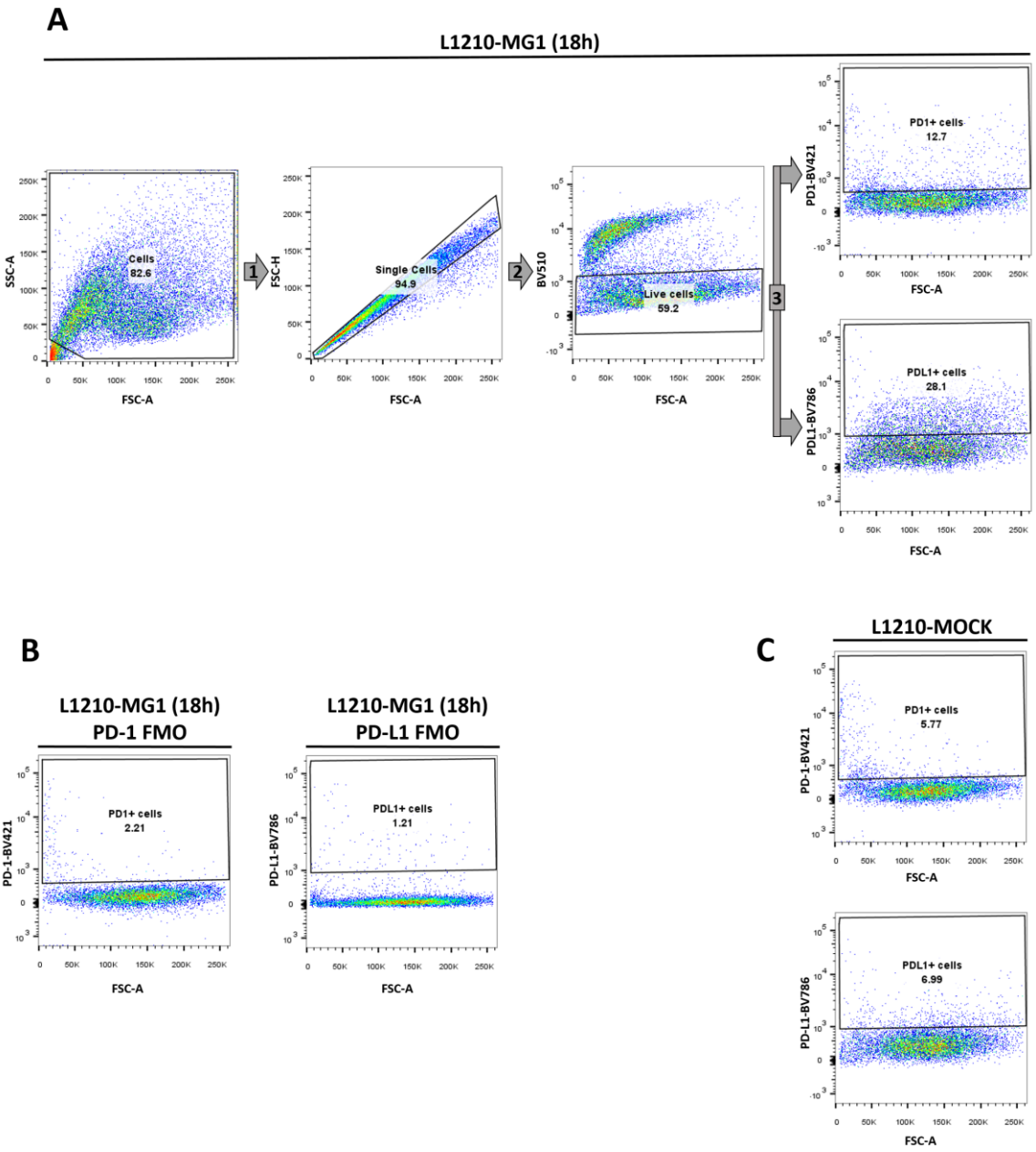
A
L1210-MG1 (18h)
SSC-A
FSC-A
Cells
82.6
1
FSC-H
Single Cells
94.9
2
BV510
Live cells
59.2
3
PD1-BV421
PD1+ cells
12.7
PDL1-BV786
PDL1+ cells
28.1
B
L1210-MG1 (18h)
PD-1 FMO
PD-1-BV421
PD1+ cells
2.21
L1210-MG1 (18h)
PD-L1 FMO
PD-L1-BV786
PDL1+ cells
1.21
C
L1210-MOCK
PD-1-BV421
PD1+ cells
5.77
PD-L1-BV786
PDL1+ cells
6.99

Supplementary Figure 4: The gating strategy employed in the data analysis from the experiment assessing the expression of PD-1 and PD-L1 on L1210 cells after MG1 infection *in vitro*.

L1210 cells were uninfected **(C)** or **(A)** infected with MG1 virus at MOI of 10 for 18 hours in cRPMI at 37°C, 5% CO_2. The infected leukemia cells were washed once with PBS (1500 RPM, 5 minutes) and resuspended in 100 µl (per 1×10^6 cells). The sample was stained with 50 µl of diluted (1:165, in PBS) FVS510 viability dye for 20 minutes in the dark and then incubated in 25 µl of diluted (1:100, in FACS buffer) Rat Anti-mouse CD16/CD32 solution for 5 minutes at 4°C in the dark. The sample was stained with PD-1 (BD Biosciences) and PD-L1 (BD Biosciences) monoclonal antibodies, both diluted (1:100) in Brilliant stain buffer with a total staining volume of 25 µl. Then the sample was washed in 150 µl of FACS buffer (1500 RPM, 5 minutes) and fixed in 200 µl of 1% PFA. The data was acquired using the BD LSR Fortessa. The PD-1+ and PD-L1+ leukemia cells were identified after eliminating cell debris (FSC-A vs SSC-A), doublets (FSC-A vs FSC-H) and dead cells (FSC-A vs BV510 positive). FlowJo software was used for data analysis. **(B)** L1210-MG1 FMO samples were used for each marker to set the positive gates for PD-1 and PD-L1.

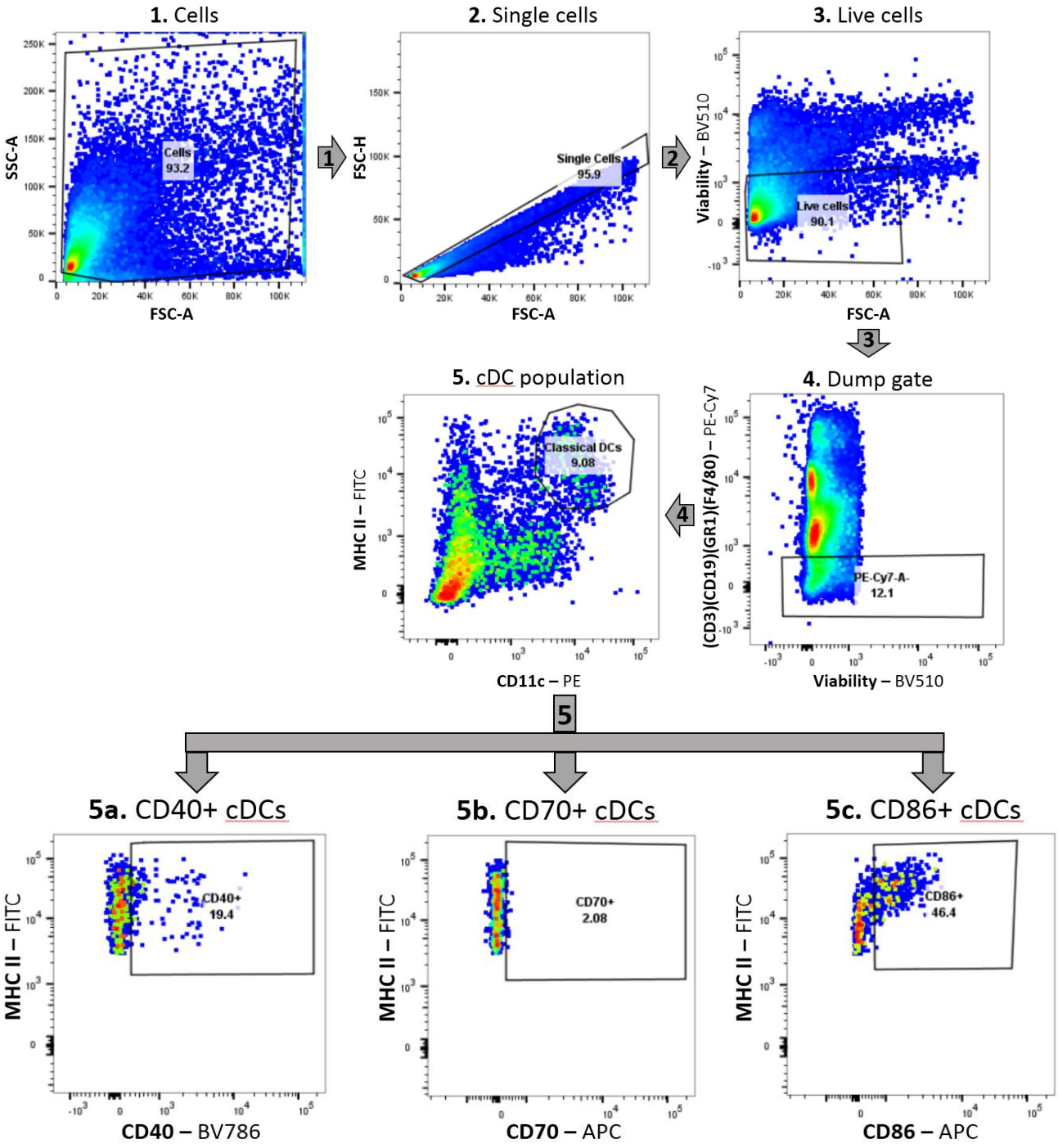
1. Cells
SSC-A
FSC-A
Cells
93.2
1
2. Single cells
FSC-H
FSC-A
Single Cells
95.9
2
3. Live cells
Viability – BV510
FSC-A
Live cells
90.1
3
4. Dump gate
(CD3)(CD19)(GR1)(F4/80) – PE-Cy7
Viability – BV510
PE-Cy7-A-
12.1
4
5. cDC population
MHC II – FITC
CD11c – PE
Classical DCs
9.08
5
5a. CD40+ cDCs
MHC II – FITC
CD40 – BV786
CD40+
19.4
5b. CD70+ cDCs
MHC II – FITC
CD70 – APC
CD70+
2.08
5c. CD86+ cDCs
MHC II – FITC
CD86 – APC
CD86+
46.4

Supplementary Figure 5: The gating strategy employed in the data analysis from the experiments assessing the *in vivo* maturation of splenic cDCs after administration of one dose of L1210-ICV.

A naïve DBA/2 mouse was immunized with one dose of L1210-ICV. After 24 hours, the spleen was processed and 1×10^6 of spleenocytes were stained with diluted (1:165, in PBS) FVS510 viability dye for 25 minutes at 4°C in the dark. The cells were washed with PBS (500g, 5 minutes) and incubated in 50 µl of diluted (1:100, in FACS buffer) Rat Anti-mouse CD16/CD32 solution for 15 minutes at 4°C in the dark. The cells were resuspended in 25 µl of a master mix in which MHC II – FITC, CD11c – PE, CD103 – BV421, CD11b – APC-Cy7, CD40 – BV784, CD86 – APC and/or CD70 – APC, CD19 – PE-Cy7, GR1 – PE-Cy7, CD3e – PE-Cy7 and F4/80 – PE-Cy7 monoclonal antibodies were diluted 1:100 in FACS buffer. The cells were incubated for 25 minutes at 4°C in the dark. The samples were washed with FACS buffer (500g, 5 minutes) and fixed in 200 µl of 1% PFA. The data was acquired using the BD LSR Fortessa and FlowJo software was used for data analysis. Cell debris (FSC-A ^{low} and SSC-A ^{low}), doublets (FSC-A vs FSC-H) and dead cells (FSC-A vs BV510 positive) were eliminated from each samples in both flow panels. The cDC population was identified in the first panel as MHC II ^{high}, CD11c ^{high} after eliminating PE-Cy7+ cell populations from the analysis. The expression of CD40 and/or CD70 and CD86 were determined the cDC population as a whole.

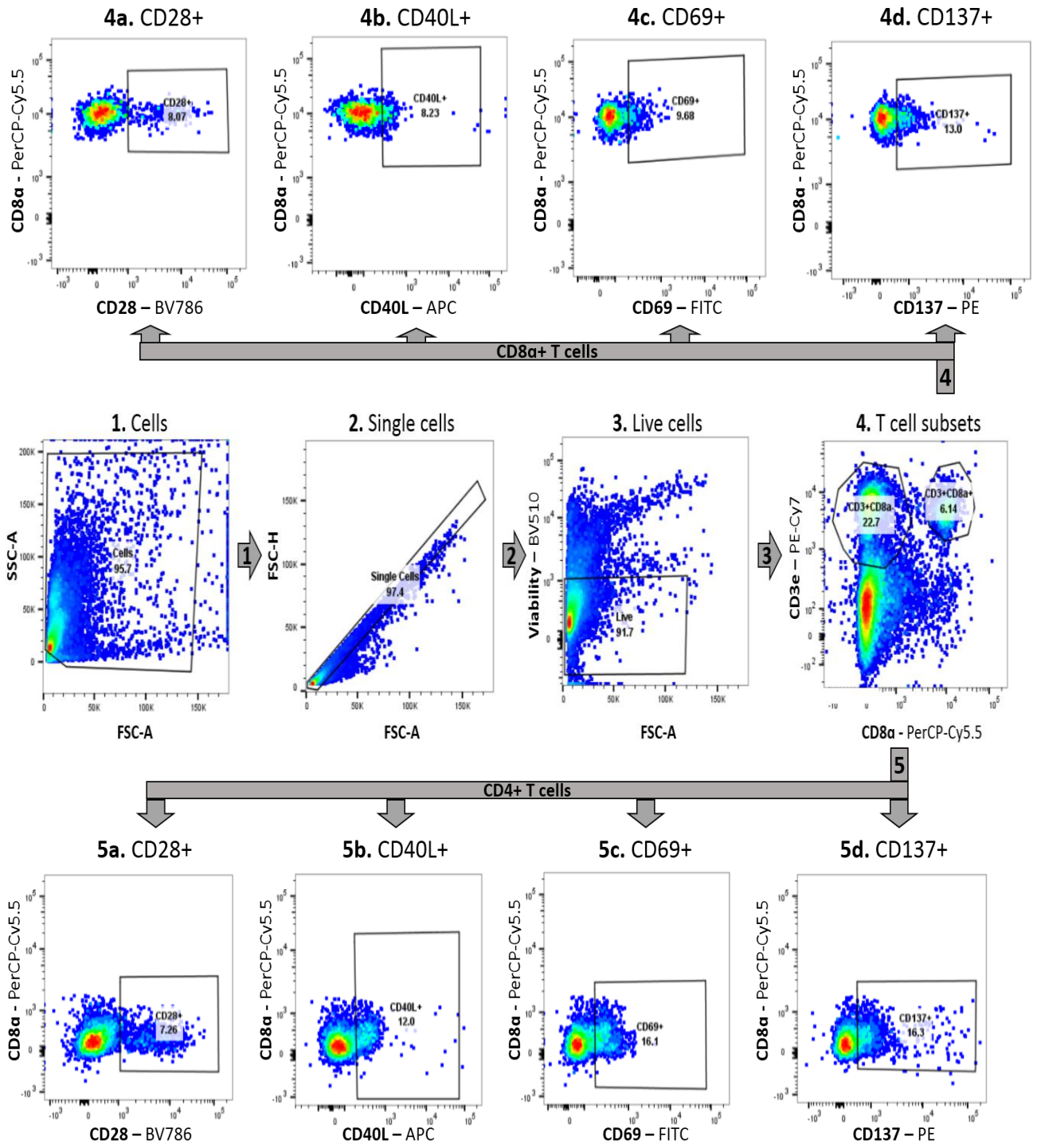
4a. CD28+
4b. CD40L+
4c. CD69+
4d. CD137+
CD8α - PerCP-Cy5.5
CD28+ 8.07
CD40L+ 8.23
CD69+ 9.68
CD137+ 13.0
CD28 – BV786
CD40L – APC
CD69 – FITC
CD137 – PE
CD8α+ T cells
4
1. Cells
2. Single cells
3. Live cells
4. T cell subsets
SSC-A
Cells 95.7
FSC-H
Single Cells 97.4
Viability – BV510
Live 91.7
CD3e – PE-Cy7
CD3+CD8a- 22.7
CD3+CD8a+ 6.14
FSC-A
CD8α - PerCP-Cy5.5
1
2
3
5
CD4+ T cells
5a. CD28+
5b. CD40L+
5c. CD69+
5d. CD137+
CD28+ 7.26
CD40L+ 12.0
CD69+ 16.1
CD137+ 16.3
CD28 – BV786
CD40L – APC
CD69 – FITC
CD137 – PE

Supplementary Figure 6: The gating strategy employed in the data analysis from the experiments assessing the *in vivo* activation of splenic T cells after administration of one dose of L1210-ICV.

A naïve DBA/2 mouse was immunized with one dose of L1210-ICV. After 1 hour, the spleen was processed and 1×10^6 of spleenocytes were stained with diluted (1:165, in PBS) FVS510 viability dye for 25 minutes at 4°C in the dark. The cells were washed PBS (500g, 5 minutes) and incubated in 50 µl of diluted (1:100, in FACS buffer) Rat Anti-mouse CD16/CD32 solution for 15 minutes at 4°C in the dark. The spleenocytes were resuspended in 25 µl of a master mix in which CD3e – PE-Cy7, CD8α – PerCP-Cy 5.5, CD28 – BV786, CD40L – APC, CD69 – FITC and CD137 – PE monoclonal antibodies were diluted 1:100 in FACS buffer. The cells were incubated for 25 minutes at 4°C in the dark. The samples were washed with FACS buffer (500g, 5 minutes) and fixed in 200 µl of 1% PFA. The data was acquired using the BD LSR Fortessa and FlowJo software was used for data analysis. Cell debris (FSC-A ^{low} and SSC-A ^{low}), doublets (FSC-A vs FSC-H) and dead cells (FSC-A vs BV510 positive) were eliminated from each samples in both flow panels. The CD8+ and CD4+ T cell subsets were identified in the second panel as CD3e+, CD8α+ and CD3+, CD8α- respectively. The expression of CD28, CD40L, CD69 and CD137 was then determined individually for both T cell subsets.

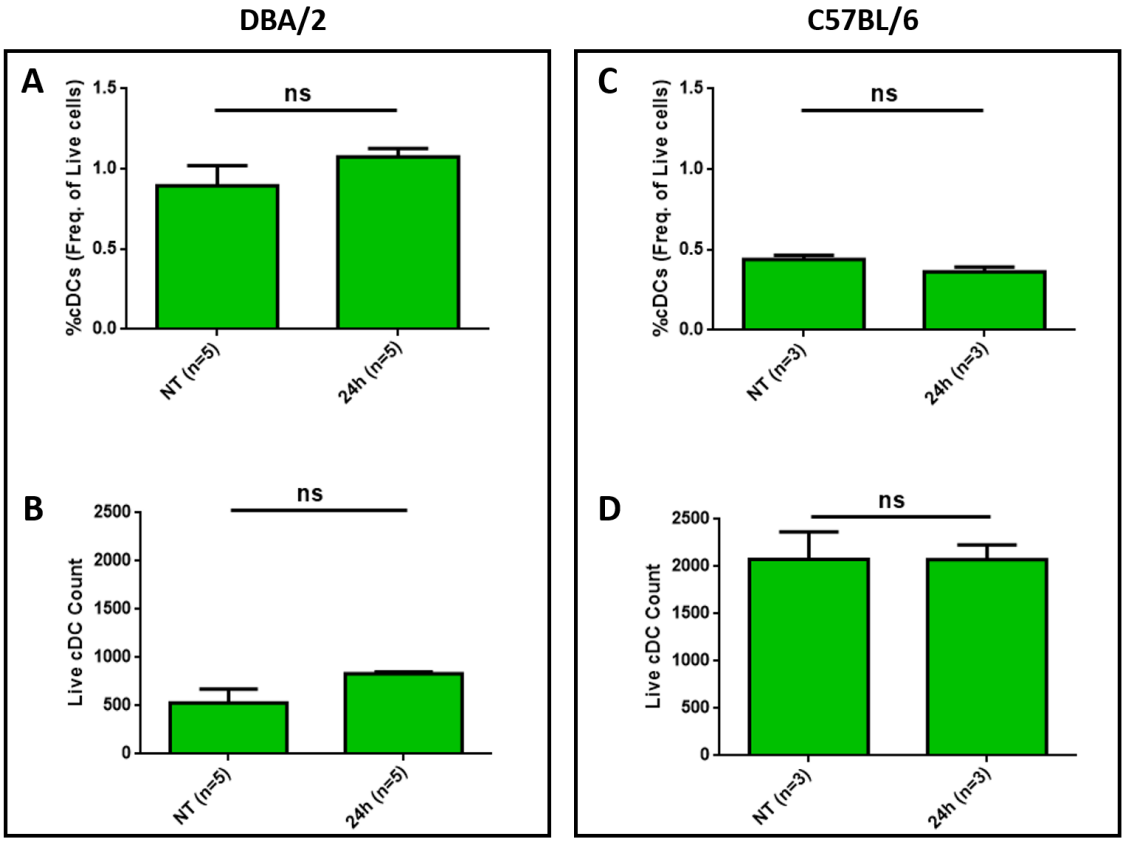
DBA/2
C57BL/6
A
%cDCs (Freq. of Live cells)
1.5
1.0
0.5
0.0
ns
NT (n=5)
24h (n=5)
B
Live cDC Count
2500
2000
1500
1000
500
0
ns
NT (n=5)
24h (n=5)
C
%cDCs (Freq. of Live cells)
1.5
1.0
0.5
0.0
ns
NT (n=3)
24h (n=3)
D
Live cDC Count
2500
2000
1500
1000
500
0
ns
NT (n=3)
24h (n=3)

Supplementary Figure 7: Changes in frequency and counts of live splenic cDCs after immunization of **(A, B)** DBA/2 mice with one dose of L1210-ICV-18h and **(C, D)** C57BL/6 mice with one dose of C1498-ICV-6h.

Naïve DBA/2 (n=5) and C57BL/6 (n=3) mice were treated with one dose of L1210-ICV-18h and C1498-ICV-6h respectively. The spleens of the immunized mice, along with the spleens of unimmunized DBA/2 (n=5) and C57BL/6 (n=3) mice were collected 24 hours later. The harvested spleenocytes from both immunized and unimmunized animals were stained for **(B, D)** CD28 receptor on CD8+ T cell sub-population and for its CD86 ligand **(A, C)** on cDC subsets to determine changes in their levels of expression. A difference in the levels of CD86+ cDC population was detected in both ICV-immunized DBA/2 mice ($p<0.05$) and C57BL/6 mice ($p<0.05$). The statistics were obtained after performing and a non-parametric, unpaired t test using the tools from GraphPad Prism.

A

DBA/2

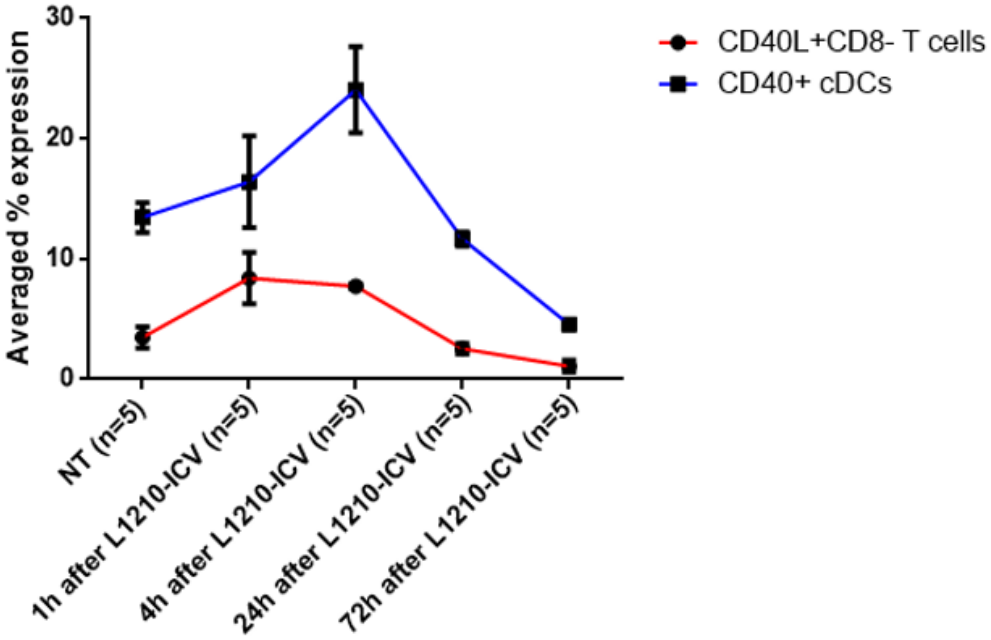

B

C57BL/6

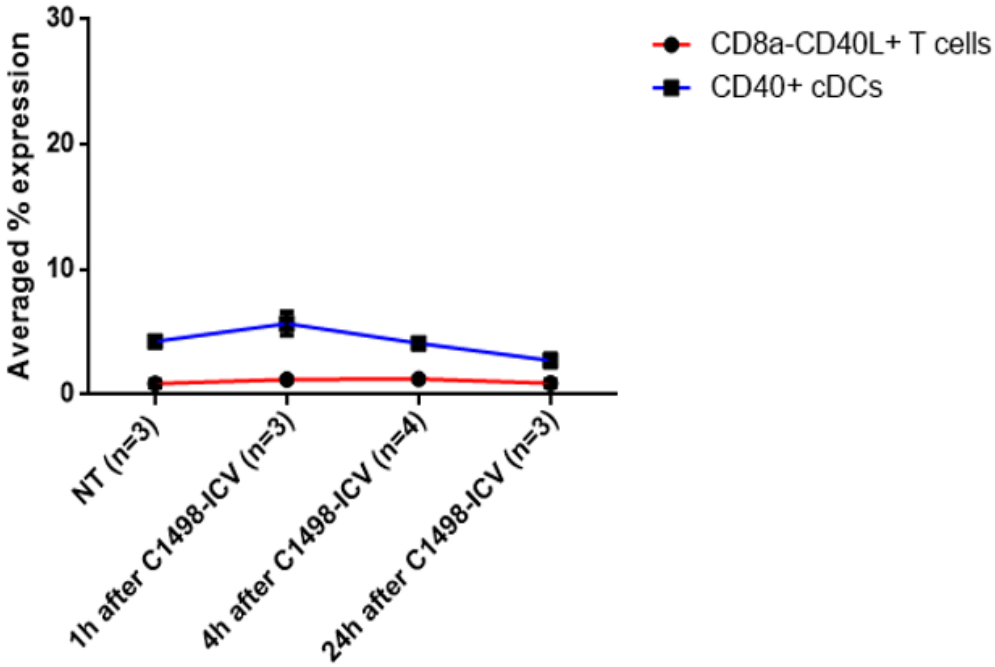

Supplementary Figure 8: Changes in CD40/40L expression of cDC and CD4+ T cell populations after immunization with **(A)** L1210-ICV-18h and **(B)** C1498-ICV-6h.

Naïve DBA/2 (n=5) and C57BL/6 (n=3) mice were treated with one dose of L1210-ICV-18h and C1498-ICV-6h respectively. The spleens of the immunized mice, along with the spleens of unimmunized DBA/2 (n=5) and C57BL/6 (n=3) mice were collected 1h, 4h, 24h or 72h later. The harvested spleenocytes from both immunized and unimmunized animals were stained for CD40L ligand on CD4+ T cell sub-population and for its receptor CD40 expressed on cDCs. The cDCs and T cells were stained in two separate panels (see the subparagraph 2.8.5 in the Materials and Methods section) and the data was acquired using LSR Fortessa.

A

T cell activation status in DBA/2 mice after one dose of L1210-ICV-18h

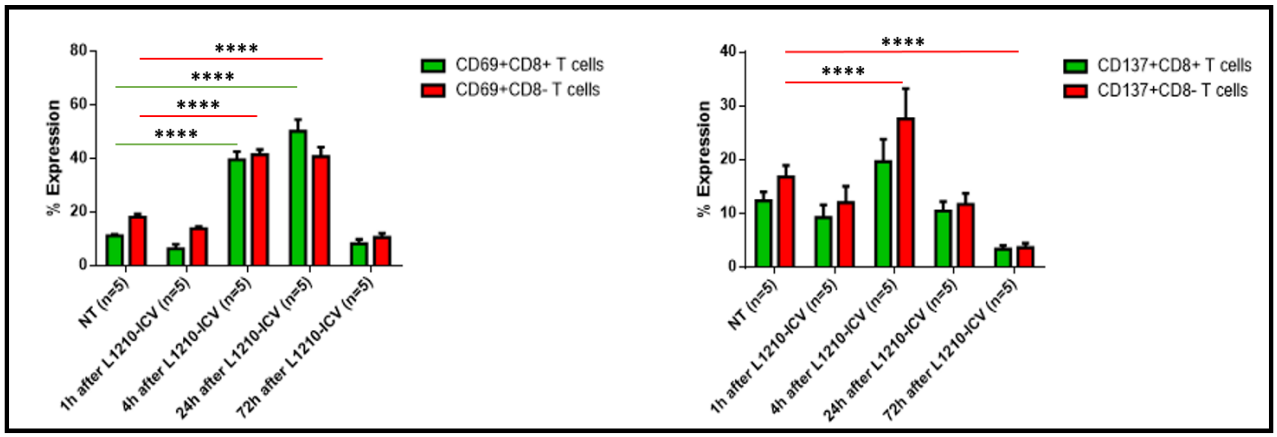

B

T cell activation status in C57BL/6 mice after one dose of C1498-ICV-6h

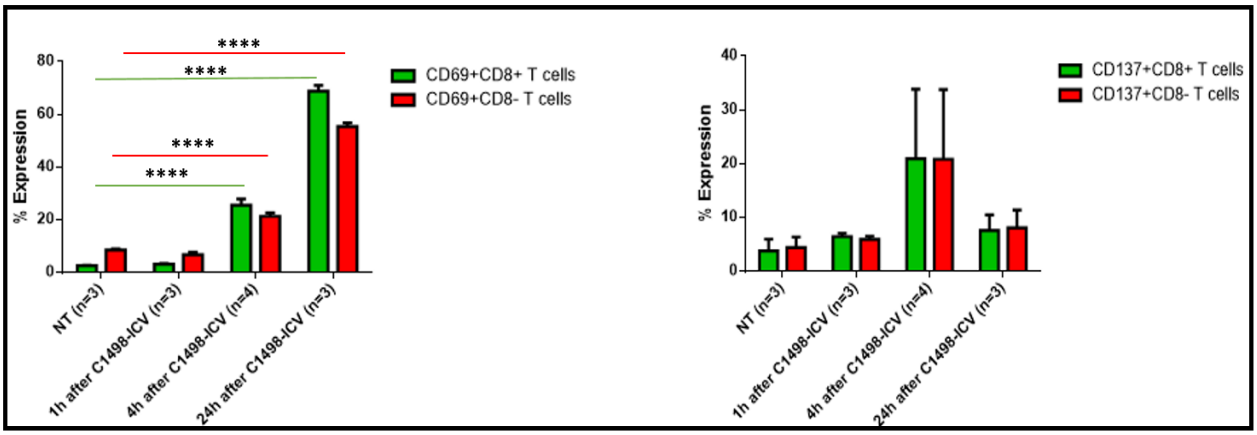

Supplementary Figure 9: Changes in the expression of CD69 and CD137 on splenic T cell subsets in **(A)** DBA/2 and **(B)** C57BL/6 mice after immunization with one dose of L1210-ICV-18h and C1498-ICV-6h respectively

Naïve DBA/2 (n=5) and C57BL/6 (n=3) mice were treated with one dose of L1210-ICV-18h and C1498-ICV-6h respectively. The spleens of the immunized mice, along with the spleens of unimmunized DBA/2 (n=5) and C57BL/6 (n=3) mice were collected 1h, 4h, 24h and/or 72h later. The harvested spleenocytes from both immunized and unimmunized animals were stained for CD69 and CD137 expression on CD8α+ T cell subsets (see the subparagraph 2.8.5 in the Materials and Methods section for more details on this experiment) The data was acquired using LSR Fortessa while GraphPad Prism was used to represent the data.

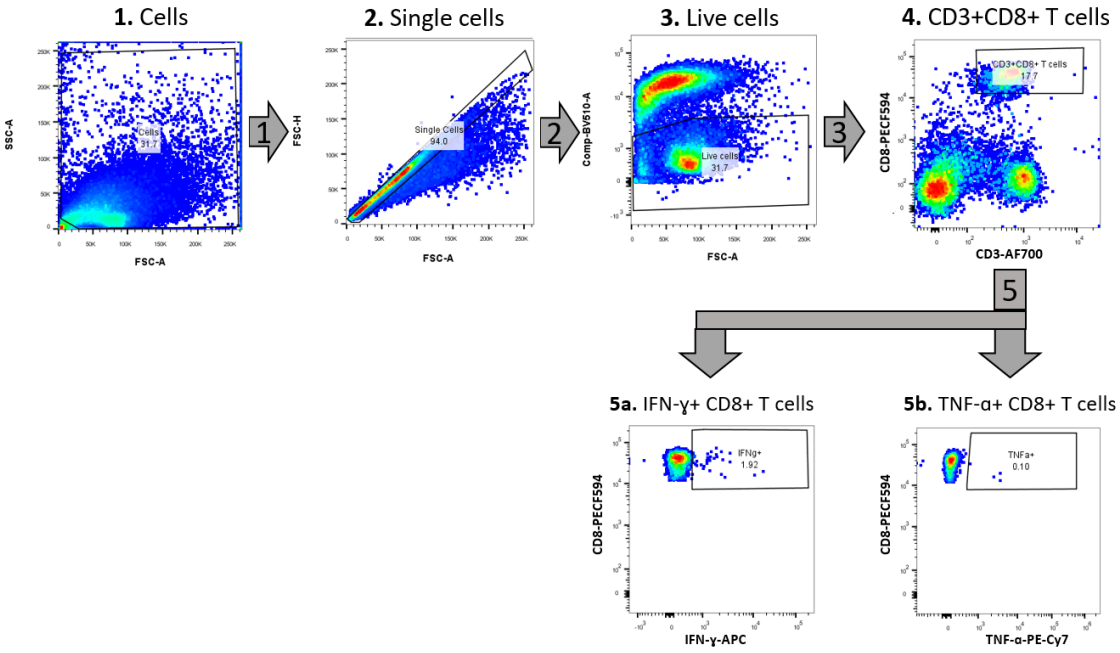
1. Cells
SSC-A
FSC-A
Cells
31.7
1
2. Single cells
FSC-H
FSC-A
Single Cells
94.0
2
3. Live cells
Comp-BV610-A
FSC-A
Live cells
31.7
3
4. CD3+CD8+ T cells
CD8-PECF594
CD3-AF700
CD3+CD8+ T cells
17.7
5
5a. IFN-γ+ CD8+ T cells
CD8-PECF594
IFN-γ-APC
IFNg+
1.92
5b. TNF-α+ CD8+ T cells
CD8-PECF594
TNF-α-PE-Cy7
TNFa+
0.10

Supplementary Figure 10: Gating strategy for identifying the activated CD8+ T cells from the saphenous blood of C1498-ICV-6h immunized C57BL/6

Naïve C57BL/6 mice were either untreated or treated with irradiated C1498 cells, C1409-ICV-18h or C1498-ICV-6h. A week after the first treatment mice were saph bleed and assayed for IFN-ɣ and TNFα expression levels on CD8α+ T cell population. Results were acquired using LSR Fortessa and are shown as percent CD8α+ T cells that are positive for both IFN-ɣ and TNFα.